

EXPERIMENTAL STUDIES OF THE DYNAMICS AND
FLOW BEHAVIORS OF COLLOIDAL NANOCCLAY
GLASSES AND GELS

BY

DEBASISH SAHA

A THESIS SUBMITTED TO THE JAWAHARLAL NEHRU UNIVERSITY
FOR THE DEGREE OF DOCTOR OF PHILOSOPHY

SOFT CONDENSED MATTER GROUP

RAMAN RESEARCH INSTITUTE

BANGALORE 560 080

MAY 2015

© Debasish Saha, 2015.

Typeset in L^AT_EX 2_ε.

Certificate:

This is to certify that the thesis entitled “**Experimental Studies of the Dynamics and Flow Behaviors of Colloidal Nanoclay Glasses and Gels**” submitted by Debasish Saha for the award of the degree of Doctor of Philosophy of Jawaharlal Nehru University is his original work. This has not been published or submitted to any other University for any other Degree or Diploma.

Prof. Ravi Subrahmanyam
(Director)
Raman Research Institute
Bangalore 560 080
India

Dr. Ranjini Bandyopadhyay
(Thesis Supervisor)

Declaration:

I hereby declare that the work reported in this thesis is entirely original. This thesis is composed independently by me at Raman Research Institute under the supervision of Dr. Ranjini Bandyopadhyay. I further declare that the subject matter presented in this thesis has not previously formed the basis for the award of any degree, diploma, membership, associateship, fellowship or any other similar title of any university or institution. I also declare that I have run it through **Turnitin** plagiarism detection software.

Dr. Ranjini Bandyopadhyay

(Thesis Supervisor)

Soft Condensed Matter Group

Raman Research Institute

Bangalore 560 080

India

Debasish Saha

Acknowledgements

I express my sincere gratitude to my thesis supervisor Dr. Ranjini Bandyopadhyay for her guidance, support and encouragement throughout the duration of thesis work and beyond. I am grateful to her for encouraging independent thinking, believing in my ability and giving me a friendly lead whenever needed. I would like to convey my sincere gratitude to Prof. Yogesh M. Joshi (Department of Chemical Engineering, Indian Institute of Technology Kanpur, India) for many encouraging discussion sessions on my thesis work, collaboration and invaluable advices. I am thankful to Prof. Rama Govindarajan (TIFR Centre for Interdisciplinary Sciences, Hyderabad, India) for many useful discussions at the initial stage and teaching me tricks to improve my presentation skills. I express my sincere gratitude to Dr. Suresh Bhat, Polymer Science and Engineering Division, CSIR-National Chemical Laboratory for his help with the Zeta potential measurements.

A very sincere note of thanks is to Prof. V. Lakshminarayanan for helping me with the conductivity experiments. I am lucky to have Dr. Sanjib Sabhapandit and Dr. Pramod Pullarkat as my student advisory committee members. I am thankful to them for their encouragement and help with many academic issues. I would like to thank Prof. Yashodhan Hatwalne, Prof. V. A. Raghunathan and other faculty members of Soft Condensed Matter Group for their helpful discussions and encouragement.

My sincerest thanks and regards to my seniors, Dr. Md. Arif Kamal and Dr. Antara Pal for helping me in countless occasions and giving me company and support

when I needed it most. I wish them best of luck with their future and a very happy and prosperous married life. I convey my deepest gratitude to Dr. Rajib Basak and Dr. Harsha Mohan Paroor for their help in every aspect of my life in last few years. I express my sincere gratitude to my lab mates, Mr. Samim Ali and Mr. Sanjay Kumar Behera for their company and help in daily basis. I thank my past lab mates, Mr. Pawan Nandakishore, Mr. Yadu Krishnan, Ms. Hafsa Syed, Mr. Skanda Vivek, Ms. Sapna Ravindran, Mr. Prakhyat Hejmady, Dr. Somnath Karmakar and Mr. Rajsekhar Das for their help with the experiments, useful discussions and pleasant company.

I am thankful to Dr. Tridib Ray, Dr. Arijit Sharma and Prof. Sadiqali Rangwala for their help with the experiments and invaluable advices at various stages of my thesis work. I express my gratitude to Mr. Ram for his help with the glass drilling job. I am thankful to Mr. A. Dhason for glass blowing job and Mrs. K. N. Vasudha for her help with the experiments. I am thankful to all members of RRI workshop for their help and support. A special note of thank Mr. Narayanaswamy for his help with the design of syringe pump and other experimental setups.

I am thankful to every student at RRI for their company, support and encouraging discussions in various academic and nonacademic tropics. I would particularly like to thank my all football team mates for giving me company in last few years and helping me relax through many fun activities. In particular, I would like to thank Jayakumar, Tridib, Rajib, Arnab, Anjan, Prasad, Samim, Shafi, Rengaraj, Rahul, Raj, Chandan, Venu, Santanu, Deepak, Varun and many more for giving me many pleasurable moments. I am thankful to all boarders at RMV hostel for being amazing friends during my stay and doing many fun activities like watching movies, playing carom, celebrating my birthday, holi, diwali etc. My sincere thanks to Arnab, Anjan, Rajib, Rituparno, Raj, Debadrita, Meera and Santanu for their help with cooking on Sundays.

I would like to express my gratitude to SCM group secretary Mr. Radhakrishna for his assistance with vehicle booking, purchasing chemicals and components, travel claim and many more things. My sincere thanks to Raja and Murali for their help in daily basis. I would like to thank all the staff members of the library for their help and

support. I am thankful to all staff members in the purchase and account departments for their help with purchasing laboratory equipments, travel claim and foreign exchange. A special thanks to the purchase officer, Mr. Ramamurthy for his effort to minimize delay regarding purchase. I would like to thank all the staff members of the computer section for their assistance to sort out countless issues regarding software installation and internet connectivity.

I express my gratitude to the director, Prof. Ravi Subrahmanyam for his help regarding various academic issues. I would like to thank the administrative officer, Mr. Krishnamaraju for his assistance with countless administrative issues. I express sincere gratitude to all staff members of administration, especially Mrs. Shailaga, Mrs. Marisa, Mrs. K. Radha and all other staff members of administration for their help and support. I acknowledge all the canteen staff members, hostel staff members, and everyone at RRI for their cooperation and encouragement.

At last, I express my deepest gratitude, love and respect for my parents Mr. Sunil Kumar Saha and Mrs. Ranu Saha, my brother Mr. Pijus Kanti Saha, my sisters Mrs. Manashi Majumder and Mrs. Tapashi Kundu and other family members for their constant support and help in every ups and downs in my life.

Synopsis

Colloidal suspensions like ink, milk, paint and many more are used in our day-to-day life. These fluids show very rich flow properties at length and time scales that are easily accessible in the laboratory. A colloidal suspension exhibits different phases depending on the effective particle volume fraction, temperature and the nature of the interaction potential between the colloidal particles. They can show aging behavior i.e. the relaxation time increases with waiting time and the system evolves spontaneously. In this thesis, we have studied the structure, dynamics and flow behavior of aging colloidal suspensions formed by a synthetic clay, Laponite.

Chapter 1 presents the background knowledge necessary to understand the thesis work. This chapter gives an overview of colloidal systems, different glass formers, the colloidal glass transition, glass transition in supercooled liquids and other glass formers, microscopic relaxation and inter-particle interactions in the context of colloidal suspensions. Next, the phase diagram and aging dynamics of Laponite (a colloidal system and the main material studied in this thesis) is discussed in details. This is followed by a detailed discussions of the flow behaviors of colloidal suspensions and the dynamics of interfaces.

Chapter 2 describes the experimental methods used in this thesis. This chapter contains the detailed descriptions of the dynamic light scattering technique, high speed imaging, rheology and sodium ion concentration measurement. Design of a falling ball

viscometer and a Hele-Shaw cell that have been used in this thesis, are also described.

Chapter 3 presents the different microscopic relaxation processes of soft colloidal suspensions formed by the synthetic clay Laponite in the context of the glass transition. The primary (α -process) and secondary (β -process) relaxation timescales of aging soft colloidal suspensions of Laponite are estimated from intensity autocorrelation functions obtained in dynamic light scattering (DLS) experiments. The dynamical slowing down of these relaxation processes are compared with the observations in fragile supercooled liquids by establishing a one-to-one mapping between the waiting time t_w since filtration of a Laponite suspension and the inverse of the temperature $1/T$ of a supercooled liquid that is rapidly quenched towards its glass transition temperature. New timescales associated with the primary and secondary relaxation processes, such as the characteristic timescale associated with the slowdown of the secondary relaxation process t_β^∞ and the glass transition time t_g , which describe the phenomenon of dynamical arrest in Laponite suspensions, are found. These results are strongly reminiscent of analogous timescales extracted from supercooled liquids approaching their glass transitions. A strong coupling exists between the primary and secondary relaxation processes of aging Laponite suspensions in the cage-forming regime. Furthermore, the experimental data clearly demonstrates the self-similar nature of the aging dynamics of Laponite suspensions within a range of sample concentrations. These observations are very useful to understand the universal behavior of the microscopic relaxation dynamics in the glass transition of two very different glass formers - colloidal glasses and supercooled liquids.

Chapter 4 describes the effects of several physicochemical parameters, such as the particle concentration, the interaction potential between particles and the temperature, on the colloidal glass transition. The microscopic dynamics of clay suspensions is studied using dynamic light scattering for different clay concentrations C_L , the concentrations of externally added salt C_S (and hence the interaction potential) and temperatures T . The α and β -relaxation times of Laponite suspensions are extracted from intensity autocorrelation functions measured at different waiting times since sample

preparation. Scaling of the microscopic timescales of clay suspensions with different clay concentrations, waiting times, salt concentrations and temperatures results in comprehensive overlap curves for both relaxation timescales. These results highlight the self-similar nature of the energy landscape of Laponite suspensions under different physicochemical conditions and the pivotal role of attractive interactions in the microscopic dynamics of spontaneously evolving Laponite suspensions.

In chapter 5, the microscopic relaxation timescales are estimated from the autocorrelation functions obtained by dynamic light scattering experiments for Laponite suspensions with different concentrations (C_L), added salt concentrations (C_S) and temperatures (T). In this chapter, the fragility parameter D , which signifies the deviation from Arrhenius behavior, is obtained from fits to the time evolutions of the structural relaxation timescales. For the Laponite suspensions studied in this work, D is seen to be independent of C_L and C_S , but is weakly dependent on T . Interestingly, the behavior of D corroborates the behavior of fragility in molecular glass formers with respect to equivalent variables. Furthermore, the stretching exponent β , which quantifies the width w of the spectrum of structural relaxation timescales is seen to depend on t_w . A hypothetical Kauzmann time t_k , analogous to the Kauzmann temperature for molecular glasses, is defined as the timescale at which w diverges. Corresponding to the Vogel temperature defined for molecular glasses, a hypothetical Vogel time t_α^∞ is also defined as the time at which the structural relaxation time diverges. Interestingly, a correlation is observed between t_k and t_α^∞ , which is remarkably similar to that known for fragile molecular glass formers. A coupling model that accounts for the t_w -dependence of the stretching exponent is used to analyze and explain the observed correlation between t_k and t_α^∞ .

A universal secondary relaxation process, known as the Johari-Goldstein (JG) β -relaxation process, appears in many glass formers. This relaxation process involves all parts of the molecule and is particularly important in glassy systems because of its very close relationship with the α -relaxation process. However, the absence of J-G β -relaxation mode in colloidal glasses, raises questions regarding its universality.

In chapter 6, we studied the microscopic relaxation processes for Laponite suspensions (a model glass former) by dynamic light scattering (DLS) experiments. The α and β -relaxation timescales are estimated from the autocorrelation functions obtained by DLS measurements for Laponite suspensions with different concentrations C_L , salt concentrations C_S and temperatures T . We measure primitive relaxation timescales from the α -relaxation time and the stretching exponent β by applying the coupling model for highly correlated systems. Our experimental results suggest that the β -relaxation process involves all parts of a Laponite particle and is coupled with the primitive relaxation process. The glass transition time is also correlated to the activation energy of the β -relaxation process for all Laponite concentrations, salt concentration and temperatures. The width of the primary relaxation process is also coupled with the secondary relaxation process. It is seen that both primary and secondary relaxation timescales are sensitive to particle concentration. These observations suggest that the β -relaxation process of colloidal glasses of Laponite carries many characteristics of the J-G β -relaxation processes seen in molecular glass formers.

In chapter 7, the microscopic relaxation processes of aging Laponite suspensions with embedded polystyrene beads, used as probe particles, are studied by dynamic light scattering (DLS) experiments. The polystyrene beads, being larger in size than the Laponite particles, behave as the less mobile regions in the suspension. Intensity autocorrelation functions measured in DLS experiments show the existence of two-step relaxation processes in these suspensions. The fast relaxation process is identified as due to the diffusion of a Laponite particle inside the cage formed by its neighbors, while the slow relaxation process is interpreted to originate due to structural relaxation events in the presence of the externally added less mobile polystyrene beads. The fragility parameter D , which quantifies the rapidity of approach towards eventual kinetic arrest, is calculated from the evolution of the structural relaxation time for different concentrations and sizes of the polystyrene beads. D is seen to increase with the concentration of polystyrene particles, but decreases as the size of the particles increases. The observed results are compared with simulation results on random pinning

in binary mixtures.

In the next two chapters, we report experimental observations of the flow behaviors of aging Laponite suspensions which show non-Newtonian rheology. Two important classes of problem are addressed which involve the motion of an object in a viscous medium and flow behaviors in porous media during enhanced oil recovery. It is seen that the falling of an object through a non-Newtonian aging suspensions leads to very interesting manifestations of Stokesian flows without any terminal velocity. In chapter 8, we report falling ball experiments on aging colloidal suspensions of Laponite. Steel balls of different sizes are dropped into the suspensions having different initial states of structure. An increase of velocity of the ball as it gets deeper into the fluid is observed. This increment is more pronounced for larger balls and for lower aging or waiting times of the suspensions. A simple rheological model is constructed based on the concepts of structural kinetics in thixotropic fluids to explain the experimental results by taking into account (i) the restructuring and destructuring processes and (ii) the dependence of the viscosity of the suspensions on structure parameter and shear rate.

Dynamics at interfaces is a vast and interesting field of research involving different kinds of instabilities (for example, Saffman-Taylor instability), fractal structure formation, viscous fingering, viscoelastic fracturing, wetting properties and many more. This kind of problem has immense significance in the context of enhanced oil recovery and in the flow in porous media. In many of these cases, interfacial properties play a major role in determining the flow behavior of complex fluids and soft solids. In chapter 9, the dynamics at the interface between different kinds of fluids (Newtonian fluids, aging non-Newtonian fluids formed by anisotropic charged clay suspensions) is studied in a confined geometry, also known as a Hele-Shaw cell. It is reported that the emergence of fractal patterns is determined by many factors, for example, the type of Newtonian fluid (miscible and immiscible fluids), the rate of injection of the second fluid, the surface tension etc. Colloidal suspensions formed by anisotropic charged clay (Laponite) transform from a liquid-like phase to a soft solid phase with time. Hence,

different kinds of interfacial phenomena are seen when an aging colloidal suspension is displaced by a miscible Newtonian fluid. For example, viscous fingering is observed by us when clay is in a liquid-like phase due to Saffman-Taylor instability, with the pattern transforming to a viscoelastic fracturing pattern later in the case of miscible flow. Suppression of the tip-splitting and side-branching with increasing elasticity are also observed. The changes observed in the fractal patterns due to the development of elasticity in the first phase (Laponite suspension) are described in this chapter.

Chapter 10 summarizes the main results reported in this thesis and discusses the scope for future work.

Dr. Ranjini Bandyopadhyay
(Thesis Supervisor)
Soft Condensed Matter Group
Raman Research Institute
Bangalore 560 080
India

Debasish Saha

Publication List

Publications from this thesis:

1. Investigation of the dynamical slowing down process in soft glassy colloidal suspensions: comparisons with supercooled liquids
Debasish Saha, Yogesh M. Joshi and Ranjini Bandyopadhyay.
Soft Matter, 2014, 10, 3292-3300, DOI: 10.1039/C4SM00187G
2. Dynamic light scattering study and DLVO analysis of physicochemical interactions in colloidal suspensions of charged disks
Debasish Saha, Ranjini Bandyopadhyay and Yogesh M. Joshi.
Langmuir, 2015, 31 (10), 30123020, DOI: 10.1021/acs.langmuir.5b00291
3. Kinetics of the glass transition of fragile soft colloidal suspensions
Debasish Saha, Yogesh M. Joshi and Ranjini Bandyopadhyay.
(To be submitted)
4. Fragile behavior of soft glassy colloidal suspensions in the presence of probe particles
Debasish Saha, Yogesh M. Joshi and Ranjini Bandyopadhyay.
(Manuscript under preparation)

Contents

Acknowledgements	v
Synopsis	viii
Publication List	xiv
1 Introduction	5
1.1 Colloidal suspensions	5
1.2 Glass transition	6
1.2.1 Colloidal glass transition	7
1.2.2 Glass transition in supercooled liquids and other glass formers	8
1.3 Interparticle interactions in colloids	13
1.3.1 van der Waals forces	14
1.3.2 Electrostatic repulsion	14
1.4 Different phases formed by Laponite nanoclay colloidal suspensions .	16
1.5 Flow behavior of colloidal dispersions	19
1.6 Thesis organization	21

References	22
2 Experimental Techniques	27
2.1 Introduction:	27
2.2 Experimental techniques:	28
2.2.1 Dynamic Light Scattering:	28
2.2.2 Ion Measurements:	35
2.2.3 Rheology and Rheometry:	38
2.2.4 High Speed Imaging:	41
2.2.5 Falling Ball Viscometer:	42
2.2.6 Hele-Shaw Cell:	46
References	48
3 The dynamical slowing down process in soft glassy colloidal suspen- sions: comparisons with supercooled liquids	51
3.1 Introduction	51
3.2 Sample preparation	55
3.3 Results and Discussions	55
3.4 Conclusions	69
References	72
4 Effects of physicochemical interactions on the aging dynamics of col- loidal suspensions of Laponite	77
4.1 Introduction	77
4.2 Sample preparation and experimental methods	79
4.3 Results and discussions	80
4.4 Conclusions	97

References	99
5 Kinetics of the glass transition of fragile soft colloidal suspensions	103
5.1 Introduction	103
5.2 Sample preparation and experimental methods	106
5.3 Results and discussions	106
5.4 Conclusions	116
References	118
6 Characteristics of the secondary relaxation process in soft glassy colloidal suspensions	121
6.1 Introduction	121
6.2 Sample preparation and experimental methods	124
6.3 Results and discussions	124
6.4 Conclusions	132
References	133
7 Fragile behavior of a soft glassy colloidal suspension in the presence of probe particles	135
7.1 Introduction	135
7.2 Sample preparation and experimental methods	138
7.3 Results and discussions	139
7.4 Conclusions	146
References	148
8 Falling ball experiments on aging colloidal suspensions	151
8.1 Introduction	151

8.2	Sample preparation and experimental methods	153
8.3	Results and discussions	154
8.4	Conclusions	163
References		164
9	Instabilities at the interface between a Newtonian fluid and an aging non-Newtonian fluid in quasi-2D geometry	167
9.1	Introduction	167
9.2	Sample preparation and experimental methods	170
9.3	Results and discussions	170
9.3.1	Pattern formation when an aging Laponite suspension is displaced by CCl_4	170
9.3.2	Pattern formation when an aging Laponite suspensions is displaced by water	174
9.4	Conclusions	177
References		180
10	Summary and future directions	183

1

Introduction

1.1 Colloidal suspensions

The word “colloid” was coined from a Greek word- “κωλλα” by Graham Thomas, meaning “glue” [1, 2] in the 19th century. A large variety of multiphasic substances, for example, suspensions, emulsions, foams, aerosol etc. are described by the word *colloid*. All these multiphasic substances are composed by particles in solid, liquid or gaseous state dispersed in a continuous phase. These systems have sizes ranging from 10 nm-10 μm [3].

A colloidal suspension, in general, is constituted by small solid particles (dispersed phase) dispersed in a liquid phase (dispersion medium). The size of the solid particle is small enough that it is affected by the thermal fluctuations in the system. A colloidal particle in a suspension is subjected to random collisions by the solvent molecules. As a result, it moves in a very random fashion and shows Brownian motion at laboratory time scales. Colloidal systems can be categorized depending on the states of the dispersion media and the dispersed phases. Various colloidal systems and typical examples [3, 4] are described in table 1.1 given below:

Colloidal systems	Dispersion medium	Dispersed phase	Examples
Foams	Liquids or solids	Gas bubbles	Shaving foam, soap bubble.
Aerosols	Gases	Solid particles or liquid droplets	Smoke, fog.
Emulsions	Liquids	Liquid droplets	Hand lotion, mayonnaise.
Suspensions	Liquid	Solid particles	Blood, paint, dispersions of clay minerals.

Table 1.1: Examples of colloidal systems.

The experimental results reported in this thesis are carried out with aqueous colloidal dispersions or suspensions formed by a synthetic clay Laponite. The main focus of this thesis is on the study of the dynamics and flow behaviors of the glasses and gels formed by Laponite suspensions. In the following sections and subsections, the basic features of the glass transition are discussed in the context of colloids and other materials. The flow behaviors of colloidal suspensions are also discussed briefly.

1.2 Glass transition

The viscosity of most liquids depend on their temperatures. In general, above the melting point, viscosity increases with decrease in temperature. Depending on the cooling conditions, two situations can arise at the melting point. Crystalline order can be achieved by many liquids if they are cooled slowly enough that liquid molecules have time to rearrange themselves. However, if a liquid is cooled down rapidly below its melting point to avoid crystallization, the molecules retain a liquid-like structure but their dynamics become extremely slow. This results in a huge increase in viscosity. This phenomena is called the glass transition and the temperature at which the transition happens is called the glass transition temperature, T_g . Typical cooling rates required to attain the glass transition are in the range $0.1-10^3$ K/sec and are highly material dependent. Below T_g , a material is in a highly disordered arrested state as it does

not have any crystalline order. Depending on the timescale, it might show solid-like or liquid-like behavior. For example, pitch or bituminous tar appear to be solid in normal condition. However, it is well-known that even pitch can flow like a liquid if we wait long enough (≈ 10 years) [5].

1.2.1 Colloidal glass transition

Like most liquids, a colloidal suspension can also achieve the glass transition. There is a large difference in the nature of the glass transition between a colloidal suspension and a liquid. The viscosity of a colloidal dispersion is dependent on the volume fraction ϕ of the colloidal particles in the suspension. For a very dilute suspension, i.e. $\phi < 10^{-5}$, the viscosity is independent of ϕ and almost equal to the viscosity of the dispersing medium. As the number of colloidal particles in a suspension increases, the viscosity of the suspension is no longer the same as that of the pure solvent. Hard sphere colloids, where interparticle interactions are present only when the particles come in contact or try to interpenetrate [6], form a liquid-like suspension below $\phi=0.494$ [7]. The volume fraction $\phi_{freeze}=0.494$ is analogous to the freezing point of a liquid. If the volume fraction ϕ is increased rapidly beyond ϕ_{freeze} , a disordered state can be achieved, with the dynamics of the colloidal particles in the suspension ceasing to exist for $\phi > 0.58$. This volume fraction $\phi_g=0.58$ is the colloidal glass transition volume fraction. Beyond this volume fraction, a colloidal suspension constituted by monodisperse colloidal particles is more likely to form a crystal and at $\phi_{rcp}=0.64$, it will achieve a random close packed structure. However, a small amount of polydispersity will allow it to be in a glassy state between $0.58 \leq \phi \leq 0.64$. In an important contribution, Marshall and Zukoski showed that the viscosity of colloidal silica depends on ϕ and it obeys the Doolittle equation given below [8]:

$$\frac{\eta}{\eta_c} = C \exp\left(\frac{AN_T v_f^*}{v_f}\right) \quad (1.1)$$

In the above expression, N_T is the number of particles in the suspension. v_f and v_f^* are the free volumes available and required for the diffusion process respectively. A is a constant. Equation 1.1 can be written in terms of ϕ as [8]:

$$\frac{\eta}{\eta_c} = C \exp\left(\frac{A\phi}{\phi_m - \phi}\right) \quad (1.2)$$

Here, $\phi_m=0.638$ and A is a constant close to unity.

Interestingly, the primary relaxation time, or the α -relaxation time τ_α , also obeys the above functional form and is given by:

$$\tau_\alpha = \tau_0 \exp\left[\frac{D\phi}{\phi_0 - \phi}\right] \quad (1.3)$$

In the above expression, $\phi_0=0.638$ and D , a dimensionless number, is called the fragility index [3].

1.2.2 Glass transition in supercooled liquids and other glass formers

A supercooled liquid is one that is quenched rapidly below its freezing point to avoid crystallization. Supercooled liquids and their glass transitions show many interesting features such as the rapid increase of viscosity near T_g , heat-capacity jump at T_g , Kauzmann entropy catastrophe, non-exponential relaxation processes and fragile behavior [9–11]. In the next few paragraphs, these features are discussed briefly.

Above the vaporization point T_v , a liquid behaves like a gas, that is, in this regime, the main transport process is collisional [10]. Molecules of a gas feel the existence of the other molecules only when they collide. As a result, a gas has negligible potential energy compared to its kinetic energy. If it is cooled down below T_v , the transport will still be collisional. It will behave like a very dense gas below T_v and intermolecular forces will have an important contribution to its behavior. In a liquid, molecules are held together by attractive van der Waals forces. In this state, the potential energy of the liquid molecule exceeds its kinetic energy. However, the nearest neighbors of

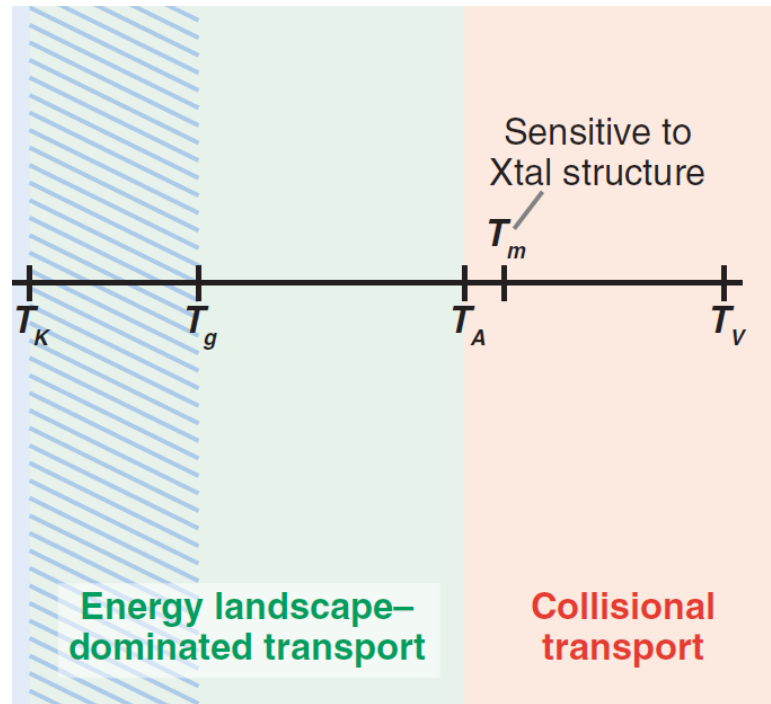


FIGURE 1.1: Regimes of the molecular phases between a dilute gas and a frozen glass. Here, T_v is the vaporization temperature, T_m the melting point. T_A is the temperature at which collisional transport ceases and the onset of activated motion is seen. T_A is usually, but not always, below T_m and transport below T_A is dominated by the underlying energy landscape below this temperature. Below the glass transition temperature T_g , the system achieves a non-equilibrium state. T_K is the Kauzmann temperature. This figure is adapted from [10].

a molecule are not fixed as two molecules do not spend much time near each other. Here, the molecular permutation timescale of a molecule is comparable to its collisional timescale. However, if the liquid is cooled below its melting point T_m at a rate greater than the rate of nucleation, crystalline order can be avoided. In this situation, a molecule can retain its nearest neighbors for a very long time and transport is no longer dominated by collisions [10]. At some temperature T_A (figure 1.1), transport properties like viscosity, diffusion etc., are dominated by activated processes. If the system is cooled further below a temperature T_g , the timescale of molecular permutations, or the α -relaxation timescale, becomes larger than the laboratory timescale. This temperature is called the glass transition temperature (T_g). In general, T_g depends on the observation timescale. In the supercooled liquids literature, T_g is the temperature at which the α -relaxation time (τ_α) is 100 sec [12]. Viscosity (η) and the α -relaxation

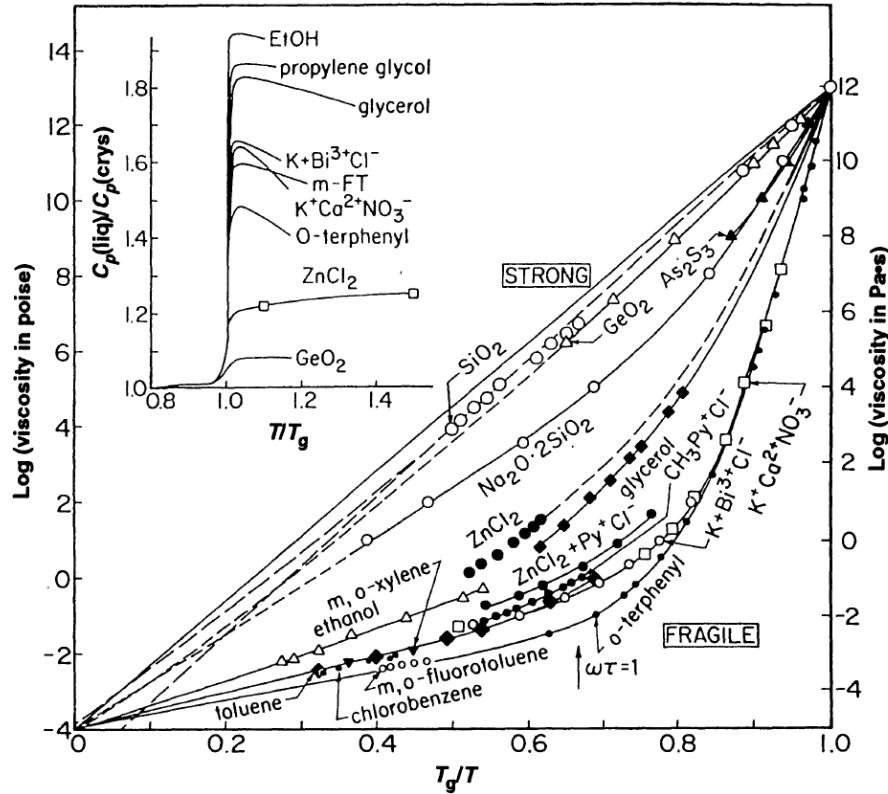


FIGURE 1.2: Angell plots of the viscosity data as functions of the inverse temperature scaled by their respective glass transition temperatures T_g/T . Straight lines in the Angell plot shows the Arrhenius dependence of viscosity on temperature seen in strong glass formers (SiO₂, GeO₂ etc.). Non-Arrhenius behaviors of viscosity is seen for fragile glass formers (o-terphenyl, toluene etc.) and represented by the deviation from the straight line. In the inset, specific heat C_p is plotted vs. T_g/T . C_p shows a jump at T_g . This figure is adapted from [9].

timescale (τ_α) increase by many decades near T_g (figure 1.2). By convention, a glassy state is achieved when $\eta \approx 10^{12}$ Pa.s and flow ceases to exist at observation timescales achievable in the laboratory. This rapid increase in viscosity near T_g is a very common feature of the glass transition in supercooled liquids. In some glass formers, the viscosity shows an Arrhenius dependence on temperature (figure 1.2) with an activation energy that is independent of temperature. Interestingly, in some other glass formers, the increase in viscosity with the inverse of temperature deviates from Arrhenius behavior and the degree of deviation is commonly defined as the fragility of the glass former. In fragile supercooled liquids, viscosity η and the structural relaxation time or the α -relaxation time τ_α each obey a Vogel-Fulcher-Tammann (VFT) temperature

dependence that is given by the following two equations:

$$\eta = \eta_0 \exp \left[\frac{DT_0}{T - T_0} \right] \quad (1.4)$$

$$\tau_\alpha = \tau_0 \exp \left[\frac{DT_0}{T - T_0} \right] \quad (1.5)$$

Here, D is known as the fragility or strength index and solely depends on the material. T_0 is called the Vogel temperature and signifies the temperature at which τ_α diverges. For “strong” glass formers (i.e. SiO_2 , GeO_2), $D \rightarrow \infty$ and the rate of change of viscosity in the whole temperature range remains the same (figure 1.2). However, for “fragile” glass formers like o-terphenyl mixtures, chlorobenzene etc., the changes in η and τ_α are very rapid near T_g and another measure for the fragility (m) or the deviation from Arrhenius behavior exists. m quantifies how rapidly η and τ_α increase as the glass transition temperature is approached and is defined as follows:

$$m = \left(\frac{\partial \log \eta}{\partial (T_g/T)} \right)_{T=T_g} \quad (1.6)$$

or,

$$m = \left(\frac{\partial \log \tau_\alpha}{\partial (T_g/T)} \right)_{T=T_g} \quad (1.7)$$

The origin of fragility is still not well understood despite many theoretical and experimental studies. A correlation is drawn between fragility of a material and its physical properties i.e. Poissons ratio or the relative strength of its shear and bulk moduli [13]. The relation between the nature of the interaction potential and fragility has also been studied for model binary mixture glass formers [14] and colloidal glass formers [15].

It has already been mentioned that collisional transport takes a back seat and energy landscape driven transport dominates below T_A (figure 1.1). The energy landscape can be visualized in terms of a multidimensional potential energy surface as a function of the particle coordinates [16]. For a dense liquid, the material properties are related to the interactions between the constituent particles. The constituent particles

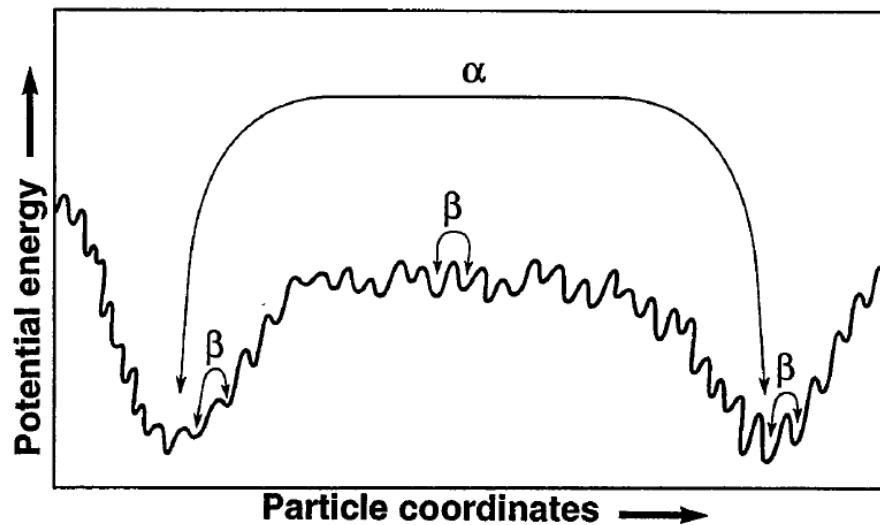


FIGURE 1.3: Potential energy landscape explored by fragile glass formers near T_g . The elementary interbasin transitions are associated with the β -relaxation process, and the large distance intercrater transitions are associated with the α -relaxation process. This figure is adapted from [17].

could be atoms, molecules, ions or a group of atoms. There exists a potential energy function $\phi(\mathbf{r}_1, \mathbf{r}_2, \dots, \mathbf{r}_N)$ for each of these particles that depends on interparticle interactions and also on their spatial positions \mathbf{r}_i [17]. For a supercooled liquid state, where each molecule is interacting with numerous molecules, the full N -body ϕ -function is needed to describe the system [16]. Therefore, the potential energy landscape (PEL) is a $3N+1$ dimensional hyperspace and is characterized by several extrema (maxima and minima), with the temporally evolving system being represented by a point in this hyperspace [16–18]. This description makes it easier to discuss the relaxation processes of glass forming liquids. In this multidimensional hyperspace, the relaxations between neighboring basins (or minima) is identified with the β -relaxation processes (figure 1.3), whereas the α -relaxation processes are represented in terms of an escape from one deep basin within a "metabasin" to another neighboring basin [17, 18].

The above description of the potential energy landscape is particularly useful for

the calculation of the configurational entropy (S_c) of a supercooled liquid [19]. According to the Adam-Gibbs relation, the configurational entropy is related to the viscosity of the liquid and is given by [12, 20]:

$$\eta = \eta_0 \exp \left[\frac{A}{TS_c} \right] \quad (1.8)$$

Here, the VFT form (equation 1.4) can be obtained if S_c is written in the following way [11, 19]:

$$TS_c = K_{AG} \left(\frac{T}{T_K} - 1 \right) \quad (1.9)$$

Here, T_K is the Kauzmann temperature or the ideal glass transition temperature, while K_{AG} is the kinetic fragility. Below T_K , $S_c = 0$.

1.3 Interparticle interactions in colloids

In general, the structure and dynamics of a colloidal suspension is extremely sensitive to its inter-particle (or pair) potential [4]. For a hard sphere colloidal suspension, the interaction potential between two particles has the simplest form. The only constraint on motion in this case is that the particles cannot penetrate each other. The interparticle interaction potential for hard sphere colloids is given by $V(r) = 0$ when $r \geq \sigma$, where σ is sum of the radii of the two interacting particles. In addition, $V(r) = \infty$ for $r < \sigma$, which signifies that the particles are impenetrable. A dilute colloidal suspension of hard spheres has no potential energy and the dynamics is solely governed by the volume fraction ϕ of the particles. However, most colloidal suspensions do not show hard sphere interaction. In general, colloidal suspensions are formed by charged particles and the interparticle interaction can be expressed as the sum of two interactions - the attractive van der Waals interaction and the screened electrostatic repulsion.

1.3.1 van der Waals forces

The van der Waals force is attractive in nature. For a molecular system having permanent dipoles, an attractive force exists between two molecules because of the dipole-dipole interaction. However, a neutral atom or molecule can be considered as a rapidly fluctuating dipole due to the rapid motion of the electrons around its nucleus and a London dispersion interaction arises as the dipoles start to couple with each other to minimize the interaction energy [21]. For colloidal particles where each particle consists of a large numbers of molecules, the London dispersion interaction manifests as the attractive van der Waals force between particles. Normally, the interaction between colloidal particles is calculated by summing over all the pairwise interactions between an atom in one particle with all the atoms in the other particle. Finally, this pairwise summation is done for all the atoms in the first particle and added together to get the total van der Waals interaction. This method of calculation was first prescribed by Hamaker in 1937 [21, 22].

For a 2:1 layer clay (i.e. Laponite in figure 1.4, the main material investigated in this thesis) the free energy per unit area due to van der Waals attraction is given by [1]:

$$W_{vdW} = -\frac{A_H}{48\pi} \left[\frac{1}{d^2} + \frac{1}{(d + \Delta)^2} - \frac{2}{(d + \Delta/2)^2} \right] \quad (1.10)$$

where d is the half-distance between two plates. Here, d is measured between the planes of the tetrahedral sheet and the centers of the oxygen atoms. A_H is the Hamaker constant (1.06×10^{-20} J) and Δ is the thickness of unit layers between the same planes (6.6 Å) [1].

1.3.2 Electrostatic repulsion

When a charged colloidal particles is added to an electrolyte solution, the counterions from the solution are attracted towards the electric charges of the particle. These counterions are always in thermal motion and diffuse around the particle. This arrangement of counterions and the opposite charges on the particle is called an electric double

layer [21]. Electrostatic repulsion arises due to overlap of the diffuse charges in the electrical double layers of two colloidal particles. This is known as electric double layer repulsion. The influence of the interaction due to double layer repulsion is experienced over a distance given by the Debye screening length ($1/\kappa$). Here, the Debye screening length, which measures the range of the electric potential that extends from the surface of a charged colloidal particle, depends on the electrolyte concentration in the suspension. It is given by the following expression [23]:

$$\frac{1}{\kappa} = \left(\frac{\epsilon_0 \epsilon_r k_B T}{\sum_i (z_i e)^2 n_i} \right)^{1/2} \quad (1.11)$$

Here, ϵ_0 is the permittivity of free space, ϵ_r is the relative permittivity of the medium, k_B is the Boltzmann constant, T is the temperature of the suspension, e is the charge of an electron and z_i is the ionic charge number of the i th species of ions of concentration n_i .

It is, however, very difficult to measure the exact potential at the surface of the colloidal particle. Stern prescribed that there is an effect of the finite size of the counterions near the particle surface and can be accounted for by considering the presence of a Stern layer, the distance of closest approach of the counterions [1, 24]. However, there exists a potential called zeta potential which is experimentally measurable. Zeta potential is the potential at the slipping plane which occurs between the moving envelop of water attached to the particle and the bulk [1, 4, 21]. As a good approximation, the zeta potential can be considered as the potential at the Stern layer.

The free energy per unit area due to double layer repulsion for a 2:1 layer clay can be written as a function of half-distance d [1]:

$$W_{DL} = \left(\frac{64nk_B T}{\kappa} \right) \gamma^2 e^{-2\kappa d} \quad (1.12)$$

where n is the number density and $\gamma = \tanh(z e \Phi_0 / 4 k_B T)$, where z is the valence of the counterions and Φ_0 is the surface electric potential.

1.4 Different phases formed by Laponite nanoclay colloidal suspensions

Hydrous sodium lithium magnesium silicate ($\text{Na}_{+0.7}[(\text{Si}_8\text{Mg}_{5.5}\text{Li}_{0.3})\text{O}_{20}(\text{OH})_4]_{-0.7}$) or Laponite belongs to a family of hectorite clay comprising 2:1 phyllosilicate. Each Laponite particle has a disk-like shape with diameter in the range 25 ± 2.5 nm and a thickness of approximately 1 nm [25]. It consists of an octahedral layer of magnesia sandwiched by two tetrahedral layers of silica (figure 1.4) [1]. The deficiency of positive charges within the particle is compensated by sodium atoms that, in the dry state, reside in the inter-layer gallery. When dispersed in aqueous media, the sodium ions dissociate such that the two faces of the Laponite particle acquire negative charges. The edge of the particle, on the other hand, is composed of anhydrous oxides dominated by MgOH groups [26], whose charge in the aqueous medium depends on the medium pH. Incorporation of Laponite powder in ultra-pure water raises its pH, due to the dissociation of OH^- ions from the edges, and leads to the edges acquiring positive charges [26, 27]. At a pH of 10, the edge of the Laponite platelet is estimated to have a weak positive charge [26]. Owing to dissimilar charges on their edges and faces, the particles can interact *via* attractive as well as repulsive interactions, thereby strongly influencing the sample microstructure [28–30]. It is observed that in an aqueous medium, Laponite particles interact *via* face-to-face long range repulsions and edge-to-face short range attractions [31]. Addition of monovalent salts such as NaCl in aqueous suspensions of Laponite increases the concentrations of cations and anions that shield the charges on the particles and effectively reduces the interparticle repulsive interactions.

Typically, for Laponite suspensions with concentrations above 2 wt%, the viscosity and the elastic modulus increase gradually as a function of time since preparation. This suggests a continuous build-up of structure in a process that is referred to as physical aging [32–34]. In dynamic light scattering experiments, physical aging is manifested by an enhancement in the suspension's relaxation time with increase in

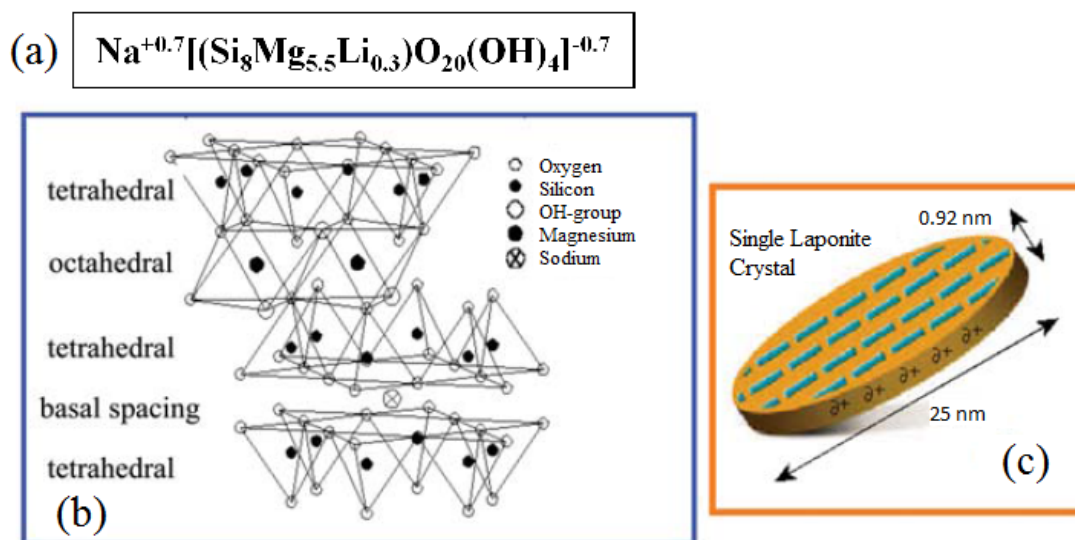


FIGURE 1.4: (a) Chemical formula for Laponite. (b) Structure of a unit cell of Laponite. (c) A single Laponite platelet. This figure is adapted from [28].

waiting time [35–37]. However, the application of a deformation field reverses the process of aging, with the viscosity, elastic modulus and relaxation time decreasing due to the breakdown of the sample microstructure [33, 38]. This process is known as rejuvenation in the colloidal glass literature and as shear melting in the traditional rheology literature [39, 40].

In the last decade, the phase behavior of aqueous suspensions of Laponite has been studied in great detail using different experimental techniques, such as static and dynamic light scattering [37, 41–48], small angle X-ray scattering [49], microscopy [50], and rheology [51–55]. Ruzicka *et. al.* summarized all the results obtained by both experimental and numerical studies in a recent review [28] and presented a fresh phase diagram of Laponite suspensions for large waiting times (figure 1.5). There is a general consensus that for concentrations below approximately 2 wt%, the microstructure is dominated by edge-to-face attractive interactions, leading to an attractive gel [28, 56]. For higher concentrations, there is a debate on whether the particles are in mutual contact due to attractive interactions or remain self-suspended in the repulsive environments of the surrounding particles, thereby forming a repulsive glass

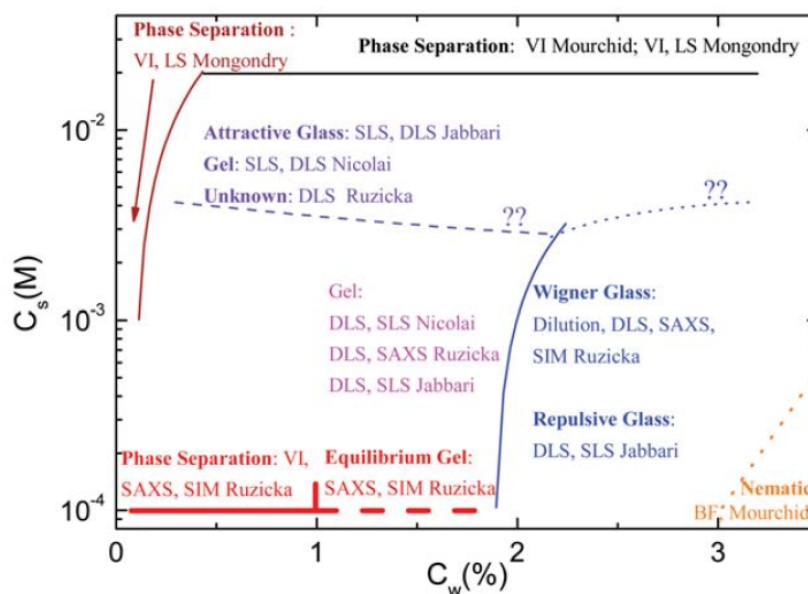


FIGURE 1.5: Phase diagram of Laponite suspensions for a large waiting time. VI, LS, SIM, SAXS, DLS and SLS refer to visual inspection, light scattering, numerical simulations, small angle X-ray scattering, dynamic light scattering and static light scattering respectively. This figure is adapted from [28].

[53, 56]. Remarkably, for $\phi > 0.004$, aqueous suspensions of Laponite undergo ergodicity breaking over a duration of days, with the free-flowing liquid getting transformed into a soft solid phase that can support its own weight. Ruzicka and co-workers studied aqueous suspensions of Laponite using small angle X-ray scattering (SAXS) and estimated that the average interparticle distance, which was around 15 nm for concentrations less than 2 wt%, increased to 40 nm at high concentrations [49]. This work, therefore, indicates the presence of an attractive gel-like morphology at low concentrations and a repulsive glass-like microstructure at high concentrations. Dissolution experiments carried out by the same group [57] showed that Laponite suspensions that were older than 7 days do not dissolve in an aqueous medium, thereby suggesting that the influence of attractive interactions on the microstructures of old samples cannot be ignored.

Ruzicka *et al.* report the existence of two different concentration-dependent

routes by which Laponite clay suspensions approach the arrested state [58, 59]. They claim that at high clay concentrations, the system forms a repulsive Wigner glass whose elementary units are single Laponite platelets, while at low clay concentrations ($1.0 \text{ wt}\% < C_w < 2.0 \text{ wt}\%$), clusters of Laponite platelets form an attractive gel. Interestingly, recent work on this subject suggests that the influence of attractive interactions cannot be ruled out even at high Laponite concentrations [53, 57]. Laponite suspensions also show very interesting phase behavior as the salt concentration is varied [60, 61]. A gel or a glass state, and a nematic gel state are observed at low salt concentrations as the clay concentration is increased. At very high ionic strengths, there is phase separation [62]. Recent experimental observations and simulations in the gel state show that for very high waiting times, suspensions at weight concentrations $C_w \leq 1.0 \text{ wt}\%$ phase separate in the absence of salt into clay-rich and clay-poor phases, while suspensions at concentrations $1.0 \text{ wt}\% < C_w < 2.0 \text{ wt}\%$ do not phase separate, giving rise to a true equilibrium gel obtained from an empty liquid [63].

1.5 Flow behavior of colloidal dispersions

In general, a liquid has negligible resistance to shear deformation compared to a solid. As a result, it starts to flow under the application of a shearing stress. For a Newtonian fluid of low viscosity like water, the mechanical properties can be described by its shear viscosity η , which depends on temperature and pressure. However, there is a large class of fluids, called complex fluids, that show deviations from simple Newtonian flow behavior. These complex fluids are intermediate between solids and liquids. For short times, they can maintain their shapes and show solid-like behavior. However, at long times, they eventually start to flow and show liquid-like behavior. This kind of intermediate flow behavior is known as viscoelasticity [64]. Typical examples of complex fluids are polymer melts, glass forming liquids and dense colloidal dispersions.

In dense colloidal suspensions, the average interparticle separation is less than the particle radius. The rheological properties of these suspensions show non-Newtonian

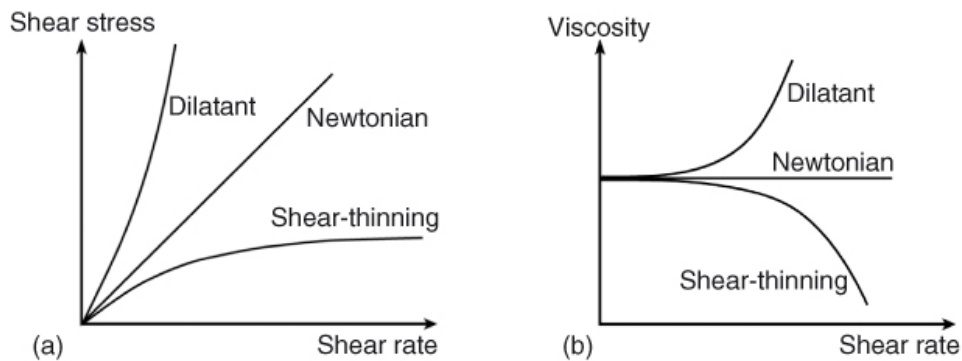


FIGURE 1.6: (a) Typical plots of shear stress vs. shear rate for Newtonian, shear thinning and shear thickening (dilatant) fluids. (b) Viscosity vs. shear rate for Newtonian, shear thinning and shear thickening fluids (dilatant). This figure is adapted from [66].

behavior. Multiple-body interactions and two-body lubrication effect are significant in dense colloidal suspensions [65]. Many colloidal suspensions, for example paint and clay suspensions, show thixotropy or aging, i.e. their viscosities are dependent on the deformation history and therefore change with time. In dense colloidal suspensions, the viscosity also depends on the rate of shear deformation (figure 1.6). Shear thinning or the decrease in viscosity with shear rate is observed in blood, polymer melts and in Laponite clay suspensions. Shear-thickening, or the increase in viscosity with shear rate, is not uncommon in dense colloidal suspensions (example, in cornstarch suspensions [67]). A considerable deviation from Stokes drag force is observed when a spherical object settles under gravity through a thixotropic colloidal suspension formed by Laponite [68]. Pattern formation or fingering instabilities are seen at the interface between two fluids when a more viscous fluid is replaced by a less viscous fluid in a porous medium or in a quasi-2D Hele Shaw geometry in many contexts [69, 70]. A transition from viscoelastic fingering to viscoelastic fracturing has been observed with increase in clay concentration when a clay suspension is displaced by water in Hele-Shaw cell [71, 72]. Colloidal suspensions of Laponite show aging behavior, i.e. their mechanical properties evolve spontaneously with time, and are characterized by complex viscoelastic properties [73]. The aging and rejuvenation of these materials

have been studied [33]. Details of many such phenomena related to the complex flow behavior of viscoelastic materials can be found in [74].

1.6 Thesis organization

This thesis presents a systematic study of the dynamics and flow behaviors of colloidal suspensions formed by Laponite. Chapter 1 contains a brief description of the glass transitions in colloidal suspensions and supercooled liquids. It also discusses interparticle interactions in colloidal suspensions and the phase behavior of Laponite suspensions. Experimental techniques used in this thesis are described in chapter 2. Chapter 3 describes the experimental measurements of the relaxation processes in aqueous suspensions of Laponite and compares these results with previous studies that investigate the dynamics of supercooled liquids. In chapter 4, more experimental work addressing the issue of the self-similarity of the relaxation processes under various physicochemical conditions and the influence of attractive interactions on the aging dynamics of Laponite suspension is reported. The kinetics of the glass transition process and the fragile behavior of aging colloidal glasses of Laponite under various physicochemical conditions are discussed in chapter 5. The characteristics of the secondary relaxation process exhibited by fragile glasses of Laponite are discussed in chapter 6. In chapter 7, the influence of the inclusion of probe particles on the relaxation dynamics of Laponite suspensions is described. The settling of a spherical object through a thixotropic colloidal suspension of Laponite is reported in chapter 8. Chapter 9 discusses the instabilities that emerge at the interface between non-Newtonian aging Laponite suspensions and Newtonian fluids when the former is displaced by the latter. In chapter 10, a summary of the experimental results is given and the scope of future research is discussed.

References

- [1] H. van Olphen, *An Introduction to Clay Colloid Chemistry*, Wiley: New York, 1977.
- [2] Graham Thomas (1861), *Liquid diffusion applied to analysis*, *Phil. Trans. Royal Soc. (London)*, **151**, 183-224.
- [3] G. L. Hunter and E. R. Weeks, *Rep. Prog. Phys.*, **75**, 066501 (2012).
- [4] T. Cosgrove, *Colloid Science: Principles, Methods and applications*, Wiley-Blackwell, 2010.
- [5] R. Johnston, *Nature News*, “*World’s slowest-moving drop caught on camera at last*”, DOI: 10.1038/nature.2013.13418.
- [6] J. D. Bernal, *Proc. R. Soc. Lond. A*, **280**, 299322 (1964).
- [7] F. Sciortino and P. Tartaglia, *Advances in Physics*, **54:6-7**, 471-524 (2005).
- [8] L. Marshall and C. F. Zukoski, *J. Phys. Chem.*, **94**, 1164-1171 (1990).
- [9] C. A. Angell, *Science*, **267**, 1924 (1995).
- [10] V. Lubchenko and P. G. Wolynes, *Annu. Rev. Phys. Chem.*, **58**, 23566 (2007).
- [11] C. A. Angell, *J. Res. NIST*, **102**, 171-185 (1997).
- [12] C. A. Angell, *J. Non-Cryst. Solids*, **131-133**, 13-31 (1991).

-
- [13] V. N. Novikov and A. P. Sokolov, *Nature*, **431**, 961-963 (2004).
- [14] S. Sengupta, F. Vasconcelos, F. Affouard and Srikanth Sastry, *J. Chem. Phys.*, **135**, 194503 (2011).
- [15] J. Mattsson, H. M. Wyss, A. Fernandez-Nieves, K. Miyazaki, Z. Hu, D. R. Reichman and D. A. Weitz, *Nature*, **462**, 83-86, (2009).
- [16] P. G. Debenedetti and F. H. Stillinger, *Nature (London)*, **410**, 259-267 (2001).
- [17] F. H. Stillinger, *Science*, **267**, 1935-1939 (1995).
- [18] F. H. Stillinger, *Phys. Rev. B*, **41**, 2409 (1990).
- [19] S. Sastry, *Nature*, **409**, 164-167 (2001).
- [20] G. Adam and J. H. Gibbs, *J. Chem. Phys.*, **43**, 139-146 (1965).
- [21] R. J. Hunter, *Foundations of Colloid Science*, Volume 1, Oxford Science Publication.
- [22] H. C. Hamaker, *Physica*, **4**, 1058 (1937).
- [23] J. N. Israelachvili, *Intermolecular and Surface Forces*, Academic Press: New York, 2010.
- [24] O. Stern, *Z. Elektrochem.*, **30**, 508-516 (1924).
- [25] M. Kroon, G. H. Wegdam and R. Sprik, *Phys. Rev. E*, **54**, 6541-6550 (1996).
- [26] S. L. Tawari, D. L. Koch and C. Cohen, *J. Colloid Interface Sci.*, **240**, 54-66 (2001).
- [27] S. Jatav and Y. M. Joshi, *Applied Clay Science*, **97-98**, 72-77 (2014).
- [28] B. Ruzicka and E. Zaccarelli, *Soft Matter*, **7**, 1268-1286 (2011).
- [29] M. Delhomme, B. Jönsson and C. Labbez, *Soft Matter*, **8**, 9691-9704 (2012).

-
- [30] M. Delhomme, B. Jönsson and C. Labbez, *RSC Adv.* (2014), DOI: 10.1039/C4RA05555A.
- [31] H. Tanaka, S. Jabbari-Farouji, J. Meunier and D. Bonn, *Phys. Rev. E*, **71**, 021402 (2005).
- [32] S. Cocard, J. F. Tassin and T. Nicolai, *J. Rheol.*, **44**, 585-594 (2000).
- [33] Y. M. Joshi, G. R. K. Reddy, A. L. Kulkarni, N. Kumar and R. P. Chhabra, *Proc. Roy. Soc. A*, **464**, 469-489 (2008).
- [34] R. Bandyopadhyay, P. H. Mohan and Y. M. Joshi, *Soft Matter*, **6**, 1462-1468 (2010).
- [35] B. Abou, D. Bonn and J. Meunier, *Phys. Rev. E*, **64**, 021510 (2001).
- [36] R. Bandyopadhyay, D. Liang, H. Yardimci, D. A. Sessoms, M. A. Borthwick, S. G. J. Mochrie, J. L. Harden and R. L. Leheny, *Phys. Rev. Lett.*, **93**, 228302 (2004).
- [37] F. Schosseler, S. Kaloun, M. Skouri and J. P. Munch, *Phys. Rev. E*, **73**, 021401 (2006).
- [38] D. Bonn, S. Tanase, B. Abou, H. Tanaka and J. Meunier, *Phys. Rev. Lett.*, **89**, 015701 (2002).
- [39] G. B. McKenna, T. Narita and F. Lequeux, *Journal of Rheology*, **53**, 489-516 (2009).
- [40] Y. M. Joshi, *Annu. Rev. Chem. Biomol. Eng.*, **5**, 181-202 (2014).
- [41] D. Saha, Y. M. Joshi and R. Bandyopadhyay, *Soft Matter*, **10**, 3292-3300 (2014).
- [42] T. Nicolai and S. Cocard, *Langmuir*, **16**, 8189-8193 (2000).
- [43] D. Bonn, H. Kellay, H. Tanaka, G. Wegdam and J. Meunier, *Langmuir*, **15**, 7534-7536 (1999).

-
- [44] B. Ruzicka, L. Zulian and G. Ruocco, *Langmuir*, **22**, 1106-1111 (2006).
- [45] H. Z. Cummins, *J. Non-Cryst. Solids*, **353**, 3891-3905 (2007).
- [46] S. Jabbari-Farouji, H. Tanaka, G. H. Wegdam and D. Bonn, *Phys. Rev. E*, **78**, 061405-061410 (2008).
- [47] R. Angelini, L. Zulian, A. Fluerasu, A. Madsen, G. Ruocco and B. Ruzicka, *Soft Matter*, **9**, 10955-10959 (2013).
- [48] D. R. Strachan, G. C. Kalur and S. R. Raghavan, *Phys. Rev. E*, **73**, 041509 (2006).
- [49] B. Ruzicka, L. Zulian, R. Angelini, M. Sztucki, A. Moussaïd and G. Ruocco, *Phys. Rev. E*, **77**, 020402-020404 (2008).
- [50] A. Mourchid, A. Delville, J. Lambard, E. Lecolier and P. Levitz, *Langmuir*, **11**, 1942-1950 (1995).
- [51] A. Shahin and Y. M. Joshi, *Langmuir*, **26**, 4219-4225 (2010).
- [52] J. P. Rich, G. H. McKinley and P. S. Doyle, *Journal of Rheology*, **55**, 273-299 (2011).
- [53] A. Shahin and Y. M. Joshi, *Langmuir*, **28**, 15674-15686 (2012).
- [54] A. S. Negi and C. Osuji, *Phys. Rev. E*, **82**, 031404 (2010).
- [55] A. S. Negi and C. Osuji, *Europhys. Lett.*, **90**, 28003 (2010).
- [56] P. Mongondry, J. F. Tassin and T. Nicolai, *J. Colloid Interface Sci.*, **283**, 397-405 (2005).
- [57] B. Ruzicka, L. Zulian, E. Zaccarelli, R. Angelini, M. Sztucki, A. Moussaïd and G. Ruocco, *Phys. Rev. Lett.*, **104**, 085701 (2010).
- [58] B. Ruzicka, L. Zulian and G. Ruocco, *J. Phys.: Condens. Matter*, **16**, S4993-S5002 (2004).

-
- [59] B. Ruzicka, L. Zulian and G. Ruocco, *Phys. Rev. Lett.*, **93**, 258301 (2004).
- [60] B. Ruzicka, L. Zulian and G. Ruocco, *Langmuir*, **22**, 1106-1111 (2006).
- [61] B. Ruzicka, L. Zulian and G. Ruocco, *Phil. Mag.*, **87**, 449-458 (2007).
- [62] H. Tanaka, J. Meunier and D. Bonn, *Phys. Rev. E*, **69**, 031404 (2004).
- [63] B. Ruzicka, E. Zaccarelli, L. Zulian, R. Angelini, M. Sztucki, A. Moussaïd, T. Narayanan and F. Sciortino, *Nature Materials*, **10**, 56-60 (2011).
- [64] R. G. Larson, *The Structure and Rheology of Complex Fluids (Topics in Chemical Engineering)*, Oxford University Press, Oxford, 1999.
- [65] J. J. Stickel and R. L. Powell, *Annu. Rev. Fluid Mech.*, **37**, 129-149 (2005).
- [66] U. Bröckel, W. Meier and G. Wanger, *Product Design and Engineering: Formulation of Gels and Pastes*, Wiley-VCH, 2007.
- [67] A. Fall, N. Huang, F. Bertrand, G. Ovarlez and D. Bonn, *Phys. Rev. Lett.*, **100**, 018301 (2008).
- [68] T. Ferroir, H. T. Huynh, X. Chateau and P. Coussot, *Phys. Fluids*, **16**, 594 (2004).
- [69] P. G. Saffmann and G. I. Taylor, *Proc. Soc. London A*, **245**, 312 (1958).
- [70] J. Nase, A. Lindner and C. Creton, *Phys. Rev. Lett.*, **101**, 074503 (2008).
- [71] H. van Damme, F. Obrecht, P. Levitz, L. Gatineau and C. Laroche, *Nature*, **320**, 731 (1986).
- [72] E. Lemaire, P. Levitz, G. Daccord, and H. van Damme, *Phys. Rev. Lett.*, **67**, 2009 (1991).
- [73] E. Lécolier, A. Mourchid and P. Levitz, *Progress in Colloid & Polymer Science*, **110**, 16-20 (1998).
- [74] R. Bandyopadhyay, *Pramana - J. Phys.*, **81**, 3-34 (2013).

2

Experimental Techniques

2.1 Introduction:

Several experimental techniques, such as dynamic light scattering (DLS), ion measurement, rheology and high speed imaging, used to perform the experiments reported in this thesis, are described in this chapter. Designs of cells for the study of interfacial instabilities in a Hele-Shaw geometry and a falling ball viscometer are also discussed. The timescales of the microscopic dynamics of colloidal suspensions are studied by DLS. Details of this experimental technique are described in the section 2.2.1. Sodium ion concentration measurements are done by an ion meter. The principles of acquiring data using this meter is explained in section 2.2.2. A stress controlled rheometer is used for bulk rheological measurements. A brief discussion of rheometry and the rheometer used in this work is included in the section 2.2.3. A high speed camera used for studying interfacial instabilities and the trajectory of the falling ball in aging clay suspensions is discussed in section 2.2.4. Section 2.2.5 describes the design of a falling ball viscometer and the data analysis protocols used here. The Hele-Shaw cell used to

study the interfacial instabilities in this thesis is described in section 2.2.6.

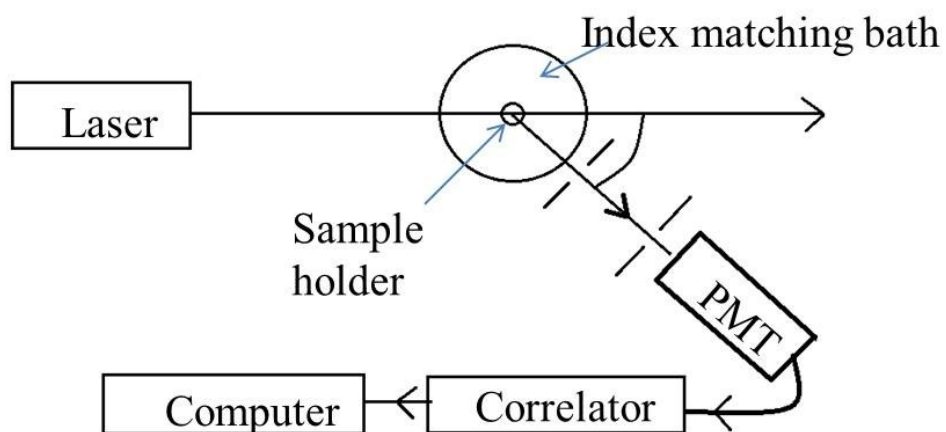
2.2 Experimental techniques:

2.2.1 Dynamic Light Scattering:

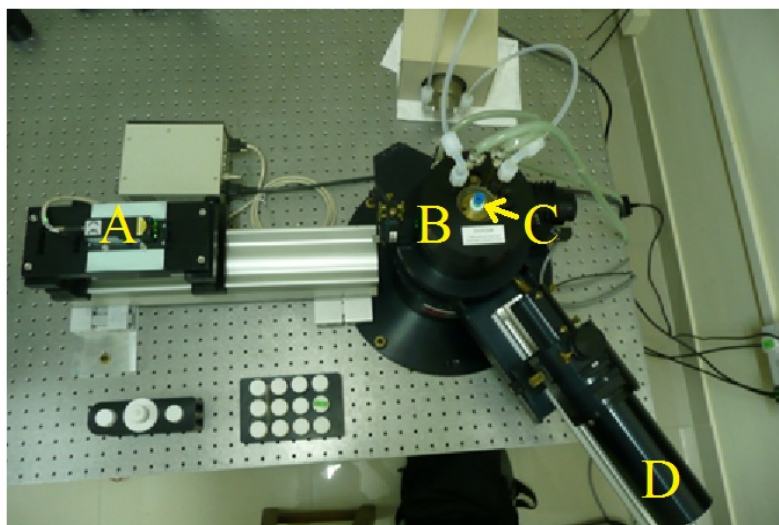
Dynamic light scattering is a very efficient technique to study the microscopic motion of scatterers in a suspension in a non-invasive way. This technique, commonly used in the determination of the structure and dynamics of soft materials, is also known as photon correlation spectroscopy.

A standard dynamic light scattering (DLS) setup has three parts, i.e. an intense monochromatic source or a laser, an index-matching bath containing the sample holder and a very fast and efficient detector (an avalanche photo diode (APD) or a photo multiplier tube (PMT)). A schematic diagram of the DLS setup is shown in figure 2.1(a). Colloidal particles in a dilute suspension undergo Brownian motion. An incident beam from a laser is scattered by the colloidal particles in every direction. The intensity of the scattered light from the scattering volume has an angular dependence and generally fluctuates rapidly due to the thermal motion of the scatterers in the suspension. The scattering volume is defined as the volume of intersection between the incident beam and scattered beam intercepted by the detector [1]. The shape and size (or the hydrodynamic radius) of the colloidal particle is measured from the angular dependence and the intensity fluctuations of the scattered light respectively. Below, a brief theory is given for the measurement of the size of monodisperse spherical scatterers diffusing in a dilute suspension.

For a scattering volume V inside a non-scattering solvent containing N identical scatterers, if an incident monochromatic plane wave, polarized perpendicular to the scattering plane and having a frequency ω_0 is scattered by the scatterers, then at a distant point R_0 and at a scattering angle θ , the light scattered by the j th scatterer is given



(a)



(b)

FIGURE 2.1: (a) Schematic diagram of dynamic light scattering (DLS) setup. (b) Snapshot of BIC 200SM DLS setup with laser (A), index-matching bath (B), sample holder (C) and photo multiplier tube (D).

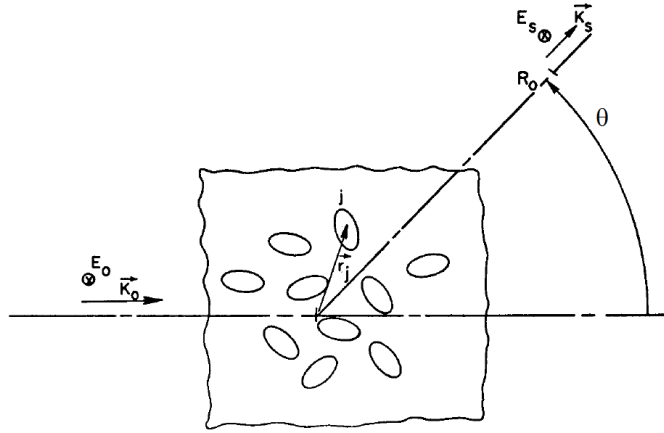


FIGURE 2.2: Schematic diagram of geometry of scattering system. This figure is adapted from [2].

by [2, 3]:

$$E_j = A_j(t) \exp(i\phi) \exp(-i\omega_0 t) \quad (2.1)$$

where A_j is the amplitude of E_j . If we choose the phase $\phi = 0$ for a scatterer at the origin and denote the position vector of the j th scatterer by \vec{r}_j with respect to the origin, then according to figure 2.2 [2],

$$\phi_j = (\vec{K}_0 - \vec{K}_s) \cdot \vec{r}_j = \vec{q} \cdot \vec{r}_j \quad (2.2)$$

where \vec{K}_0 and \vec{K}_s are the incident and scattered wave vectors respectively. For quasi-elastic light scattering, $|\vec{K}_0| \approx |\vec{K}_s|$ and $|\vec{q}| = 2|\vec{K}_0| \sin(\theta/2) = \frac{4\pi n}{\lambda} \sin(\theta/2)$, where n and λ are the refractive index of the medium and the wavelength of the laser light respectively [1, 4]. The total scattered field E_s at a distant point R_0 is given by [2]:

$$E_s = \sum_{j=1}^N A_j(t) e^{i\vec{q} \cdot \vec{r}_j} e^{-i\omega_0 t} \quad (2.3)$$

Hence, the average scattered intensity at R_0 is given by $I_s = \langle |E_s|^2 \rangle$, where $\langle \rangle$ denotes the time average. Now, if the motion of the scatterers are independent and uncorrelated, all cross terms in the expression of I_s in the time average vanish to give $I_s = \left\langle \sum_j |A_j|^2 \right\rangle = N \langle |A|^2 \rangle$ [2]. The following expression for the spectrum of the scattered light can be obtained from the Wiener-Khintchine theorem [5] which relates the electric field autocorrelation of a stationary random process with its spectrum through spectral decomposition:

$$I(\omega) = \frac{1}{2\pi} \int_{-\infty}^{\infty} C(\tau) e^{i\omega\tau} d\tau \quad (2.4)$$

where the autocorrelation function $C(\tau)$ is given by the following expression:

$$C(\tau) = \langle E_s^*(t) E_s(t + \tau) \rangle \quad (2.5)$$

Here, E_s^* is the complex conjugate of E_s . Replacing the values of E_s and E_s^* in equation 2.3 gives,

$$C(\tau) = \left\langle \sum_{j=1}^N A_j^*(t) e^{-i\vec{q} \cdot \vec{r}_j(t)} e^{i\omega_0 t} \sum_{l=1}^N A_l(t + \tau) e^{i\vec{q} \cdot \vec{r}_l(t+\tau)} e^{-i\omega_0(t+\tau)} \right\rangle \quad (2.6)$$

If we assume that the positions and orientations of all the scatterers are independent, then all cross terms ($j \neq l$) in the above equation vanishes. Since all N scatterers are identical and have the same autocorrelation function,

$$C(\tau) = N e^{-i\omega_0\tau} \langle A^*(t) A(t + \tau) \rangle \left\langle e^{-i\vec{q} \cdot \vec{r}(t)} e^{i\vec{q} \cdot \vec{r}(t+\tau)} \right\rangle \quad (2.7)$$

Substituting the value of $C(\tau)$ in equation 2.4, for identical and statistically independent scatterers we have,

$$I(\omega) = \frac{N}{2\pi} \int_{-\infty}^{\infty} e^{i(\omega - \omega_0)\tau} [C_A(\tau)] [C_\phi(\tau)] d\tau \quad (2.8)$$

For identical spherical scatterers undergoing translational diffusion, $[C_A(\tau)] = 1$ as the scattering amplitude $A(t)$ is constant. The phase autocorrelation function is given by $[C_\phi(\tau)] = e^{-Dq^2\tau}$ [2], where D is the translational diffusion coefficient and related to the hydrodynamic radius r_h of the scatterer by the Stokes-Einstein relation,

$$D = \frac{k_B T}{6\pi\eta r_h} \quad (2.9)$$

Here k_B is the Boltzmann constant, η is the viscosity of the medium at temperature T . Using equations 2.8 and 2.9, it is seen that the spectrum of the scattered light ($I(\omega)$) is given by a Lorentzian centered at $\omega = \omega_0$ [2].

$$I(\omega) = N |A|^2 \frac{1}{2\pi} \int_{-\infty}^{\infty} e^{i(\omega-\omega_0)\tau} e^{-Dq^2\tau} d\tau = N |A|^2 \left\{ \frac{Dq^2/\pi}{(\omega - \omega_0)^2 + (Dq^2)^2} \right\} \quad (2.10)$$

There are two types of measurement techniques, namely homodyne and heterodyne methods, that depend on the optical mixing protocol of the scattered spectrum. In the homodyne method, the scattered spectrum is mixed with itself. However, for heterodyne measurements, a part of the incident beam is mixed with the scattered beam.

The homodyne measurement technique is used to perform all the experiments reported in this thesis. In this method, the output of the detector is either analyzed by an autocorrelator to generate the autocorrelation function or is sent to a spectrum analyzer. One assumption is that the optical field is spatially coherent over the detector. The instantaneous intensity $I(t)$ of the optical field is related to the electric field $E(t)$ by $I(t) = E^*(t)E(t)$. If $W^{(1)}(t)$ is the probability per unit time that a secondary electron will be emitted, then the average output current of the detector is given by $\langle i(t) \rangle = e \langle W^{(1)}(t) \rangle = e\beta \langle I \rangle$, where β is the quantum efficiency of the detector and e is the charge of an electron. Again, if $W^{(2)}(t, t + \tau)$ is the joint probability per unit time that one secondary electron will be emitted at t and another at $t + \tau$, then $\langle W^{(2)}(t, t + \tau) \rangle = \beta^2 \langle E^*(t)E(t)E^*(t + \tau)E(t + \tau) \rangle = \beta^2 \langle I \rangle^2 g^{(2)}(\tau)$, where the second

order correlation function $g^{(2)}(\tau)$ is given by [2]:

$$g^{(2)}(\tau) = \langle E^*(t)E(t)E^*(t+\tau)E(t+\tau) \rangle / \langle E^*E \rangle^2 \quad (2.11)$$

The current autocorrelation function is given by [2]:

$$C_i(\tau) = \langle i(t)i(t+\tau) \rangle = e^2 \langle W^{(1)}(t)W^{(1)}(t+\tau) \rangle \quad (2.12)$$

In the present experimental setup, a digital autocorrelator receives $i(t)$ from the output of the detector as infinitely narrow discrete pulses. Clearly, for two distinct secondary electrons at t and $t+\tau$, $\langle W^{(1)}(t)W^{(1)}(t+\tau) \rangle = \langle W^{(2)}(t, t+\tau) \rangle = \beta^2 \langle I \rangle^2 g^{(2)}(\tau)$, while for the same electron we get $\langle W^{(1)}(t)W^{(1)}(t+\tau) \rangle = \langle W^{(1)}(t) \rangle \delta(\tau) = \beta \langle I \rangle \delta(\tau)$. So, $C_i(\tau)$ can be written as follows [2]:

$$C_i(\tau) = e^2 \beta \langle I \rangle \delta(\tau) + e^2 \beta^2 \langle I \rangle^2 g^{(2)}(\tau) = e \langle i \rangle \delta(\tau) + \langle i \rangle^2 g^{(2)}(\tau) \quad (2.13)$$

We know from the central limit theorem [6] that the optical field for light scattered by a very dilute solution of independent scatterers is a Gaussian random field. The second-order intensity autocorrelation function $g^{(2)}(\tau)$ can therefore be related to the first order electric field autocorrelation function by the Siegert relation [7]:

$$g^{(2)}(\tau) = 1 + |g^{(1)}(\tau)|^2 \quad (2.14)$$

where $g^{(1)}(\tau) = \langle E^*(t)E(t+\tau) \rangle / \langle E^*(t)E(t) \rangle$ and the autocorrelation function is given by $C_i(\tau) = e \langle i \rangle \delta(\tau) + \langle i \rangle^2 (1 + |g^{(1)}(\tau)|^2)$. Now, for a dilute suspension of identical spherical scatterers, $g^{(1)}(\tau) \propto e^{-Dq^2\tau}$ [2] and therefore $|g^{(1)}(\tau)|^2 \propto e^{-2Dq^2\tau}$.

The DLS experiments reported here are performed with a Brookhaven Instruments Corporation (BIC) BI-200SM spectrometer equipped with a 150 mW solid state laser (NdYVO₄, Coherent Inc., Spectra Physics) having an emission wavelength of 532 nm

(figure 2.1(b)). A refractive index-matching bath filled with decaline contains the cuvette filled with the sample. The temperature of the bath is maintained by water circulation with a temperature controller (Polyscience Digital). The scattered photons give rise to secondary electrons in the detector which set off voltage pulses in the PMT detector. The output of the detector is attached to a Brookhaven BI-9000AT digital autocorrelator which is used to measure the intensity autocorrelation function of the light scattered from the samples. There are 522 channels (maximum) in the autocorrelator that are controlled by high-speed, medium-speed and low-speed circuits [8]. These channels can be programmed to be spaced logarithmically, linearly or otherwise. The intensity autocorrelation function $g^{(2)}(t)$ is obtained by the autocorrelator using the following expression [8]:

$$g^{(2)}(\tau_j) = \lim_{N \rightarrow \infty} \frac{1}{N} \sum_{i=1}^N n_i n_{i-j} \quad j = 1, 2, 3, \dots, M \quad (2.15)$$

Here, N is the total number of samples and τ_j is the j th delay time, n_i and n_{i-j} are the number of pulses in the time interval $\Delta\tau$ (or sampling time) centered at t and $t - \tau_j$ and M is the total number of channels [8].

For a very dilute suspension of polystyrene beads (purchased from Bangs Lab, NT05N, NIST particle size standard, nominal size 95.6 nm, polydispersity 3.7%), the normalized intensity autocorrelation function $C(\tau) = g^{(2)}(\tau) - 1$ as a function of delay time τ is plotted in figure 2.3 for several scattering angles at temperature $T = 25^\circ\text{C}$. A dilute polystyrene suspension (volume fraction $\phi = 10^{-5}$) is prepared from a supplied stock suspension. The second order autocorrelation function is given by $g^{(2)}(\tau) = \frac{\langle I(0)I(\tau) \rangle}{\langle I(0) \rangle^2} = 1 + A|g^{(1)}(\tau)|^2$, [1], where $I(\tau)$ is the intensity at a delay time τ , $g^{(1)}(\tau)$ is the normalized electric field autocorrelation function, A is the coherence factor, and the angular brackets $\langle \rangle$ represents an average over time. The duration of data collection is kept long enough to ensure a large photon count. The autocorrelation functions $C(\tau)$ are acquired at six different scattering angles (i.e. six different q , figure 2.3) and are fitted to exponential decays $C(\tau) = \exp(-\tau/\tau_1)$. Here, τ_1 is the relaxation time

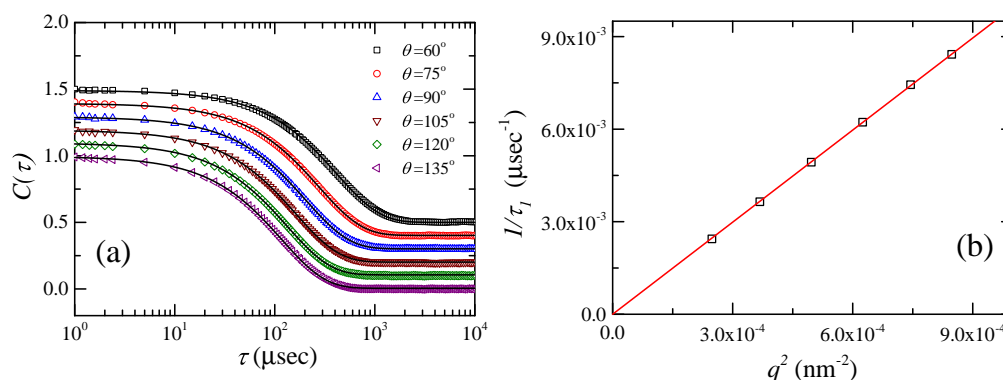


FIGURE 2.3: (a) The normalized intensity autocorrelation functions $C(\tau)$ vs. the delay time τ at 25°C and scattering angle (60° (\square), 75° (\circ), 90° (\triangle), 105° (∇), 120° (\square) and 135° (\blacktriangleleft)) for polystyrene beads in a dilute aqueous suspension ($\phi = 10^{-5}$). The solid lines are fits to simple exponential function. (b) $1/\tau_1$ vs. q^2 plot showing diffusive motion of the scatterers. Diffusion coefficient D of the scatterers is extracted from the slope of the plot which yields 96.1 ± 0.6 nm as size of the scatterers.

of the scatterers. τ_1 values obtained from the fits to the $C(\tau)$ data for six q values and $1/\tau_1$ are plotted vs. q^2 (figure 2.3(b)). A straight line passing through the origin indicates diffusive behavior *i.e.* $\tau_1 = 1/Dq^2$. Here D is the diffusion coefficient and is obtained from the slope of the $1/\tau_1$ vs. q^2 plot. The size of the polystyrene beads dispersed in aqueous medium ($\eta = 0.89$ mPa.s at 25°C) is calculated by applying the Stokes-Einstein relation (equation 2.9). The calculated size of the polystyrene sphere is 96.1 ± 0.6 nm which agrees fairly well with the size supplied by the manufacturer.

2.2.2 Ion Measurements:

An ion selective membrane is needed to determine the concentration of a specific ion in suspension. In this thesis, the concentration of sodium ions (Na^+) is measured by a Eutech CyberScan 2100 pH/ion meter (figure 2.4). This meter is equipped with an electrode (ROSS Sure-Flow) with a sodium ion-selective membrane. An ion-selective membrane allows only a particular species of ion or a specific set of ions to permeate (figure 2.5). For this reason, an electrical potential develops across the membrane over time. A sodium ion selective membrane senses the activity of the sodium ion

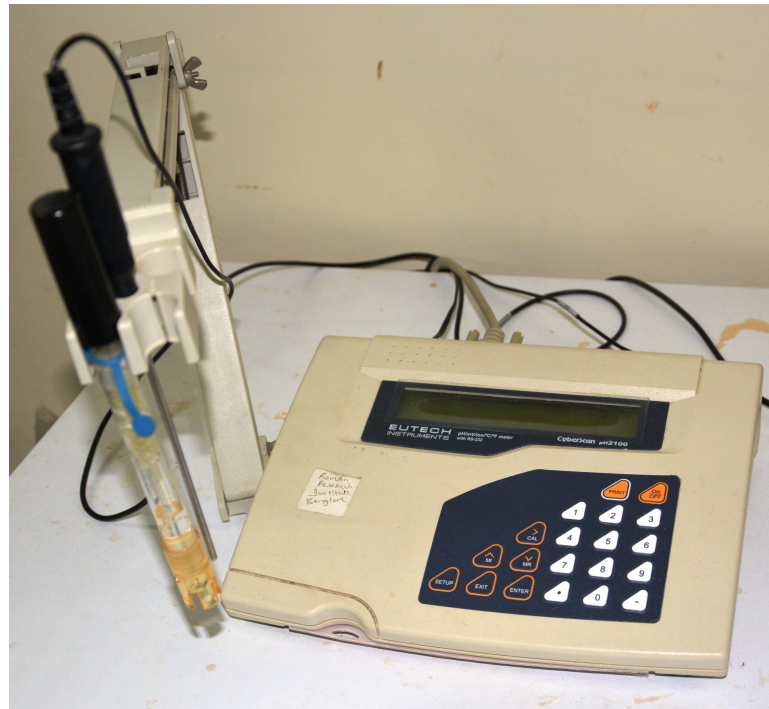


FIGURE 2.4: Snapshot of the Eutech CyberScan 2100 pH/ion meter.

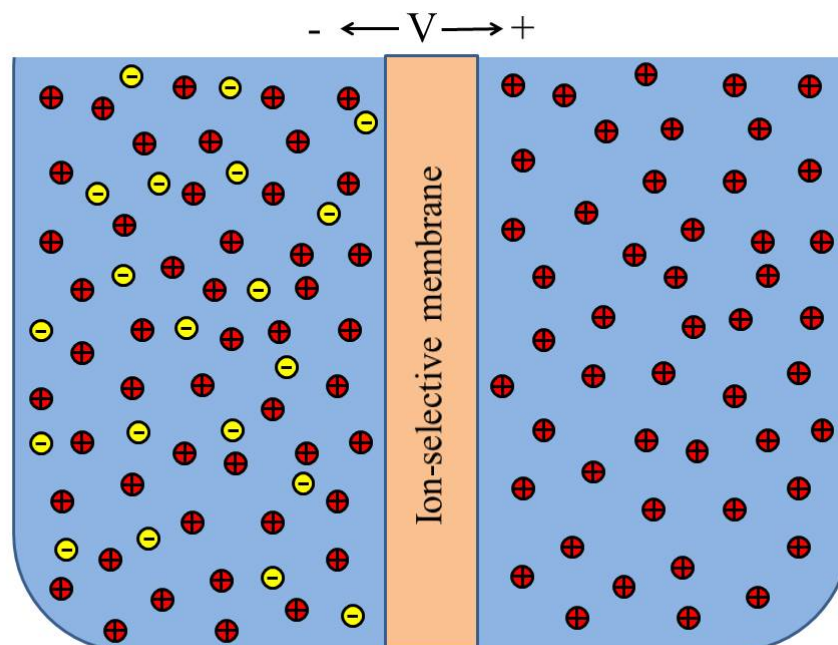


FIGURE 2.5: Schematic diagram of an ion-selective membrane. Potential V develops across the membrane because it is permeable to a particular ion. Red and yellow circles denote two different species of ions.

dissolved in the colloidal suspension and converts it into an electrical potential. This potential is measured and is used to determine the concentration of sodium ions in the suspension. The potential developed at this membrane is measured using two internal electrochemical cells- a sensing reference cell and a second reference cell. These two cells are connected in such a way that the change in potential happens only due to the change in the concentration of sodium ions. The measured potential is given by the Nernst equation which relates the concentration gradient of a species or a specific ion (in case of an ion selective electrode) at equilibrium to the electric potential that balances it [9, 10]:

$$V = V_0 + S \log A \quad (2.16)$$

Here V_0 is the constant potential dependent on the reference electrode, A is the sodium ion activity and S is the electrode slope. Calibration is done for several known concentrations of Na^+ ions (0.01 mM, 0.1 mM, 1 mM, 10 mM and 100 mM) to determine the electrode parameters (V_0 and S). The Laponite suspension is loaded in a narrow-mouth bottle and the electrode is dipped inside for measurement. The opening between the mouth of the bottle and electrode wall is sealed. The temperature of the suspension is maintained at the desired value by water circulation throughout the duration of the experiment. It is seen from equation 2.16 that the Nernst equation relates the potential directly to the activity but not to the concentration of a specific ion. However, the activity A_i of an ion (i^{th} species or sodium ion) is related to its concentration c_i in the following way [11]:

$$A_i = \gamma_i c_i \quad (2.17)$$

Here, γ_i is called the activity coefficient which, in the case of a chemical solution or mixture, is a measure of the deviation from ideal behavior. For low concentrations of sodium ions, the activity coefficient is close to unity [11] and the activity A in the Nernst equation (equation 2.16) can be replaced by the concentration of sodium ions.

2.2.3 Rheology and Rheometry:

The word ‘‘Rheology’’ was coined by Bingham to describe the study of the deformation and flow of matter [12]. For an ideal elastic solid, the deformation or strain (γ) is directly proportional to the stress (σ) applied to it. Here, the Hookes’ law is used to relate stress and strain, with $\sigma = G\gamma$ [13], where G is the proportionality constant known as rigidity modulus or modulus of elasticity. An ideal liquid, on the other hand, offers no resistance to shear deformation and has no elasticity. However, in a liquid, the applied stress (σ) is proportional to strain rate ($\dot{\gamma} = \frac{d\gamma}{dt}$), $\sigma = \eta\dot{\gamma}$. Here η is called the coefficient of viscosity [14] and is the measure of the liquid’s resistance to flow. As discussed in the introduction, many soft matter systems, including the Laponite suspensions studied in this thesis, show viscoelastic behavior. Depending on the amount of stress or strain in the material, two different kinds of behavior, linear and non-linear viscoelasticity, are observed. In the linear viscoelastic regime *i.e.* for small stresses or strains, a linear relationship exists between σ and $\dot{\gamma}$ which is described by the linear differential equation below.

$$\sigma(t) = \int_{-\infty}^t G(t - t_1)\dot{\gamma}(t_1)dt_1 \quad (2.18)$$

In the above equation, $G(t - t_1)$ is the stress relaxation function. It is a function of $t - t_1$ where t_1 is a past time variable. However, in the non-linear regime which occurs for higher values of stresses and strains, G also depends on the amount of instantaneous strain. In this regime, the stress can be written as $\sigma(t) = G(t, t_1, \gamma)\dot{\gamma}(t)$. Normal stress differences, shear thinning and shear thickening are observed in this regime [15].

In the laboratory, a rheometer is employed to measure the different rheological parameters. In general, measurements may be performed by applying both rotational and oscillatory stresses. All rheological measurements reported in this thesis are performed in a stress controlled modular Anton Paar MCR 501 rheometer (figure 2.6). This rheometer consists of a synchronous motor, an air bearing support with a normal

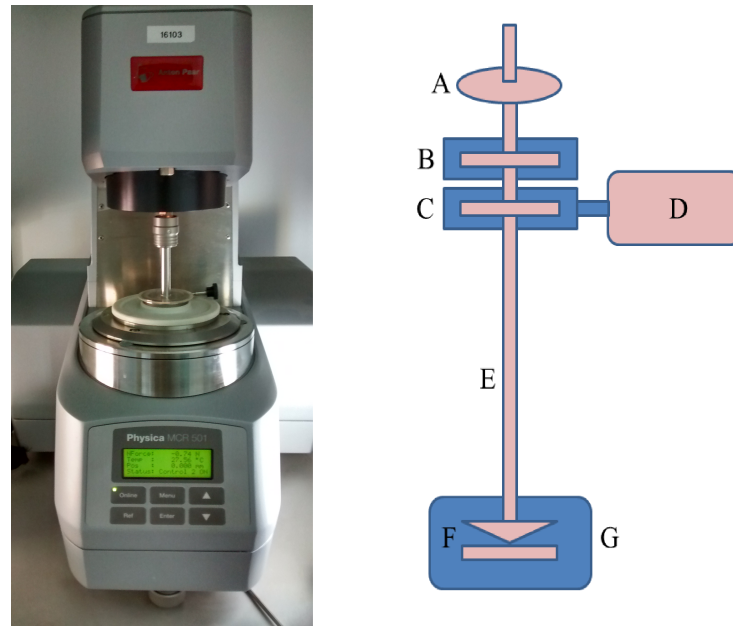


FIGURE 2.6: Anton Paar MCR 501 rheometer (left) and the schematic diagram of the rheometer (right) consisting of the optical encoder (A), synchronous motor (B), air bearing support (C), compressor (D), measuring rod (E), measuring geometry (F) and temperature controller (G).

Specification	Concentric cylinder	Double gap
Model no.	CC17	DG26.7/Q1
Description	Co-axially arranged cylindrical cup with a rotating cylindrical bob. Gap between cup and bob is 0.71 mm (figure 2.7(a))	Modified concentric cylinder geometry with an inner hollow cylinder. Two gaps between the inner and outer cylinder surfaces (figure 2.7(b))
Effective Length	24.99 mm	40 mm
Sample volume	4.72 ml	3.8 ml
Range of shear stress	771.345×10^{-6} Pa and 17740.935 Pa	109.407×10^{-6} Pa and 2516.361 Pa
Range of shear strain	$> 1.23 \times 10^{-5}$	$> 2.93 \times 10^{-5}$
Range of strain rate	$1.283 \times 10^{-7} \text{s}^{-1}$ and $3.849 \times 10^3 \text{s}^{-1}$	$3.0697 \times 10^{-7} \text{s}^{-1}$ and $9.209 \times 10^3 \text{s}^{-1}$.

Table 2.1: Specifications of measuring geometries used in this thesis.

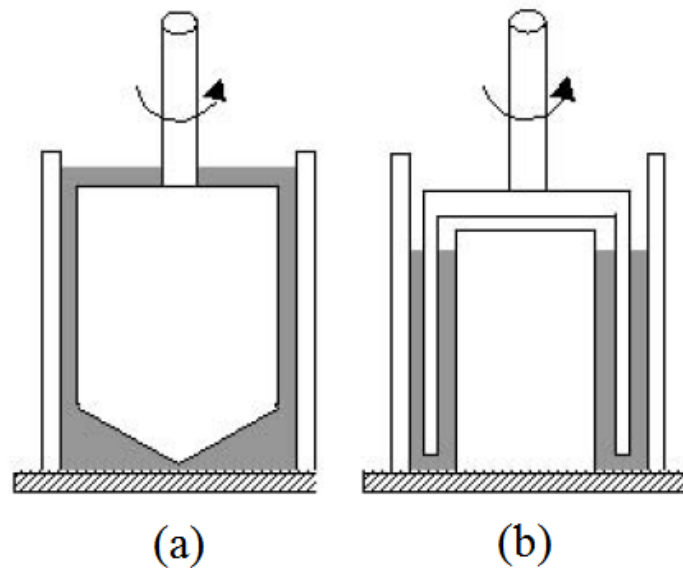


FIGURE 2.7: Schematic diagram of the measuring geometries (a) CC17 and (b) DG26.7/Q1 used in this thesis. This picture is adapted from [16].

force transducer, a compressor, an optical encoder, a measuring rod, a measuring geometry and a temperature controller as shown in the schematic diagram (figure 2.6). A synchronous motor is used to directly control the torque or stress applied to the system under observation. A feedback mechanism is used for the measurements that need strain control. Compressed air from the compressor is sent to the air bearing support attached to the motor to reduce the friction between the rotor and the stator of the synchronous motor. In this way, the rheometer is capable of measuring torques down to 2 nN.m with a resolution of 0.01 nN.m [16]. Angular deflection is measured with very high resolution and precision by employing an optical encoder (resolution < 1 mrad). The temperature of the sample in the measuring geometry is controlled by water circulation using a temperature controller (Viscotherm VT2) [16]. All data is acquired and saved using the Rheoplus 3.40 software in the computer. Different geometries, depending on the system under study, are used to acquire data. The specifications of two measuring geometries (concentric cylinder and double gap, figure 2.7) are given in the table 2.1. A sample flow curve of glycerol, obtained in a double gap geometry

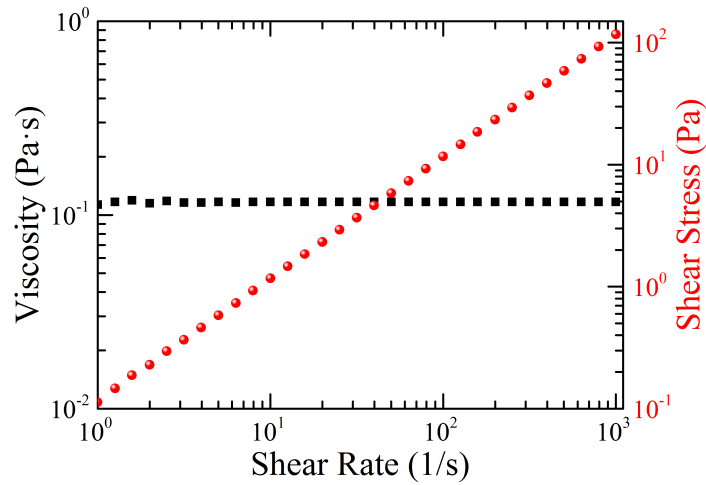


FIGURE 2.8: Flow curve of glycerol using DG26.7/Q1 where viscosity (■) and stress (●) are plotted vs. shear rate. From the picture, it is seen that the stress is proportional to shear rate and the viscosity is constant at 0.12 Pa.s in the applied shear rate regime, confirming the Newtonian flow behavior of glycerol.

(DG26.7/Q1), is shown in figure 2.8.

2.2.4 High Speed Imaging:

High speed imaging was done with an IDT MotionPro Y4-S2 CMOS camera equipped with a Nikon AF-S NIKKOR 12-24mm lens (figure 2.9). The specifications of the camera are given in the table 2.2 [17]:



FIGURE 2.9: Snapshot of the IDT MotionPro Y4-S2 CMOS camera equipped with a Nikon AF-S NIKKOR 12-24mm lens.

Key features	Specifications
Maximum fps @ maximum resolution	4500 @ 1016x1016
No. of pixels	1016x1016
Minimum exposure time	1 μ s
Sensitivity ASA (mono)	6000
Sensitivity ASA (color)	6000
Memory/DRAM Internal	8 GB
Sensor Type	CMOS-Polaris II
Sensor Size	13.9 x 13.9 mm
Array Size	1 Megapixel
Pixel Size	13.68 x 13.68 μ m
Pixel Fill factor	40 %
Dynamic Range	60 dB
Quantum Efficiency (QE)	50%
Pixel Depth (mono)	10-bit
Pixel Depth (color)	30-bit
Internal clock	166.66 MHz

Table 2.2: Specifications of high speed camera.

2.2.5 Falling Ball Viscometer:

The main principle behind a falling ball viscometer is that the buoyant weight of an object settling through a viscous fluid is balanced by the viscous drag on it. In this condition, the object achieves terminal velocity. The viscosity of the medium can be calculated from the terminal velocity by applying Stokes' law [18]. According to Stokes' law, a drag force is generated against the motion of the ball and is proportional to the instantaneous velocity of the ball. At some point of time, this drag force is large enough to cancel the buoyant weight of the falling ball. Thus, the ball stops accelerating due to gravity and attains a terminal velocity when the drag force and gravitational force balance each other. The drag force F is related to the terminal velocity v by Stokes' law for an infinite medium (*i. e.* in the absence of wall) and without any inertial effect and is given by [18],

$$F = 6\pi\eta r v \quad (2.19)$$

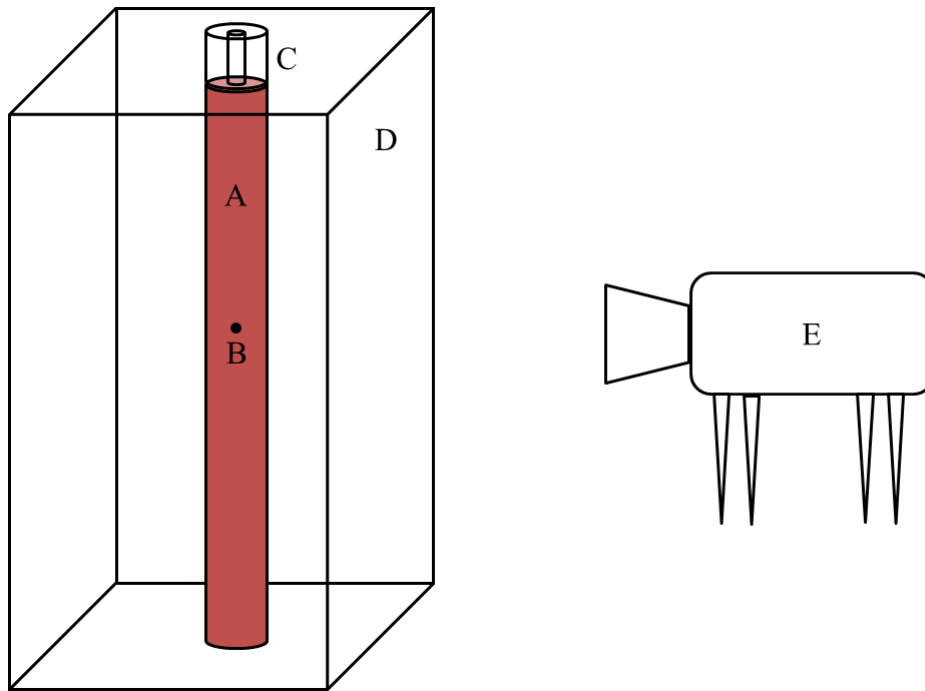


FIGURE 2.10: Schematic diagram of the falling ball viscometer. (A) Cylindrical tube, (B) ball, (C) guide tube, (D) thermal bath and (E) high speed camera.

where η is the coefficient of viscosity of the medium and r is the radius of the ball dropped. If this force is equal to the buoyant weight of the ball, then we have,

$$\frac{4}{3}\pi r^3(\rho_{ball} - \rho)g = 6\pi\eta r v \quad (2.20)$$

which yields the expression for terminal velocity,

$$v = \frac{2}{9} \frac{r^2(\rho_{ball} - \rho)g}{\eta} \quad (2.21)$$

Often in an experiment, conditions are not ideal and the fluid through which the ball falls has a finite extent. There can then be wall effects due to the closeness of the cylinder walls to the falling ball (figure 2.10) as well as inertial effects. In general, the presence of the wall reduces the terminal velocity v as the drag on the ball is more.



FIGURE 2.11: Snapshot of the falling ball viscometer inside a thermal bath and with a solenoid based ball release mechanism.

The correction to the terminal velocity due to the wall effect is given by Faxen for a cylindrical tube with a diameter D [19]:

$$v_{Faxen} = v(1 - 2.104(d/D) + 2.089(d/D)^3 + \dots)^{-1} \quad (2.22)$$

where d is the diameter of the ball. The correction due to the inertial effect is given by Oseen's approximation [20]. The corrected terminal velocity in the presence of inertia is given by:

$$v_{Oseen} = v \left(1 + \frac{3}{16} Re \right)^{-1} \quad (2.23)$$

where Re , the Reynolds number, is the ratio of the inertial force to the viscous drag, and is given by:

$$Re = \frac{\rho v d}{\eta} \quad (2.24)$$

Here, ρ is the density of the fluid through which the ball is falling. Other higher order corrections to the terminal velocity are given by Goldstein [21] and Proudman and Pearson [22] and the corresponding equations are given by the following two equations.

$$v_{Goldstein} = v \left(1 + \frac{3}{16} Re - \frac{19}{1280} Re^2 + \frac{71}{20480} Re^3 + \dots \right)^{-1} \quad (2.25)$$

$$v_{Proudman} = v \left(1 + \frac{3}{16} Re + \frac{9}{160} Re^2 \ln\left(\frac{Re}{2}\right) + \dots \right) \quad (2.26)$$

In our design of a falling ball viscometer, the fluid under observation is loaded into a cylindrical tube of height 61 cm approximately and diameter 3.6 cm (figures 2.10 and 2.11). The tube is kept inside a thermal bath made of acrylic. A temperature controller (Polyscience Digital) is attached to the thermal bath. The temperature is maintained by water circulation. Spherical steel balls are used as the objects settling through the medium inside the cylinder under gravity (the falling ball). The path followed by the ball is recorded with an IDT MotionPro Y4-S2 high speed camera. From the frames obtained, the motion of the ball is tracked using a LabView based tracking program [23] to obtain the displacement of the ball with time. It should be noted that after the ball reaches terminal velocity v , the slope of the displacement vs. time graph for a Newtonian fluid gives the value of its terminal velocity. In this work, the ball is dropped using a solenoid based release mechanism at the center of the cylinder through a guide tube (figures 2.10 and 2.11). This ensures that the ball falls through the center of the cylindrical viscometer and minimizes wall effects.

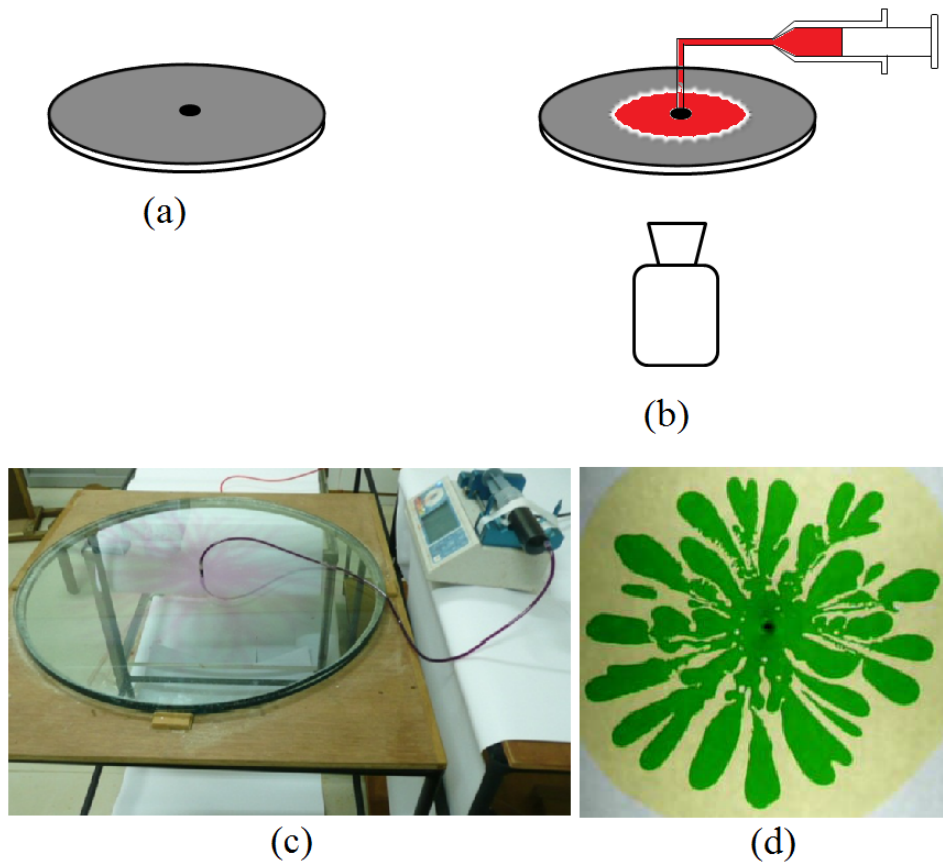


FIGURE 2.12: (a) Schematic of a radial Hele-Shaw cell. (b) Schematic of a flow experiment in a Hele-Shaw set up. (c) Snapshot of the experimental set up. (d) Viscous fingering pattern when mustard oil ($\eta = 60$ mPa.s) is displaced by colored (green) water ($\eta = 0.89$ mPa.s).

2.2.6 Hele-Shaw Cell:

The interface between two fluids, in general, is unstable when a fluid of higher viscosity is displaced by a fluid of lower viscosity under pressure. This leads to the formation of finger-like intrusions and the creation of fractal patterns. This phenomenon is known as viscous fingering [24]. Tongues of water in oil have often been reported in the context of secondary oil recovery. The study of viscous fingering is performed in a confined geometry or a Hele-Shaw cell. In the Hele-Shaw cell, named after the English mechanical and automobile engineer Henry Selby Hele-Shaw, two glass plates with spacers between them are used to confine the more viscous fluid. This geometry

is used to study the Stokes flow between two parallel plates separated by an infinitesimally small gap (a quasi 2 dimensional geometry). If the glass plates are very close (separation < 0.02 inch) then the flow is laminar at all velocities [25]. This simplifies many problems in fluid mechanics and the phenomenon of interfacial instabilities can be studied by analytical, numerical and experimental methods. Rheologists use different types of geometries to study viscous fingering. In the conventional radial Hele-Shaw cell, the less viscous fluid is pushed through a hole in the center of one of the glass plates (upper or lower) by applying pressure. A lifting Hele-Shaw cell is a special example of a confined geometry where the force of adhesion can be estimated by determining the force required to separate the plates. There have been many instances of the study of viscous fingering in modified Hele-Shaw cells. In some recent experiments, an external perturbation was introduced by etching grooves in the lower plate [26, 27] or by stretching a piece of cloth across the lower plate [28]. In this thesis a conventional radial Hele-Shaw cell (figure 2.12) is used to study the fingering instabilities at the interface between an aging non-Newtonian fluid (Laponite suspension) and a Newtonian fluid (oil or water). Circular glass plates of thickness 10 mm and diameter 60 cm are used for the experiment. 10 mm thick glass plates are found to give good mechanical stability. This also improves the uniformity of the gap between the glass plates by reducing sagging. A hole of approximately 4.2 mm is drilled on the upper glass plate for fluid injection. A syringe pump (Fusion 400, Chemyx Inc.) is used to inject the fluid at a controlled rate. The Hele-Shaw cell is kept on a mechanically stable table. Imaging is done from below by the IDT MotionPro Y4-S2 high speed camera (figure 2.12(b)).

References

- [1] B. J. Berne and R. Pecora, *Dynamic Light Scattering: With Applications to Chemistry, Biology, and Physics*, Wiley-Interscience, New York, 1976.
- [2] H. Z. Cummins, F. D. Carlson, T. J. Herbert and G. Woods. *Biophys. J.*, **9**, 518-546 (1969).
- [3] Donald A. McQuarrie. *Statistical Mechanics*. Harper & Row, Publishers, Inc., New York, 1976.
- [4] R. Pecora, *Dynamic Light Scattering: Applications of Photon Correlation Spectroscopy*, Plenum Press, New York, 1985.
- [5] Norbert Wiener. *Time Series*. M.I.T. Press, Cambridge, Massachusetts. p. 42, 1964.
- [6] W. Feller. The fundamental limit theorems in probability. *Bull. Amer. Math. Soc.* 51, 800-832, 1945.
- [7] A. J. F. Siegert, M.I.T. Rad. Lab. Rep., No. 465, 1943.
- [8] BI-200SM and BI-9000AT user manual, Brookhaven Instruments Corporation.
- [9] User Guide ROSS® Sodium Ion Selective Electrode. Thermo Fisher Scientific Inc., Beverly, MA 01915 USA, 2008.

-
- [10] John T. Stock and Mary Virginia Orna. *Electrochemistry, past and present*. American Chemical Society, Washington, DC, 1989.
- [11] A. D. McNaught and A. Wilkinson, *IUPAC Compendium of Chemical Terminology*, 2nd ed. (the “Gold Book”). Blackwell Scientific Publications, Oxford, 1997.
- [12] H. A. Barnes, J. F. Hutton and K. Walters, *An Introduction to Rheology*, Elsevier, Amsterdam, 1989.
- [13] R Hooke, *Lectures de Potentia Restitution*, John Martyn, London, 1678.
- [14] I. S. Newton, *Philosphiae Naturalis Principia Mathematica*, Royal Society of London, 1687.
- [15] C. W. Macosko, *Rheology: Principles, Measurements and Applications*, VCH Publishers, New York, 1993.
- [16] Anton Paar MCR 501 rheometer user manual.
- [17] IDT Cameras Specification Manual, Integrated Design Tools, Inc., 2010.
- [18] G. K. Batchelor, *An Introduction to Fluid Dynamics*, Cambridge University Press, Cambridge, 1967.
- [19] H. Faxen, *Ark Matematik Astron. Fys.*, **17**,1 (1923).
- [20] C.W. Oseen, *Ark Matematik Astron. Fys.*, **9**,1 (1913).
- [21] S. Goldstein, *Proc.R. Soc.*, 123A, 225 (1929).
- [22] I. Proudman and J.R.A. Pearson, *J. Fluid Mech.*, **2**, 237 (1957).
- [23] Particle Tracking Resource Page, <http://grahammilne.com/tracker.htm>.
- [24] G. M. Homsy, *Ann. Rev. Fluid Mech.*, **19**, 271-311 (1987).

- [25] B. Gustafsson, R. Teodorescu, A. Vasilev, Classical and Stochastic Laplacian Growth, Springer, 2014.
- [26] S. Sinha, S.K. Kabiraj, T. Dutta and S. Tarafdar. Eur. Phys. J. B, **36**, 297-300 (2003).
- [27] K. V. McCloud and J. V. Maher, Phys. Rep., **260**, 139 (1995).
- [28] M. Ben Amar, R. Combescot and Y. Couder, Phys. Rev. Lett., **70**, 3047 (1993).

3

The dynamical slowing down process in soft glassy colloidal suspensions: comparisons with supercooled liquids

3.1 Introduction

Two-step relaxation processes are ubiquitous in supercooled liquids [1]. The faster (β) decay corresponds to the diffusion of the particle within a cage formed by its neighbours, while the slower (α) decay corresponds to its cooperative diffusive dynamics between cages. The transport properties (i.e. viscosity, diffusivity etc.) and the relaxation timescales of a glass former change sharply as the glass transition is

approached [2]. The primary or the α -relaxation time becomes increasingly slow and diverges in the vicinity of the glass transition. The dependence of this relaxation time on temperature in a strong glass former is nearly Arrhenius and the degree of deviation from Arrhenius behaviour is measured as ‘fragility’. For fragile glass formers, the α -relaxation time shows a Vogel-Fulcher-Tammann (*VFT*) dependence on temperature (T), with the fragility index depending solely on the material [3]. The density of potential energy minima of the configurational states in the potential energy landscape determines the strong or fragile behaviors of supercooled liquids [4]. Strong glasses have a lower density of minima and their entropy increases slowly with decreasing temperature, thereby resulting in nearly Arrhenius behavior [5]. In contrast, fragile glasses have a larger density of minima which causes super-Arrhenius behavior of the α -relaxation. Other secondary relaxation processes also simultaneously take place in the same temperature range. In supercooled liquids and molecular glasses, one of them is the Johari-Goldstein (JG) β -relaxation process [6–9], which is the slowest of the secondary relaxation processes and is strongly coupled with the α -relaxation process [10–12].

In the last two decades, colloidal glasses have emerged as excellent model candidates for the study of glasses and glass formers. While supercooled liquids can be driven towards their glass transitions by rapidly quenching their temperatures, the glass transition in colloidal suspensions can be achieved by increasing the volume fraction ϕ . For a colloidal suspension of hard spheres, increasing ϕ towards a glass transition volume fraction ϕ_g plays the same role as supercooling a liquid towards its glass transition temperature T_g [13, 14].

In recent years, colloidal glasses formed by the synthetic clay Laponite have been studied extensively [15–24]. Interestingly, aging Laponite suspensions show many similarities with supercooled liquids and molecular glasses. These include the observation of well-separated fast and slow timescales [25], the absence of thermorheological simplicity [26, 27], asymmetry in structural recovery following a step temperature

change [28, 29], probe size-dependent diffusion [30] and the presence of more complex phenomena such as overaging [31, 32].

The ergodic-to-nonergodic transition is observed in colloidal Wigner glasses and is discussed in detail by Tanaka *et. al.* in the context of aging dynamics of Laponite suspensions [21]. Two very distinct regimes in the temporal change of τ_α (α -relaxation time) are observed by the authors. The initial regime, when the system is ergodic and τ_α increases exponentially with waiting time, is called the ‘cage-forming’ regime, while the later stage, where τ_α increases linearly with waiting time, is called the ‘full-aging’ regime. In the cage-forming regime, the effective particle volume fraction increases with waiting time. The system gradually approaches a glass transition and finally enters the nonergodic full-aging regime. It should be noted that the aging dynamics of Laponite suspensions in the ergodic cage-forming regime is totally different from the aging of supercooled liquids just below the glass transition temperature.

In an aging Laponite clay suspension, the effective volume fraction changes spontaneously and continuously with waiting time due to the exfoliation of Laponite particles from Laponite tactoids [33] and by the simultaneous spontaneous evolution of inter-particle electrostatic interactions [18, 22, 34]. In this chapter, we report dynamic light scattering (DLS) experiments that are performed to measure the time-evolution of the primary and secondary relaxation processes of aging Laponite suspensions in the ergodic cage-forming regime. We use our data to establish connections between aging Laponite suspensions undergoing dynamical arrest and fragile supercooled liquids approaching their glass transitions. We show here that increasing the waiting time t_w of aging Laponite suspensions is equivalent to decreasing the thermodynamic temperature T of supercooled liquids. While the Vogel-Fulcher-Tammann (VFT) functional form (with $1/T$ mapped to sample age t_w) was demonstrated to work for the slower α -relaxation timescale of aging Laponite suspensions [16], we show here that β -relaxation follows an Arrhenius form (with $1/T$ again mapped to sample age t_w) as expected for supercooled liquids [9, 35]. A correspondence between temperature (T) and the waiting time since sample preparation (t_w) was reported in numerical studies of

physical and chemical gelation [36] and in Monte Carlo simulations of patchy-particle models of Laponite discs [37]. In a recent work, the role of thermodynamic temperature in the dynamical slowing down process of a colloidal glass produced by tethering polymers to the surface of inorganic nanoparticles has been investigated in the context of soft glassy rheology [38].

Furthermore, we demonstrate novel analogies between colloidal suspensions of Laponite and supercooled liquids. We extract new timescales (the timescale t_β^∞ associated with the fast relaxation process and the glass transition time t_g) to demonstrate several remarkable similarities that exist between supercooled liquids and soft glassy materials. We demonstrate a coupling between t_β^∞ and the glass transition time t_g . An analogous coupling between the glass transition temperature of a supercooled liquid and the activation energy corresponding to its β -relaxation process has been suggested and experimentally verified for supercooled liquids [10–12], but has never been demonstrated in soft materials. It has been shown in the literature that the autocorrelation decay corresponding to the primary relaxation time can be successfully modeled as a stretched exponential process [39]. We show here that the stretching exponent β decreases linearly with waiting time. This observation is analogous to that in fragile supercooled liquids, where β is seen to decrease linearly with $1/T$ while approaching the glass transition. This further establishes the soundness of our mapping between the waiting time of a Laponite suspension and the inverse of the temperature of a supercooled liquid. Our DLS data also provides indirect evidence of an exfoliation process of the nature seen earlier [33]. It also demonstrates the self-similar time-evolutions of the fast and slow relaxation times, the stretching exponents β , and the width and non-Gaussian parameters (α_1 and α_2) characterizing the distributions of the slow relaxation time with changing Laponite concentration. Finally, we show that the fragility index D is concentration-independent and interpret this result in terms of the self-similar nature of the intricate potential energy landscape of aging Laponite suspensions approaching the glass transition.

3.2 Sample preparation

All the experiments reported in this chapter are performed with Laponite RD procured from Southern Clay Products. Before every experiment, Laponite powder is dried in an oven at 120°C for at least 16 hours. Appropriate amounts of powder are added slowly and carefully to double-distilled and deionized Millipore water of resistivity 18.2 MΩ-cm. The mixture is stirred vigorously until it becomes optically clear. The resulting suspension is filtered using a syringe pump (Fusion 400, Chemyx Inc.) at a constant flow rate (3.0 ml/min) by passing through a 0.45 μm Millipore Millex-HV syringe-driven filter unit. The filtered suspension is loaded and sealed in a cuvette for DLS experiments. Laponite suspensions of concentrations 2.0% w/v, 2.5% w/v, 3.0% w/v and 3.5% w/v are used in this study. Here, the concentration (% w/v) is the weight of Laponite in 100 ml of water. The mechanical properties of all the suspensions evolve spontaneously with time and exhibit the typical signatures of soft glassy rheology [40]. To avoid any kind of disturbance, the sample, once loaded in the sample holder of the DLS set up, is not removed until the end of the experiment.

3.3 Results and Discussions

The relaxation dynamics of a medium can be analyzed by monitoring the temporal behavior of the intensity autocorrelation function $g^{(2)}(t)$. In figure 3.1, the normalized intensity autocorrelation function, $C(t) = g^{(2)}(t) - 1$, is plotted for a 3.0% w/v Laponite suspension as a function of delay time, t , for experiments carried out at different waiting times t_w since filtration of the sample. $C(t)$ shows a two-step decay, suggesting the presence of two distinct relaxation timescales. In addition, the decay in the autocorrelation function slows down progressively as the sample ages. For a glassy suspension, the two-step decay of $C(t)$ can be described as a squared sum of an exponential and a

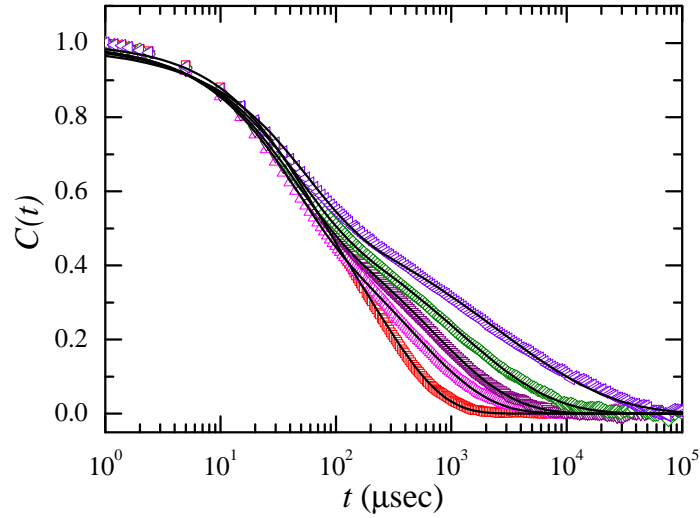


FIGURE 3.1: The normalized intensity autocorrelation functions $C(t)$ vs. the delay time t at 25°C and scattering angle $\theta = 90^\circ$ for 3.0% w/v Laponite suspension at several different waiting times t_w (from left to right): 0.5 hours (\square), 6.0 hours (\triangle), 9.0 hours (∇), 12.0 hours (\diamond) and 15.0 hours (\leftarrow). The solid lines are fits to equation 3.1.

stretched exponential decay given by [16]:

$$C(t) = \left[a \exp\{-t/\tau_1\} + (1 - a) \exp\left\{-(t/\tau_{ww})^\beta\right\} \right]^2 \quad (3.1)$$

The fits to equation 3.1 (shown by the solid lines in figure 3.1) describe the decays of the normalized autocorrelation functions for a range of waiting times t_w and for all the aging Laponite suspensions studied in this work. The fits are used to estimate the two relaxation timescales: τ_1 , the fast relaxation timescale that is associated with the secondary β -relaxation process, and τ_{ww} , the slow timescale that is associated with the primary α -relaxation process. In addition, the fits also provide values of the stretching exponent β which is connected to the distribution of the α -relaxation timescales.

In figure 3.2(a), we plot the evolutions of τ_1 with increasing t_w for Laponite suspensions of different concentrations. Interestingly, τ_1 evolves in two steps. At very small t_w , τ_1 initially decreases before increasing rapidly at large t_w . This is shown by

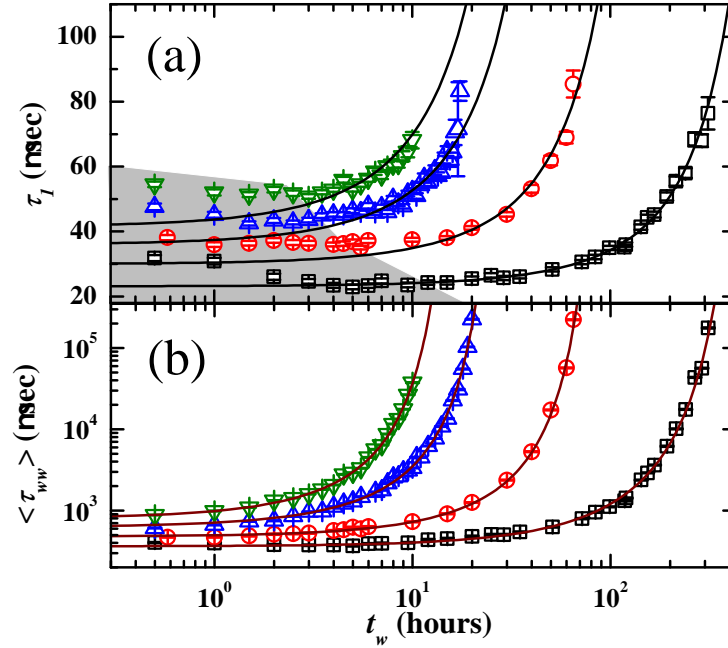


FIGURE 3.2: (a) The fast relaxation times, τ_1 vs. waiting time t_w for Laponite samples prepared at 25°C and at concentration 2.0% w/v (\square), 2.5% w/v (\circ), 3.0% w/v (Δ) and 3.5% w/v (∇). The solid lines show fits to the modified Arrhenius functions, $\tau_1 = \tau_1^0 \exp(t_w/t_\beta^\infty)$ (equation 3.2). Data are shifted vertically by an additive constant for better representation. The shaded portion highlights the initial decrease in τ_1 . (b) The mean α -relaxation times $\langle \tau_{ww} \rangle$, vs. waiting time t_w , are plotted for the same samples. The solid lines show fits to the modified VFT functions, $\langle \tau_{ww} \rangle = \langle \tau_{ww} \rangle^0 \exp(Dt_w/(t_\alpha^\infty - t_w))$ (equation 3.3).

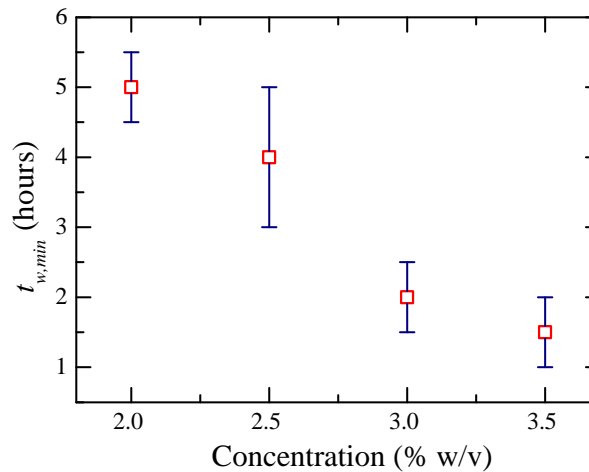


FIGURE 3.3: The waiting times associated with the minima in τ_1 ($t_{w,min}$) vs. concentration of Laponite.

the shaded portion in figure 3.2(a). It is also seen that the evolution of τ_1 shifts to smaller t_w with increasing Laponite concentration.

As noted earlier, the slow timescale τ_{ww} is identified with the α -relaxation process. The average value of τ_{ww} is given by $\langle \tau_{ww} \rangle = (\tau_{ww}/\beta)\Gamma(1/\beta)$, where Γ is the Euler Gamma function [41]. In figure 3.2(b), the evolution of $\langle \tau_{ww} \rangle$ is plotted as a function of t_w for different concentrations of Laponite. In contrast to the initial non-monotonic behavior of τ_1 , $\langle \tau_{ww} \rangle$ remains almost constant at small t_w . At larger t_w , $\langle \tau_{ww} \rangle$ shows a sharp increase. Furthermore, as in the case of τ_1 , the onset of the evolution of $\langle \tau_{ww} \rangle$ shifts to smaller t_w with increase in concentration of Laponite.

We now try to explain the non-monotonic nature of the initial time-evolution of the fast relaxation time. We note that the hydration of clay takes place soon after mixing dry Laponite powder in water. The water molecules diffuse into the inter-layer gallery causing the clusters to swell. Filtration of these suspensions breaks the clusters. After filtration, these broken clusters undergo further fragmentation [42]. In both cases, τ_1 is expected to decrease until the swelling clusters or the fragmented parts undergo dynamical arrest due to strong inter-platelet interactions that evolve spontaneously [33]. The waiting time at which τ_1 shows a minimum can therefore be considered as a measure of the time required for the onset of jamming. The waiting time associated with the minimum, $t_{w,min}$, decreases with increase in Laponite concentration as shown in figure 3.3. As the Laponite concentration increases, the increase in the number of cage-forming particles can be associated with a decrease in the free space that is required for cage expansion and swelling of the clusters. The minimum in τ_1 ($t_{w,min}$) therefore shifts to smaller t_w with increase in Laponite concentration.

The stretching exponents β associated with $\langle \tau_{ww} \rangle$ are obtained from fits of the data to equation 3.1 and are plotted as a function of t_w in figure 3.4. For small values of t_w , β is close to unity. However with increase in t_w , β decreases linearly, which signifies the broadening of the distribution associated with $\langle \tau_{ww} \rangle$. The decrease in β also shifts to smaller t_w with increase in the concentration of Laponite.

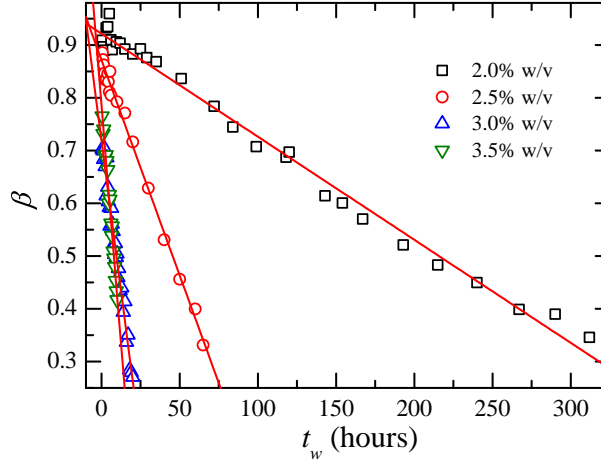


FIGURE 3.4: The stretching exponent, β , vs. waiting time, t_w , for 2.0% w/v (\square), 2.5% w/v (\circ), 3.0% w/v (\triangle) and 3.5% w/v (∇) Laponite suspensions. The solid lines are linear fits.

Because of the self-similar curvatures in the evolutions of both τ_1 (the monotonically increasing parts) and $\langle \tau_{ww} \rangle$, the data plotted in figure 3.2 can be superposed upon horizontal and vertical shifting. This is shown in figure 3.5(a). The corresponding shift factors (the horizontal shift factors for τ_1 and $\langle \tau_{ww} \rangle$ are denoted by t_β^∞ and t_α^∞ respectively, and the vertical shift factors for τ_1 and $\langle \tau_{ww} \rangle$ are denoted by τ_1^0 and $\langle \tau_{ww} \rangle^0$ respectively) are plotted in figure 3.5(b). It is observed that $\langle \tau_{ww} \rangle^0$ (\bullet in figure 3.5(b)) increases with Laponite concentration. This observation can be explained by considering that at higher concentrations, the particles are more easily confined in deep wells and can therefore be kinetically constrained at earlier times. If $q' = 1/t_\alpha^\infty$ is defined as a rate at which the system approaches the glass transition, it is seen from figure 3.6 that q' increases exponentially with concentration. This is connected to our observation that Laponite particles are trapped in progressively deeper energy wells as the Laponite concentration is increased. This again confirms that the sluggishness of the α -relaxation process increases with increasing Laponite concentration. In addition to τ_1 and τ_{ww} , β also shows superposition after appropriate shifting through a vertical shift factor (V) obtained as the value of β at $t_w/t_\alpha^\infty \rightarrow 0$. This is shown in figure 3.7.

The self-similarity and sharp enhancement of τ_1 and $\langle \tau_{ww} \rangle$ with increase in t_w

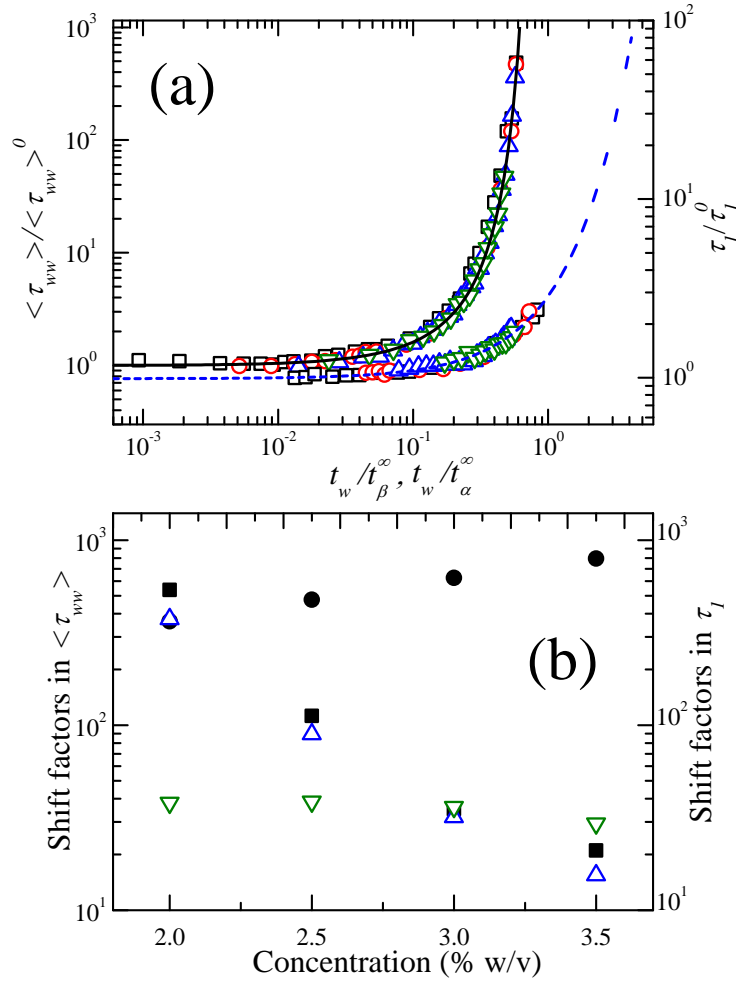


FIGURE 3.5: In (a), Superpositions of normalized τ_1 and normalized $\langle \tau_{ww} \rangle$ when plotted vs. t_w/t_β^∞ and t_w/t_α^∞ , respectively, for 2.0% w/v (\square), 2.5% w/v (\circ), 3.0% w/v (Δ) and 3.5% w/v (∇) Laponite suspensions. Dashed and solid lines are fits of normalized τ_1 and normalized $\langle \tau_{ww} \rangle$ to the modified Arrhenius and modified VFT functions (equations 3.2 and 3.3) respectively. In (b), the shift factors are plotted vs. Laponite concentration. The horizontal shift factors t_β^∞ (hours) and t_α^∞ (hours), corresponding to the fast and slow relaxation processes respectively, are denoted by Δ and \blacksquare , respectively. The vertical shift factors, τ_1^0 (μsec) and $\langle \tau_{ww} \rangle^0$ (μsec), are denoted by ∇ and \bullet , respectively.

are reminiscent of the changes that are observed in the fast (β) and slow (α) timescales of supercooled liquids that are quenched rapidly towards their glass transition temperatures T_g [1, 35]. In supercooled liquids, the fast relaxation shows an Arrhenius dependence on temperature T given by: $\tau_1 = \tau_1^0 \exp(E/k_B T)$. Here, τ_1^0 is the fast relaxation time when $T \rightarrow \infty$, E is the depth of the energy well associated with particle motion

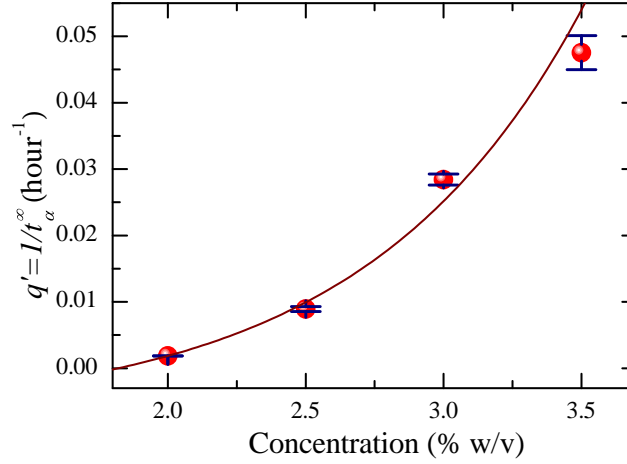


FIGURE 3.6: The rate $q'=(1/t_\alpha^\infty)$ at which the system approaches the glass transition is plotted vs. Laponite concentration. The solid line is an exponential fit.

within the cage and k_B is the Boltzmann constant. The slow α -relaxation time, which represents the timescale associated with cage diffusion in supercooled liquids, demonstrates a dependence on temperature T that is given by the Vogel-Fulcher-Tammann (*VFT*) law: $\langle \tau_{ww} \rangle = \langle \tau_{ww} \rangle^0 \exp(DT_0/(T - T_0))$. Here, the temperature T_0 at which $\langle \tau_{ww} \rangle$ diverges is called the Vogel temperature and D is the fragility of the material. The Arrhenius equation is, therefore, a special case of the *VFT* equation in the limit $T_0 \rightarrow 0$ [43]. Clearly, for nonzero values of T_0 , the slow timescale $\langle \tau_{ww} \rangle$ diverges more rapidly than the fast timescale τ_1 . In figure 3.5(a), we see a very similar situation, wherein $\langle \tau_{ww} \rangle$ diverges much more rapidly when compared to τ_1 . It can therefore be appreciated that the slowdown observed in aqueous Laponite suspensions is equivalent to that seen in supercooled liquids, with the inverse of the temperature ($1/T$) in the latter case mapped with the waiting time (t_w) in the former. In order to assess the validity of the proposed mapping, we write a modified Arrhenius equation:

$$\tau_1 = \tau_1^0 \exp(t_w/t_\beta^\infty) \quad (3.2)$$

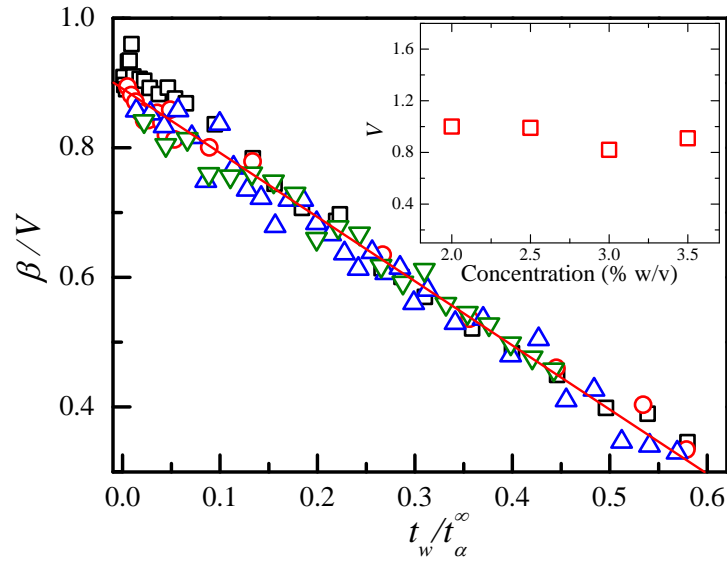


FIGURE 3.7: Superposition of the normalized stretching coefficients β when plotted vs. t_w/t_α^∞ for 2.0% w/v (\square), 2.5% w/v (\circ), 3.0% w/v (\triangle) and 3.5% w/v (∇) Laponite suspensions. The straight line is a linear fit. In the inset: vertical shift factor (V) vs. Laponite concentration.

Here, t_β^∞ is a characteristic timescale associated with the slowdown of the fast relaxation process. Similarly, the modified *VFT* equation for the mean α -relaxation time is written as:

$$\langle \tau_{ww} \rangle = \langle \tau_{ww} \rangle^0 \exp(Dt_w/(t_\alpha^\infty - t_w)), \quad (3.3)$$

where t_α^∞ is identified as a Vogel time and $\langle \tau_{ww} \rangle$ is calculated from the distribution of slow relaxation times $\rho_{ww}(\tau)$ which is obtained by inverting the stretched exponential part of the autocorrelation decay. D is the fragility index and will be discussed later. The expression for $\rho_{ww}(\tau)$ is given by [41],

$$\rho_{ww}(\tau) = -\frac{\tau_{ww}}{\pi\tau^2} \sum_{k=0}^{\infty} \frac{(-1)^k}{k!} \sin(\pi\beta k) \Gamma(\beta k + 1) \left(\frac{\tau}{\tau_{ww}}\right)^{\beta k + 1} \quad (3.4)$$

In equations 3.2 and 3.3, the inverse of temperature $1/T$ in the Arrhenius and the *VFT* forms for supercooled liquids is mapped with t_w and $1/T_0$ is mapped with t_α^∞ . It can be seen in figures 3.2 and 3.5(a) that equations 3.2 and 3.3 fit the time-evolution of the τ_1 and $\langle \tau_{ww} \rangle$ data extremely well.

It is to be noted that multispeckle autocorrelation decay data report an initial cage-forming regime followed by a power-law full-aging regime [18, 44]. While multispeckle spectroscopy probes the ballistic dynamics of Laponite particle rearrangements over longer timescales ($10^3 - 10^5$ s), the DLS data presented here probes the diffusive particle dynamics at much smaller timescales ($10^{-5} - 1$ s). In contrast to multispeckle spectroscopy, DLS is an extremely useful technique to estimate the faster relaxation times ($10^{-5} - 1$ s) of Laponite suspensions in the ergodic cage-forming regime. In the present work, a linear or power-law dependence of the slow relaxation time on the suspension waiting time, such as those seen in earlier reports using multispeckle techniques [18, 44], is absent. We note here that while we have restricted our observations to the ergodic cage-forming regime only, *i.e.* to a regime in which the autocorrelation functions decay fully and complex viscosity and Na^+ ion concentration increase with waiting time (figure 3.8). The multispeckle data reported earlier predominantly probed the ballistic dynamics in the full-aging regime.

In an activated process, the dependence of a characteristic timescale on temperature is used to calculate the activation energy associated with that relaxation phenomenon. For an Arrhenius relaxation process represented by $\tau_1 = \tau_1^0 \exp(E/k_B T)$, E is the activation energy and k_B is the Boltzmann constant. For a VFT relaxation process described by $\langle \tau_{ww} \rangle = \langle \tau_{ww} \rangle^0 \exp(DT_0/(T - T_0))$, the apparent activation energy is given by: $E_{VFT} = k_B d(\ln \tau)/d(1/T) = k_B D T_0^2 / (T - T_0)^2$ [2, 45]. The activation energies associated with the modified Arrhenius and VFT processes in aging Laponite suspensions can be estimated by comparing with the corresponding relations for a supercooled liquid, with $1/T$ mapped with t_w and $1/T_0$ with t_α^∞ . These calculations yield the following results:

$$E = (k_B c_1) / t_\beta^\infty \quad (3.5)$$

and

$$E_{VFT} = (k_B c_2) [D t_\alpha^\infty / (t_\alpha^\infty - t_w)^2] \quad (3.6)$$

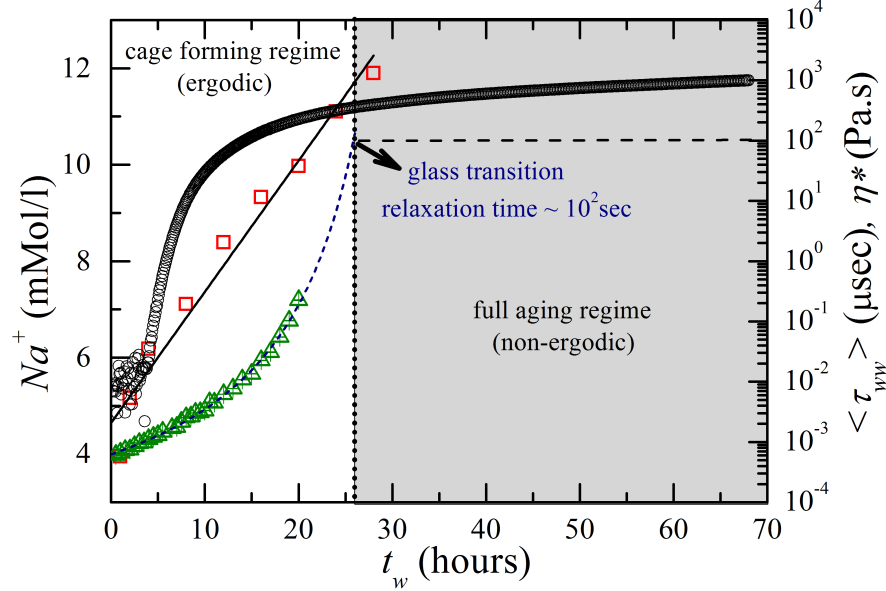


FIGURE 3.8: The simultaneous time-evolution of the sodium ion concentration (\square), the complex viscosity (\circ) and the mean slow relaxation time (Δ) of a 3.0% w/v Laponite sample. The vertical dotted line indicates the glass transition as defined in [3].

Here, equation 3.5 represents activation energy (E) associated with τ_1 , while equation 3.6 represents the apparent activation energy (E_{VFT}) associated with $\langle \tau_{ww} \rangle$. In these equations, k_B is the Boltzmann constant, D is the fragility parameter, and c_1 and c_2 are constants with dimensions $[\text{time}] \times [\text{temperature}]$. It can be seen in the inset of figure 3.9 that the activation energy E associated with τ_1 is independent of t_w and shows a power-law dependence on c , the concentration of Laponite ($E \propto c^{5.7 \pm 0.3}$). E_{VFT} associated with $\langle \tau_{ww} \rangle$, on the other hand, remains constant at small t_w ($\ll t_w^\infty$), but shows a strong dependence on t_w for large t_w . In addition, E_{VFT} shifts to smaller waiting times with increase in concentration of Laponite. This agrees with our earlier results that Laponite suspensions of higher concentrations are driven faster towards an arrested state. Furthermore, our data implies that the evolution of the potential energy landscape with increasing t_w is governed only by the α -relaxation process. The self-similar nature of E_{VFT} with changes in Laponite concentration is apparent when the data is scaled appropriately (figure 3.10(a)). The same horizontal shift factor t_w^∞ , used

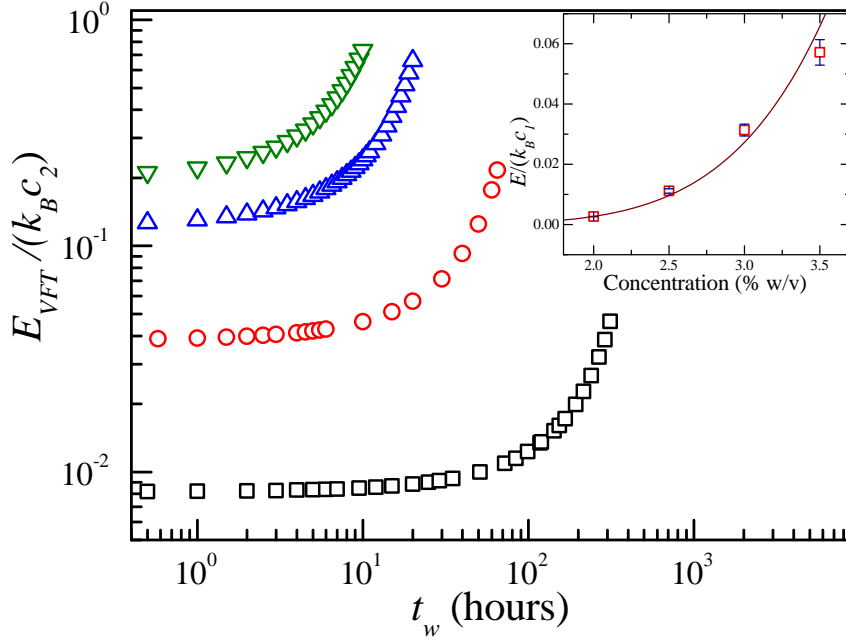


FIGURE 3.9: The normalized apparent activation energy ($E_{VFT}/k_B c_2$) associated with the α -relaxation process vs. waiting time (t_w) for 2.0% w/v (\square), 2.5% w/v (\circ), 3.0% w/v (\triangle) and 3.5% w/v (∇) Laponite suspensions. In the inset, the normalized activation energy associated with the β -relaxation process ($E/k_B c_1$) is plotted vs. Laponite concentration c . The solid line is a power law fit ($E = c^{5.7 \pm 0.3}$).

earlier to superpose the $\langle \tau_{ww} \rangle$ data, is also used here.

Following the definition proposed by Angell for supercooled liquids, we define the glass transition time t_g as the time since sample preparation at which $\langle \tau_{ww} \rangle = 100$ seconds for each Laponite concentration [3]. The Angell plot corresponding to the α -process of Laponite suspensions is shown in figure 3.10(b). Our data shows the same behaviour expected for fragile supercooled liquids (shown by the dotted line, where $1/T$ is mapped onto t_w , as discussed in equations 3.2 and 3.3). The straight dashed line corresponds to strong glassformers for which the α -relaxation timescale shows Arrhenius behavior. Furthermore, it is observed that the value of the fragility index D remains almost constant over the Laponite concentration range explored here (inset of figure 3.10(b)). It has been pointed out earlier that caged particles can get trapped in deeper energy wells with increase in the concentration of a glassformer [46]. However,

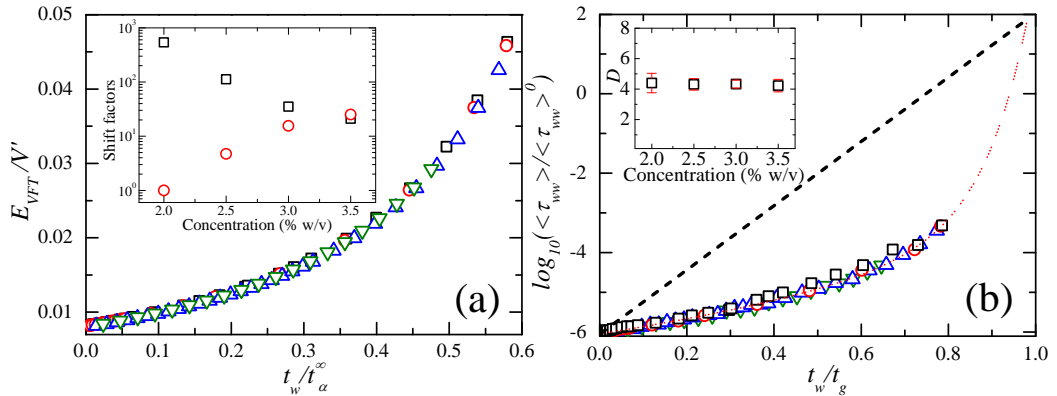


FIGURE 3.10: (a) Superposition of the normalized apparent activation energies (E_{VFT}) associated with the α -relaxation process is plotted as a function of (t_w/t_α^∞) for 2.0% w/v (\square), 2.5% w/v (\circ), 3.0% w/v (\triangle) and 3.5% w/v (∇) Laponite suspensions. Inset shows the horizontal (t_α^∞ denoted by \square) and vertical (V' denoted by \circ) shift factors vs. Laponite concentration. (b) Angell plot for 2.0% w/v (\square), 2.5% w/v (\circ), 3.0% w/v (\triangle) and 3.5% w/v (∇) Laponite suspensions. The dashed diagonal straight line is the Angell plot for strong supercooled liquids, while the dotted curve is for a fragile glassformers. In the inset, fragility index (D) is plotted vs. concentration of Laponite suspensions.

our observation that D is independent of Laponite concentration suggests that the overall topology of the potential energy landscape of aging Laponite suspensions remains unchanged even when Laponite concentration is changed [35].

The simultaneous enhancements of the fast and slow timescales at high t_w (figures 3.2 and 3.5) suggests the possibility that both these processes are strongly correlated with each other. In figure 3.11, the timescale t_β^∞ associated with the fast relaxation process and obtained from fits to equation 3.2 is plotted vs. the glass transition time t_g . It is observed that these two timescales are strongly coupled. A linear fit to the data (solid line in figure 3.11) yields $t_\beta^\infty = (1.10 \pm 0.05)t_g$. It should be noted that for supercooled liquids, the activation energy associated with the β -relaxation process was demonstrated to be proportional to the glass transition temperature T_g , with the exact relationship being given by $E_\beta = (24 \pm 3)RT_g$, where R is the universal gas constant [10–12]. The fast relaxation process in Laponite glasses has previously been identified as a β -relaxation process [25]. The coupling between t_β^∞ and t_g seen in figure 3.11 is

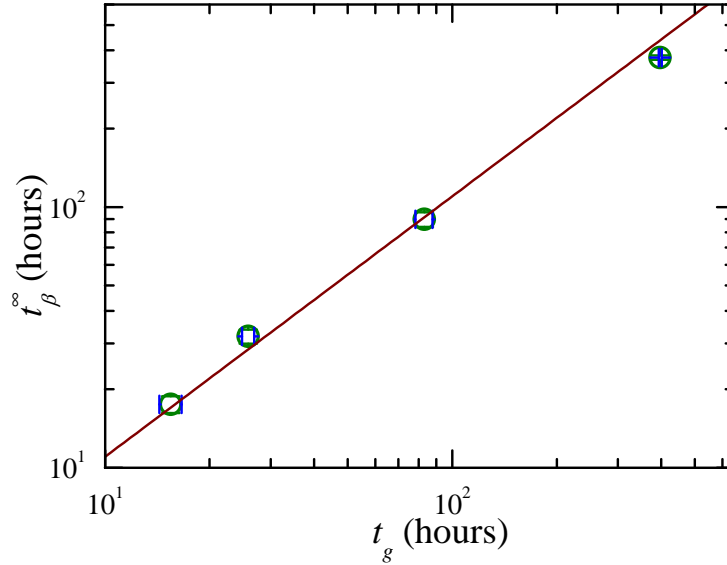


FIGURE 3.11: The fast relaxation timescale t_{β}^{∞} vs. the glass transition time t_g (from left to right - 3.5% w/v, 3.0% w/v, 2.5% w/v and 2.0% w/v). The solid line ($t_{\beta}^{\infty} \approx (1.10 \pm 0.05)t_g$) is a linear fit passing through origin.

not new in the context of the relaxation dynamics in supercooled liquids. The Johari-Goldstein (JG) β -relaxation seen in supercooled liquids, for example, is seen to be coupled with the α -relaxation [9–12]. Using ultrasound attenuation spectroscopy, Ali *et. al.* demonstrated the fragmentation of Laponite tactoids comprising more than one Laponite platelet, in addition to the slow absorption of one or two layers of water by these tactoids [33]. Both these processes contribute to an increase in the effective volume fraction and can result in the observed slowdown of the fast relaxation process. We would like to point out here that the fragmentation of clusters into smaller entities is verified by the DLS results reported here (shaded region in figure 3.2(a)). Both the relaxation processes reported here therefore slow down due to an increase in effective volume fraction, which explains the observed coupling between them.

The linear decrease of β with t_w (figures 3.4 and 3.7) as the Laponite suspensions approach the glass transition is similar to the observation in fragile supercooled liquids (such as *o*-terphenyl mixtures [47]) where β decreases linearly with $1/T$ while approaching its glass transition. This shows that the mapping between the waiting time

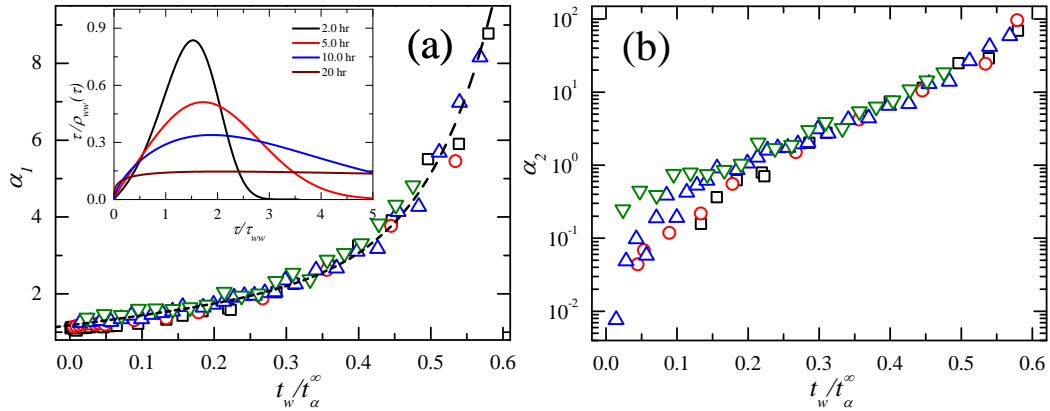


FIGURE 3.12: (a). Width parameter α_1 vs. t_w/t_α^∞ for 2.0% w/v (\square), 2.5% w/v (\circ), 3.0% w/v (\triangle) and 3.5% w/v (∇) Laponite suspensions. In the inset: distributions of the α -relaxation timescales plotted for 3.0% w/v Laponite suspension at 2 hr, 5 hr, 10 hr and 20 hr (from top to bottom). (b) The non-Gaussian parameter α_2 vs. t_w/t_α^∞ for 2.0% w/v (\square), 2.5% w/v (\circ), 3.0% w/v (\triangle) and 3.5% w/v (∇) Laponite suspensions.

of a Laponite suspension in the cage-forming regime and the inverse of the temperature of a supercooled liquid is valid even though the mechanism by which the glass transition is approached is totally different in these two cases.

We now analyze the distributions of the α -relaxation timescales for various Laponite concentrations. The distributions of the α -relaxation timescales for a 3.0% w/v Laponite suspension, $\rho_{ww}(\tau)$, at four different t_w values (2 hr, 5 hr, 10 hr and 20 hr) are estimated using equation 3.4 and are plotted in the inset of figure 3.12(a). In all the samples studied, the distributions broaden significantly with increasing waiting time t_w . We define a width parameter $\alpha_1 = \langle \tau_{ww}^2 \rangle - \langle \tau_{ww} \rangle^2 / \langle \tau_{ww} \rangle^2$ as a measure of the broadening of $\rho_{ww}(\tau)$. The calculated values of α_1 are seen to superpose when plotted vs. t_w/t_α^∞ for all the Laponite concentrations in figure 3.12(a).

We next calculate the non-Gaussian parameter $\alpha_2 = (3\langle \tau_{ww}^4 \rangle / 5\langle \tau_{ww}^2 \rangle^2) - 1$ associated with the distribution $\rho_{ww}(\tau)$ of the α -relaxation timescales. In figure 3.12(b), α_2 , when plotted vs. t_w/t_α^∞ , is seen to superpose for all four Laponite concentrations. It is seen that α_2 is very small when t_w is small. However, α_2 increases sharply at higher t_w for all four Laponite concentrations. In all the superpositions presented here, it is observed that the horizontal shift factor t_α^∞ decreases rapidly with increasing Laponite

concentration (figure 3.5(b) and the inset of figure 3.10(a)). The observed superpositions of α_1 and α_2 , which is achieved without any vertical shift for all the Laponite concentrations, is an additional verification of the self-similarity of the dynamical slowing down process.

3.4 Conclusions

In this work, we have extracted the primary and secondary relaxation timescales of aging Laponite suspensions by modeling the intensity autocorrelation functions obtained from dynamic light scattering measurements. We have compared the dynamical slowing down process of these samples with the slowing down observed in fragile supercooled liquids. While colloidal suspensions of Laponite approach the glass transition spontaneously with increasing waiting time t_w , supercooled liquids are obtained by quenching the temperature of a liquid towards its glass transition temperature at a rate that is rapid enough to avoid crystallization. It is proposed in the literature that the faster β -relaxation process of a supercooled liquid exhibits an Arrhenius temperature-dependence, while the slower α -relaxation time exhibits a *VFT* temperature-dependence [1]. The work reported in this chapter demonstrates the remarkable similarities that exist in the relaxation processes of soft colloidal suspensions approaching dynamical arrest and fragile supercooled liquids approaching the glass transition temperature. This is done by performing a simple one-to-one mapping between the waiting time since filtration of an aging Laponite suspension and the inverse of the thermodynamic temperature of a supercooled liquid ($t_w \leftrightarrow 1/T$).

We have identified the secondary and the primary relaxation processes of aging Laponite suspensions with, respectively, the β and the α -relaxation processes of fragile supercooled liquids. We observe here that the secondary relaxation time of aging Laponite suspensions exhibits exponential dependence on waiting times and is strongly coupled with α -relaxation process. This kind of coupling with the α -relaxation process is seen for the Johari-Goldstein β -relaxation process reported for supercooled liquids

in polarization-sensitive measurements. Furthermore, we have shown that the evolutions of both the primary and secondary relaxation processes are self-similar with increasing Laponite concentration. Our estimates for the apparent activation energy corresponding to the α -relaxation process, the widths of the distributions of the α -relaxation timescales and the non-Gaussian parameters characterizing these distributions also confirm the self-similar dynamics of Laponite suspensions with increasing Laponite concentrations.

A simple relation is known to exist between the glass transition temperature T_g and energy scale E (the activation energy corresponding to the β relaxation process) of supercooled liquids. In this work, we have calculated the glass transition time t_g [3], and have defined a new timescale corresponding to the secondary relaxation process, t_β^∞ , to characterize the dynamical slowing down process in Laponite suspensions. We demonstrate the existence of a relationship between these timescales that is strongly reminiscent of the relationship that was established between the glass transition temperature and the energy scale corresponding to the β -relaxation process of supercooled liquids approaching their glass transitions.

A comparison of our data with the results obtained for suspensions of hard spheres near the glass transition shows that a suspension of Laponite platelets evolves in the same way with increasing waiting time as a suspension of hard spheres whose volume fraction is increased towards the random close packing fraction of $\phi_c = 0.638$ [14]. It has been noted earlier that the particle exfoliation process and the inter-platelet interactions in aging Laponite suspensions evolve spontaneously with waiting time, resulting in an increase in the effective volume fraction and a simultaneous decrease in the accessible volume available to the system. This eventually leads to dynamical arrest. In the present case, the increase of the volume fraction is driven by a very complex interplay between the fragmentation/exfoliation process, and the evolution of the sodium ion concentration, which results in an evolution of the inter-particle interaction. It has been observed that precise experimental determination of volume fractions of colloidal suspensions remains a challenging problem [48]. In hard sphere suspensions,

the volume fraction plays the same qualitative role as the inverse of temperature in the glass transition of molecular glasses and supercooled liquids [13, 14]. The mapping ($t_w \leftrightarrow 1/T$) established here demonstrates that aging Laponite suspensions, hard sphere glasses and fragile supercooled liquids approach their glass transitions in very similar manners, thereby confirming that aqueous suspensions of Laponite are model glass formers.

References

- [1] W. Gotze and L. Sjogren, *Rep. Prog. Phys.*, **55**, 241-376 (1992).
- [2] M. D. Ediger, C. A. Angell and S. R. Nagel, *J. Phys. Chem.*, **100**, 13200-13212 (1996).
- [3] C. A. Angell, *J. Non-Cryst. Solids*, **131-133**, 13-31 (1991).
- [4] C. A. Angell, *J. Phys. and Chem. of Solids*, **49**, 863-871 (1988).
- [5] G. Adam and J. H. Gibbs, *J. Chem. Phys.*, **43**, 139-146 (1965).
- [6] G. P. Johari and M. Goldstein, *J. Chem. Phys.*, **53**, 2372-2388 (1970).
- [7] G. P. Johari and M. Goldstein, *J. Chem. Phys.*, **55**, 4245-4252 (1971).
- [8] M. S. Thayyil, S. Capaccioli, D. Prevosto and K. L. Ngai, *Phil. Mag.*, **88**, 4007-4013 (2008).
- [9] K. L. Ngai, *J. Chem Phys.*, **109**, 6982-6994 (1998).
- [10] A. Kudlik, C. Tschirwitz, S. Benkhof, T. Blochowicz and E. Rössler, *Europhys. Lett.*, **40**, 649-654 (1997).
- [11] A. Kudlik, C. Tschirwitz, T. Blochowicz, S. Benkhof, E. Rössler, *J. Non-Cryst. Solids*, **235**, 406-411 (1998).

-
- [12] S. Vyazovkin and I. Dranca, *Pharm. Res.*, **23**, 422-428 (2006).
- [13] P. N. Pusey and W. van Megen, *Nature*, **320**, 340-342 (1986).
- [14] L. Marshall and C. F. Zukoski, *J. Phys. Chem.*, **94**, 1164-1171 (1990).
- [15] D. Bonn, H. Tanaka, G. Wegdam, H. Kellay and J. Meunier, *Europhys. Lett.*, **45**, 52-57 (1999).
- [16] B. Ruzicka, L. Zulian and G. Ruocco, *J. Phys.: Condens. Matter*, **16**, S4993-S5002 (2004).
- B. Ruzicka, L. Zulian and G. Ruocco, *Phys. Rev. Lett.*, **93**, 258301 (2004).
- [17] B. Ruzicka and E. Zaccarelli, *Soft Matter*, **7**, 1268-1286 (2011).
- [18] R. Bandyopadhyay, D. Liang, H. Yardimci, D. A. Sessoms, M. A. Borthwick, S. G. J. Mochrie, J. L. Harden and R. L. Leheny, *Phys. Rev. Lett.*, **93**, 228302 (2004).
- [19] F. Schosseler, S. Kaloun, M. Skouri and J. P. Munch, *Phys. Rev. E*, **73**, 021401 (2006).
- [20] S. Kaloun, R. Skouri, M. Skouri, J. P. Munch and F. Schosseler, *Phys. Rev. E*, **72**, 011403 (2005).
- [21] H. Tanaka, S. Jabbari-Farouji, J. Meunier and D. Bonn, *Phys. Rev. E*, **71**, 021402 (2005).
- [22] A. Shahin and Y. M. Joshi, *Langmuir*, **28**, 15674-15686 (2012).
- [23] A. S. Negi and C. O. Osuji, *Phys. Rev. E*, **82**, 031404 (2010).
- [24] R. Angelini, L. Zulian, A. Fluerasu, A. Madsen, G. Ruocco and B. Ruzicka, *Soft Matter*, **9**, 10955 (2013).
- [25] B. Abou, D. Bonn and J. Meunier, *Phys. Rev. E*, **64**, 021510 (2001).

-
- [26] A. Shahin and Y. M. Joshi, *Phys. Rev. Lett.*, **106**, 038302 (2011).
- [27] L. C. E. Struik, *Physical aging in amorphous polymers and other materials*, (Elsevier, Houston, 1978).
- [28] T. P. Dhavale, S. Jadav and Y. M. Joshi, *Soft Matter*, **9**, 7751-7756 (2013).
- [29] A. J. Kovacs, *J. Polym. Sci.*, **30**, 131-147 (1956).
- [30] D. R. Strachan, G. C. Kalur and S. R. Raghavan, *Phys. Rev. E*, **73**, 041509 (2006).
- [31] D. J. Lacks and M. J. Osborne, *Phys. Rev. Lett.*, **93**, 255501 (2004).
- [32] R. Bandyopadhyay, P. H. Mohan and Y. M. Joshi, *Soft Matter*, **6**, 1462-1466 (2010).
- [33] S. Ali and R. Bandyopadhyay, *Langmuir*, **29**, 12663-12669 (2013).
- [34] R. Bandyopadhyay, D. Liang, J. L. Harden and R. L. Leheny, *Solid State Comm.*, **139**, 589-598 (2006).
- [35] F. H. Stillinger, *Science*, **267**, 1935-1939 (1995).
- [36] F. Sciortino, C. D. Michele, S. Corezzi, J. Russo, E. Zaccarelli and P. Tartaglia, *Soft Matter*, **5**, 2571-2575 (2009).
- [37] B. Ruzicka, E. Zaccarelli, L. Zulian, R. Angelini, M. Sztucki, A. Moussad, T. Narayanan and F. Sciortino, *Nat. Mater.*, **10**, 56-60 (2011).
- [38] P. Agarwal, S. Srivastava and L. A. Archer, *Phys. Rev. Lett.*, **107**, 268302 (2011).
- [39] B. Ruzicka, L. Zulian, E. Zaccarelli, R. Angelini, M. Sztucki, A. Moussaid and G. Ruocco, *Phys. Rev. Lett.*, **104**, 085701 (2010).
- [40] K. Miyazaki, H. M. Wyss, D. A. Weitz and D. R. Reichman, *Europhys. Lett.*, **75**, 915-921 (2006).
- [41] C. P. Lindsey and G. D. Patterson, *J. Chem. Phys.*, **73**, 3348-3357 (1980).

- [42] Y. M. Joshi, *J. Chem. Phys.*, **127**, 081102 (2007).
- [43] R. G. Larson, *The structure and rheology of complex fluids*, Clarendon Press: Oxford, **1999**.
- [44] M. Bellour, A. Knaebel, J. L. Harden, F. Lequeux and J. P. Munch, *Phys. Rev. E*, **67**, 031405 (2003).
- [45] M. T. Shaw and W. J. MacKnight, *Introduction to polymer viscoelasticity*, Wiley-Interscience, John Wiley & Sons, 205, pp. 271.
- [46] M. Goldstein, *J. Chem. Phys.*, **51**, 3728 (1969)).
- [47] P. K. Dixon and S. R. Nagel, *Phys. Rev. Lett.*, **61**, 341-344 (1988).
- [48] W. C. K. Poon, E. R. Weeks and C. P. Royall, *Soft Matter*, **8**, 21-30 (2012).

4

Effects of physicochemical interactions on the aging dynamics of colloidal suspensions of Laponite

4.1 Introduction

Interparticle interactions in colloidal dispersions determine their microstructures, which, in turn, influence their physical properties. In the limit of small concentrations, colloidal particles scarcely interact with each other, with the dispersions existing in the liquid state. Upon increasing the concentration, enhanced interparticle interactions can lead to self-assembled structures that strongly depend upon the charges and the shapes of the particles [1, 2]. The complexity of the structure is expected to increase if the particles possess dissimilar charges and anisotropic shapes [3]. Moreover, in some cases,

the spontaneously formed structures may not be in thermodynamic equilibrium and can continue to evolve with time over the observation timescales [4]. In this chapter, we study the relaxation dynamics of aqueous colloidal dispersions of the smectite clay Laponite. Laponite particles are characterized by their anisotropic shapes, dissimilar charges and time dependent structures in aqueous suspensions even at very small particle concentrations [3].

A series of rheological studies were carried out by Shahin and Joshi on Laponite suspensions [5–7]. They monitored the evolution of the elastic moduli of the suspensions as a function of time for different control variables, *viz.* Laponite concentration (C_L), externally added salt (C_S), temperature (T) and the time, t_i , at which shear melting was carried out after preparation of the Laponite suspension. Due to the weak sample microstructure expected during the first few days after sample preparation, the authors explored the aging behavior of only older samples ($t_i \geq 7$ days for Laponite suspensions without externally added salt and $t_i < 7$ days for suspensions with high concentrations of externally added salt) [5]. This study reveals that older shear-melted suspensions have larger elastic moduli than the younger shear-melted ones. This indicates that the permanent structures in aged Laponite suspensions cannot be destroyed even by applying very large shear deformations. For the older samples, therefore, the aging dynamics subsequent to shear-melting begins at a matured low energy level. The evolution of the elastic modulus was observed to take place at a faster rate with increase in C_L , C_S and T , indicating that the process of structure buildup is faster for increasing values of these three variables. Finally, ionic conductivity was also measured as a function of these variables and it was demonstrated that the Debye screening lengths of Laponite suspensions decrease with increase in Laponite and salt concentrations. The interparticle interaction between two approaching parallel plates was estimated using DLVO (Derjagun-Landau-Verwey-Overbeek) theory for various electrostatic screening conditions. It was observed that increasing the concentrations of particles and salt and the sample temperature increases the heights of the repulsive energy barriers while simultaneously decreasing their widths. The observations in [5] can be understood in

terms of the dissociation of Na^+ ions from the faces of the Laponite particles which increases the electronegativity of each particle face and induces an attraction between the edges and the faces of the Laponite discs. These results therefore clearly emphasize that the influence of attractive interactions in older Laponite suspensions cannot be ignored and are in close agreement with the observations of Ruzicka and co-workers [8].

In this chapter, we employ dynamic light scattering (DLS) to study the relaxation dynamics of Laponite suspensions whose ages are much smaller than those in Shahin and Joshi's work [5]. These dynamics are studied as a function of the concentrations of Laponite (C_L) and salt (C_S) and the sample temperature (T). The spontaneously evolving Laponite suspensions used here are less than three days old (aging time or waiting time, $t_w < 3$ days) and therefore can be classified as comparatively younger than the samples used in [5]. The present study, therefore complements the rheological studies performed on the much older samples [5]. We extract the evolution of the relaxation dynamics of Laponite suspensions from our DLS data to understand the complex aging dynamics of the samples. To gain further insight into the dynamics and microstructures, we measure the ionic strengths of the samples and analyze the physicochemical interactions in Laponite suspensions using the DLVO theory.

4.2 Sample preparation and experimental methods

All the experiments reported in this chapter are done using Laponite RD[®]. The details of preparation of Laponite suspensions are given in chapter 3. A sodium chloride (NaCl procured from Sigma-Aldrich) solution of a predetermined concentration is added to the filtered Laponite suspension using a pipette. The suspension is vigorously stirred during addition of the salt solution. The sample is then filled and sealed properly in a cuvette for the DLS experiments. The waiting time or the aging time t_w is calculated from the moment the sample is sealed. The measure of concentration in %

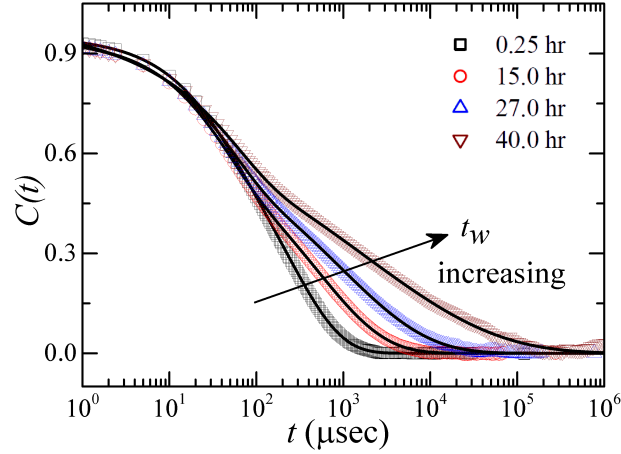


FIGURE 4.1: The normalized intensity autocorrelation functions $C(t)$, vs. the delay time t , at 15°C and scattering angle $\theta = 90^\circ$, for 3.0% w/v Laponite suspension with 0.05 mM salt at several t_w . The solid lines are fits to equation 4.1.

w/v refers to the weight of Laponite in grams that is mixed in 100 ml (100 gm) of Millipore water. Details of the experimental techniques (DLS and sodium ion concentration measurement) used to perform the experiments are described in chapter 2.

4.3 Results and discussions

The evolution of the relaxation time of an aging Laponite suspension is estimated by analyzing the intensity autocorrelation function $g^{(2)}(t)$ for different waiting times, t_w , after the sample is sealed in the cuvette. The normalized intensity autocorrelation function, $C(t) = g^{(2)}(t) - 1$, as a function of delay time t , for a 3.0% w/v Laponite suspension with 0.05 mM salt concentration at 15°C is plotted in figure 4.1 for different waiting times t_w . It is observed from figure 4.1 that the decay in $C(t)$ slows down with increasing t_w . Furthermore, $C(t)$ exhibits a two-step decay which is typical of glass-forming materials as they approach the glass transition [9] and is discussed in detail in the previous chapters.

For a molecular glass former where the glass transition is driven by a rapid decrease in temperature, the faster β -relaxation process shows an Arrhenius temperature dependence, while the slower structural α -relaxation process exhibits a Vogel-Fulcher-Tammann (VFT) temperature dependence [10–12]. In chapter 3, it was shown that the glass transition of spontaneously evolving Laponite suspensions is waiting time (t_w) driven and can be compared to the glass transition of supercooled liquids by a one-to-one mapping between the waiting time (t_w) of the former and the inverse of the temperature ($1/T$) of the latter [13]. The two-step relaxation in $C(t)$ shown in figure 4.1 can be expressed in the following way [13–15]:

$$C(t) = [a \exp\{-t/\tau_1\} + (1 - a) \exp\{-(t/\tau_{ww})^\beta\}]^2 \quad (4.1)$$

Equation 4.1 fits all the autocorrelation data acquired in DLS experiments for Laponite suspensions characterized by different C_L , C_S and T . In all the fits, a , τ_1 , τ_{ww} and β as the fitting parameters. It is seen from the fits that the relaxation time τ_1 associated with the exponential relaxation process are always faster than the slow relaxation time τ_{ww} . τ_1 is therefore associated with the fast relaxation process of the soft glassy Laponite suspension and is believed to arise from the motion of particles within cages formed by their neighbors [16]. The intercept a is a measure of the relative strength of this fast relaxation process. The slow non-exponential relaxation process, which yields the slow relaxation time τ_{ww} , is associated with the cooperative diffusion of a particle out of its cage [13, 14, 17]. The mean value of τ_{ww} is defined by $\langle \tau_{ww} \rangle = (\tau_{ww}/\beta)\Gamma(1/\beta)$ [18], where β is the stretching exponent ($\beta < 1$) and Γ is the Euler Gamma function.

In figure 4.2(a), $\langle \tau_{ww} \rangle$ is plotted as a function of t_w for Laponite suspensions of several different C_L , and $C_S = 0.05$ mM at $T = 25^\circ\text{C}$. It is apparent from the figure that the time-evolutions of $\langle \tau_{ww} \rangle$ possess self-similar curvatures at different Laponite concentrations. The superposition of the slow relaxation times that is achieved by suitably normalizing both axes by shift factors for different concentrations is shown in figure 4.3(a). The horizontal and vertical shift factors are plotted in figure 4.3(b). In

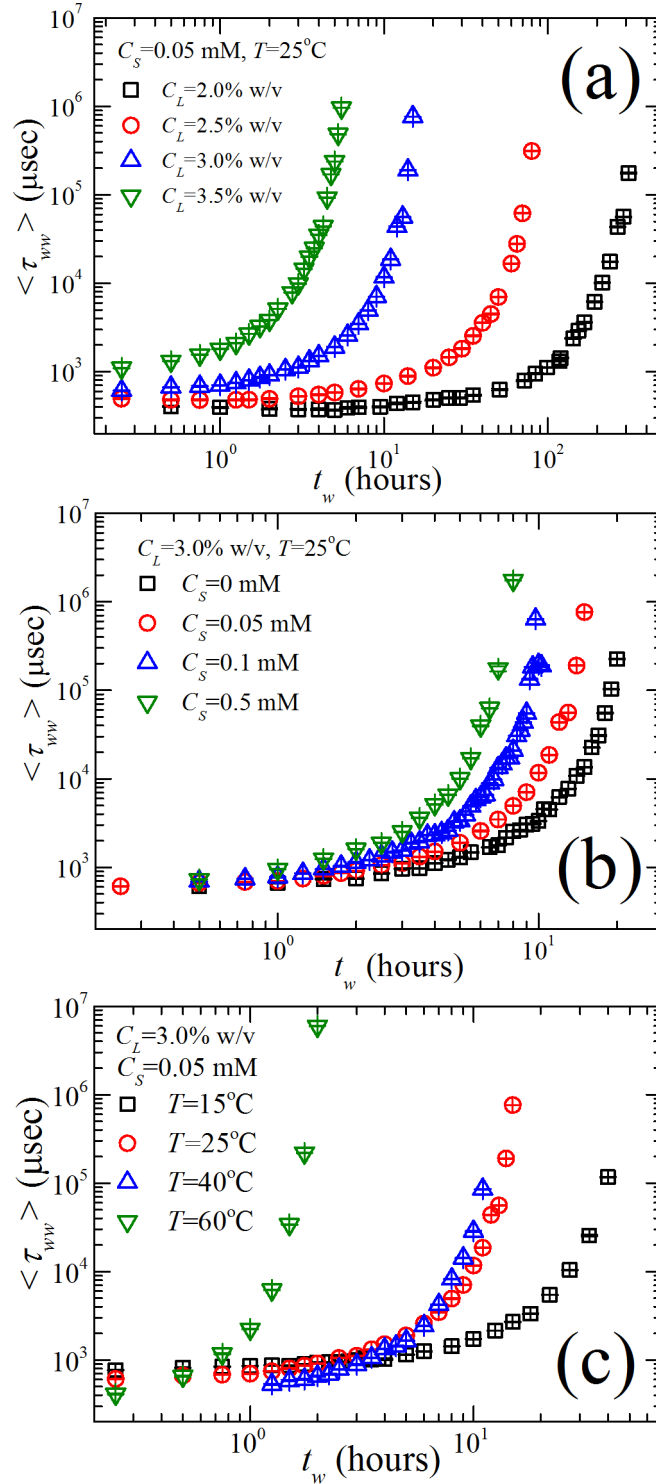


FIGURE 4.2: Mean slow relaxation times $\langle \tau_{ww} \rangle$, obtained by fitting the $C(t)$ data to equation 4.1, are plotted vs. t_w for different C_L , C_S and T values in (a)-(c).

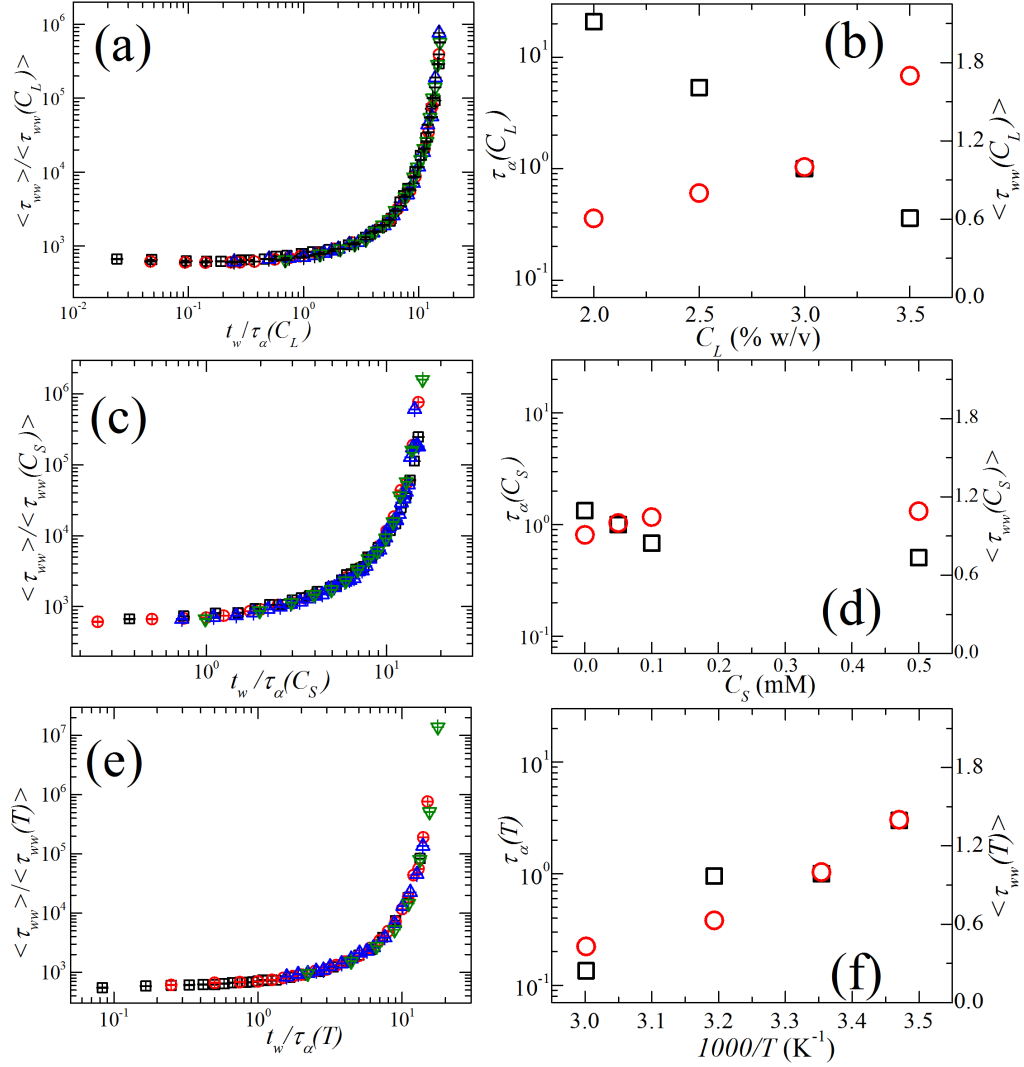


FIGURE 4.3: (a) Superposition of mean slow relaxation times $\langle \tau_{ww} \rangle / \langle \tau_{ww}(C_L) \rangle$ is shown vs. $t_w / \tau_\alpha(C_L)$ for four different Laponite concentrations ($C_L = 2.0\%$ w/v (□), 2.5% w/v (○), 3.0% w/v (△) and 3.5% w/v (∇)) with 0.05 mM salt at 25°C . (b) Horizontal and vertical shift factors, $\tau_\alpha(C_L)$ (□) and $\langle \tau_{ww}(C_L) \rangle$ (○) respectively, are plotted vs. C_L . (c) Superposition of mean slow relaxation times $\langle \tau_{ww} \rangle / \langle \tau_{ww}(C_S) \rangle$ is shown vs. $t_w / \tau_\alpha(C_S)$ for 3.0% w/v Laponite suspensions with four different salt concentrations ($C_S = 0$ mM (□), 0.05 mM (○), 0.1 mM (△) and 0.5 mM (∇)) at 25°C . (d) Horizontal and vertical shift factors, $\tau_\alpha(C_S)$ (□) and $\langle \tau_{ww}(C_S) \rangle$ (○) respectively, are plotted vs. C_S . (e) Superposition of mean slow relaxation times $\langle \tau_{ww} \rangle / \langle \tau_{ww}(T) \rangle$ is shown vs. $t_w / \tau_\alpha(T)$ for 3.0% w/v Laponite suspensions with 0.05 mM salt and at four different temperatures ($T = 15^\circ\text{C}$ (□), 25°C (○), 40°C (△) and 60°C (∇)). (f) Horizontal and vertical shift factors, $\tau_\alpha(T)$ (□) and $\langle \tau_{ww}(T) \rangle$ (○) respectively, are plotted vs. inverse of temperature ($1000/T$).

figure 4.2(b), we plot $\langle \tau_{ww} \rangle$ vs. t_w for Laponite suspensions having different C_S with $C_L = 3.0\%$ w/v at $T = 25^\circ\text{C}$, while in figure 4.2(c), we plot the evolutions of $\langle \tau_{ww} \rangle$ with t_w for Laponite suspensions of $C_L = 3.0\%$ and $C_S = 0.05$ mM at several T values. Clearly, all the plots in figures 4.2(b) and (c) also show self-similar curvatures. The superpositions of the above data with changing C_S and T are plotted in figures 4.3(c) and (e) respectively and the corresponding shift factors used for the superpositions are shown in figures 4.3(d) and (f) respectively.

Similar to the data for $\langle \tau_{ww} \rangle$, τ_1 and β are also observed to be very sensitive to C_L , C_S and T (figures 4.4 and 4.5). A comparison of the data in figures 4.2 and 4.4 reveals that the increase in $\langle \tau_{ww} \rangle$ with t_w is much stronger than for τ_1 for all the samples investigated here. This results in a separation of the α and β relaxation timescales as the sample ages, with the two-step relaxation process being very clearly visible for the older samples (figure 4.1). It is seen from figure 4.5 that β decreases linearly with t_w when C_L , C_S and T are changed. As in the case of $\langle \tau_{ww} \rangle$, τ_1 and β also show self-similar time evolutions when C_L , C_S and T are varied. This is seen in figures 4.6(a)-(f) and figures 4.7(a)-(f), where the superimposed time-evolution curves and the horizontal and vertical shift factors used to obtain the superpositions are plotted. It is important to note that the time-evolutions of $\langle \tau_{ww} \rangle$, τ_1 and β shift to smaller waiting times with increase in C_L , C_S and T . Interestingly, for a given C_L , C_S and T , the horizontal shift factors used to superpose the $\langle \tau_{ww} \rangle$ and β data (plotted in figures 4.3 and 4.7) are approximately the same.

In figure 4.8(a), we plot the comprehensive Laponite concentration - salt concentration - temperature - time superpositions of the $\langle \tau_{ww} \rangle$ data (figure 4.2). Similar comprehensive overlaps are also observed for τ_1 (figure 4.4) and β (figure 4.5), and are shown in figure 4.8. The excellent superpositions suggest that the temporal evolutions of the relaxation processes in Laponite suspensions are self-similar when C_L , C_S and T are varied, indicating that the underlying energy landscapes remain self-similar when these variables are changed. These results are similar to the ones reported earlier for

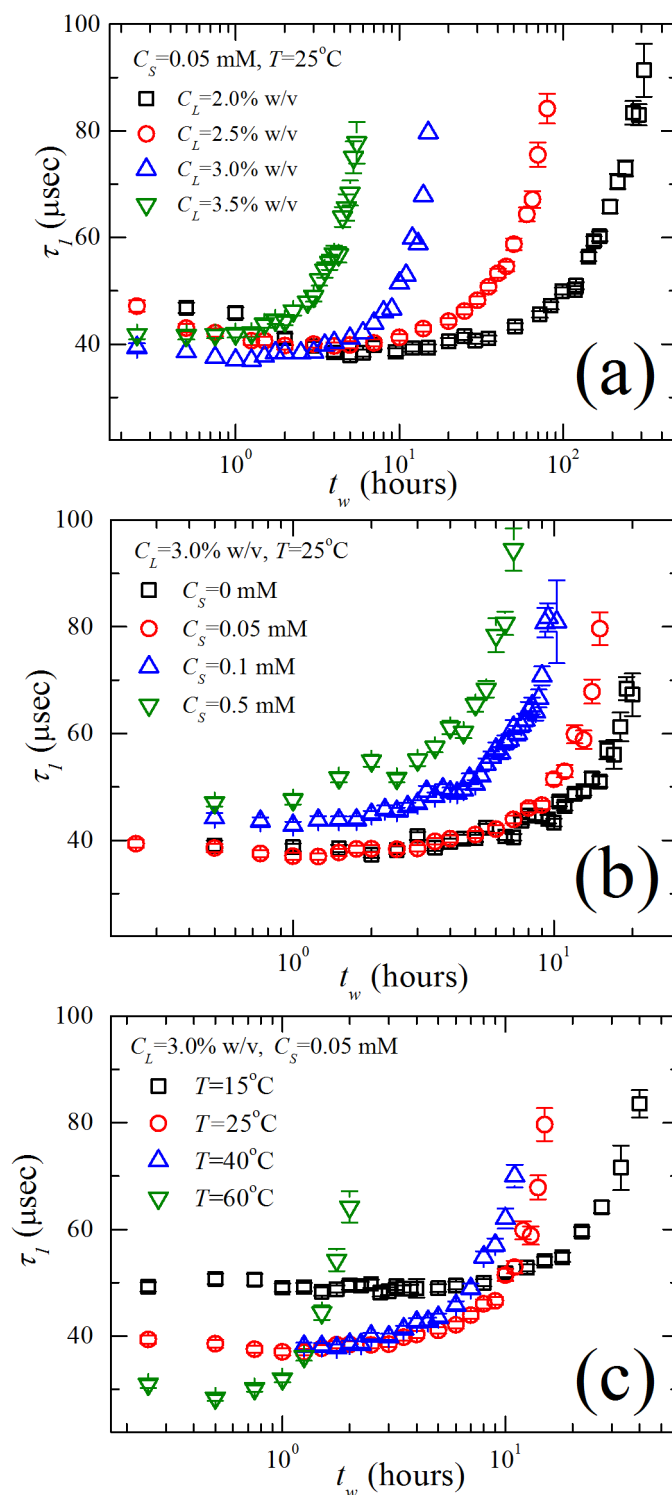


FIGURE 4.4: Fast relaxation times τ_1 are plotted vs. waiting times t_w for different C_L , C_S and T values in (a)-(c).

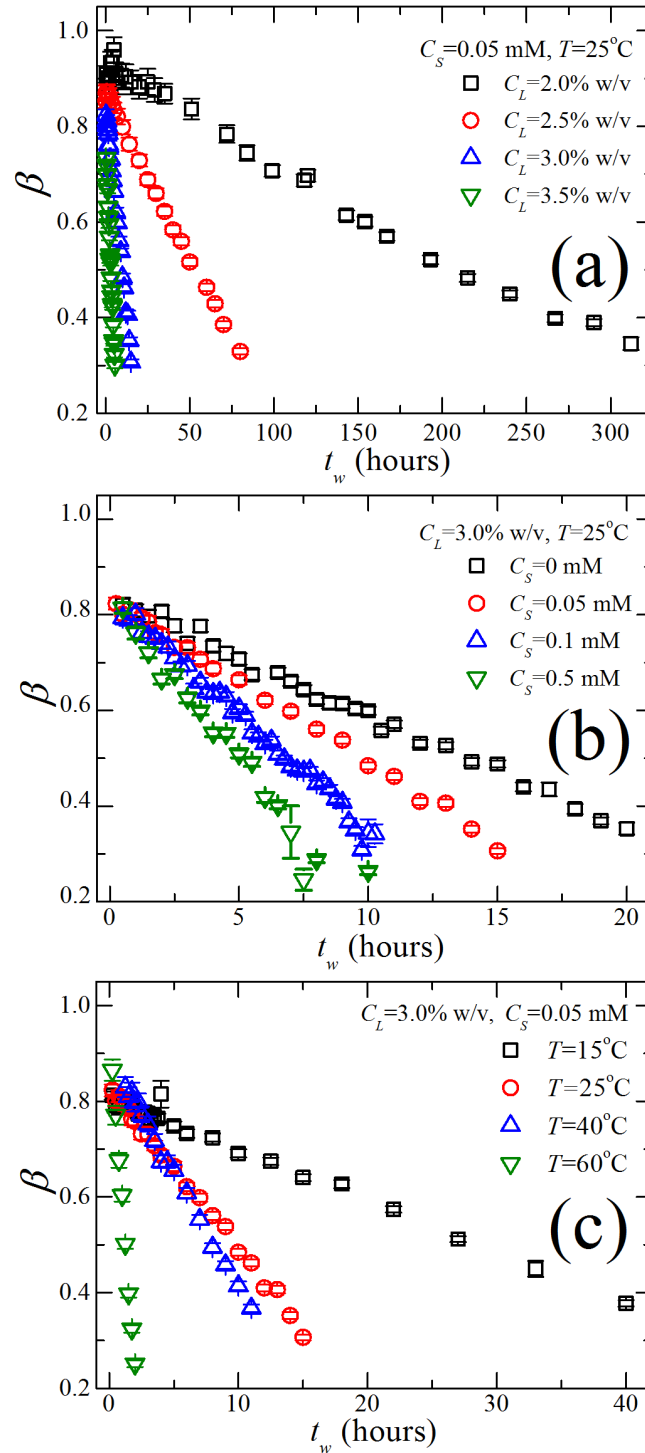


FIGURE 4.5: Stretching exponents β are plotted vs. t_w for different C_L , C_S and T values in (a)-(c).

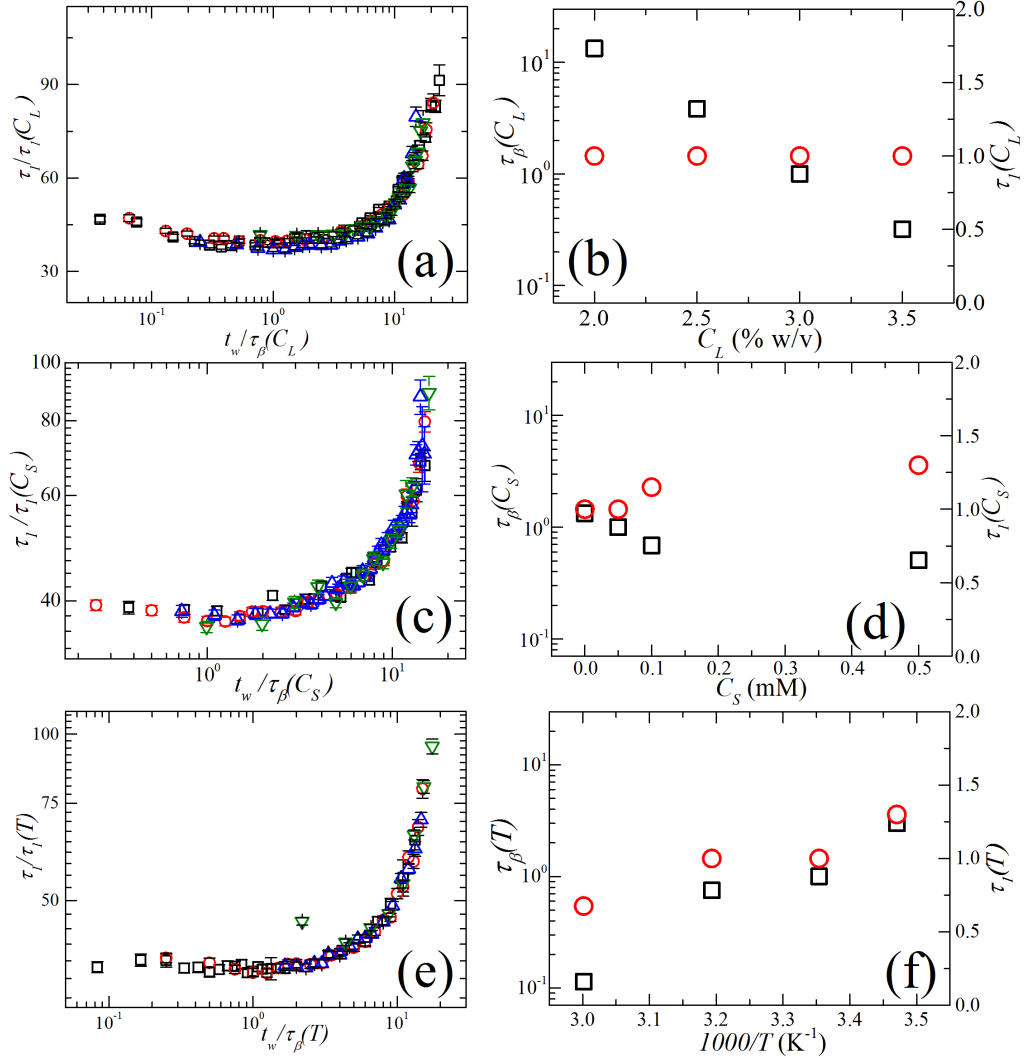


FIGURE 4.6: (a) Superposition of fast relaxation times $\tau_1/\tau_1(C_L)$ is shown vs. $t_w/\tau_\beta(C_L)$ for four different Laponite concentrations ($C_L=2.0\%$ w/v (\square), 2.5% w/v (\circ), 3.0% w/v (Δ) and 3.5% w/v (∇)) with 0.05 mM salt at 25°C . (b) Horizontal and vertical shift factors, $\tau_\beta(C_L)$ (\square) and $\tau_1(C_L)$ (\circ) respectively, are plotted vs. C_L . (c) Superposition of fast relaxation times $\tau_1/\tau_1(C_S)$ is shown vs. $t_w/\tau_\beta(C_S)$ for 3.0% w/v Laponite suspensions with four different salt concentrations ($C_S=0$ mM (\square), 0.05 mM (\circ), 0.1 mM (Δ) and 0.5 mM (∇)) at 25°C . (d) Horizontal and vertical shift factors, $\tau_\beta(C_S)$ (\square) and $\tau_1(C_S)$ (\circ) respectively, are plotted vs. C_S . (e) Superposition of fast relaxation times $\tau_1/\tau_1(T)$ is shown vs. $t_w/\tau_\beta(T)$ for 3.0% w/v Laponite suspensions with 0.05 mM salt and at four different temperatures ($T=15^\circ\text{C}$ (\square), 25°C (\circ), 40°C (Δ) and 60°C (∇)). (f) Horizontal and vertical shift factors, $\tau_\beta(T)$ (\square) and $\tau_1(T)$ (\circ) respectively, are plotted vs. inverse of temperature ($1000/T$).

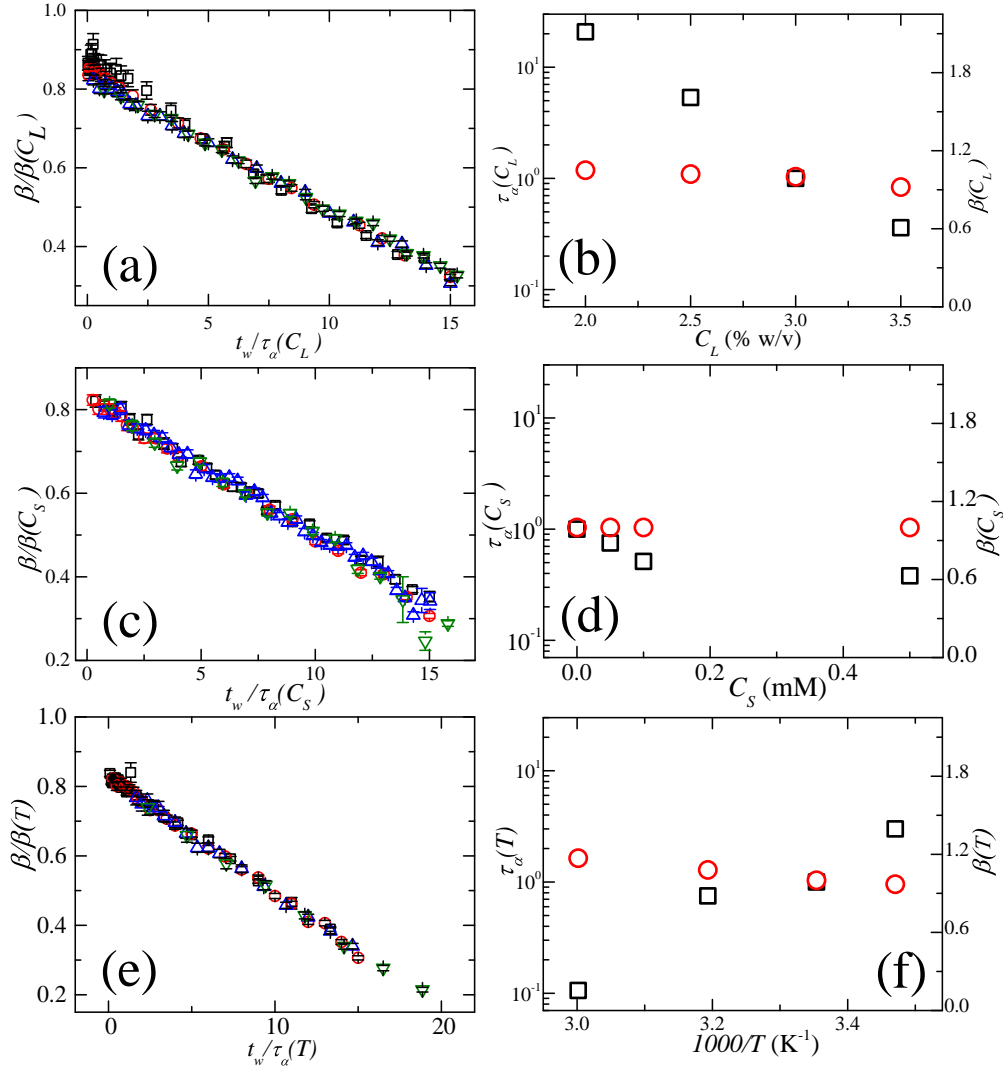


FIGURE 4.7: (a) Superposition of stretching exponents $\beta/\beta(C_L)$ is shown vs. $t_w/\tau_\alpha(C_L)$ for four different Laponite concentrations ($C_L=2.0\%$ w/v (□), 2.5% w/v (○), 3.0% w/v (△) and 3.5% w/v (∇)) with 0.05 mM salt at 25°C . (b) Horizontal and vertical shift factors, $\tau_\alpha(C_L)$ (□) and $\beta(C_L)$ (○) respectively, are plotted vs. C_L . (c) Superposition of stretching exponents $\beta/\beta(C_S)$ is shown vs. $t_w/\tau_\alpha(C_S)$ for 3.0% w/v Laponite suspensions with four different salt concentrations ($C_S=0$ mM (□), 0.05 mM (○), 0.1 mM (△) and 0.5 mM (∇)) at 25°C . (d) Horizontal and vertical shift factors, $\tau_\alpha(C_S)$ (□) and $\beta(C_S)$ (○) respectively, are plotted vs. C_S . (e) Superposition of stretching exponents $\beta/\beta(T)$ is shown vs. $t_w/\tau_\alpha(T)$ for 3.0% w/v Laponite suspensions with 0.05 mM salt and at four different temperatures ($T=15^\circ\text{C}$ (□), 25°C (○), 40°C (△) and 60°C (∇)). (f) Horizontal and vertical shift factors, $\tau_\alpha(T)$ (□) and $\beta(T)$ (○) respectively, are plotted vs. inverse of temperature ($1000/T$).

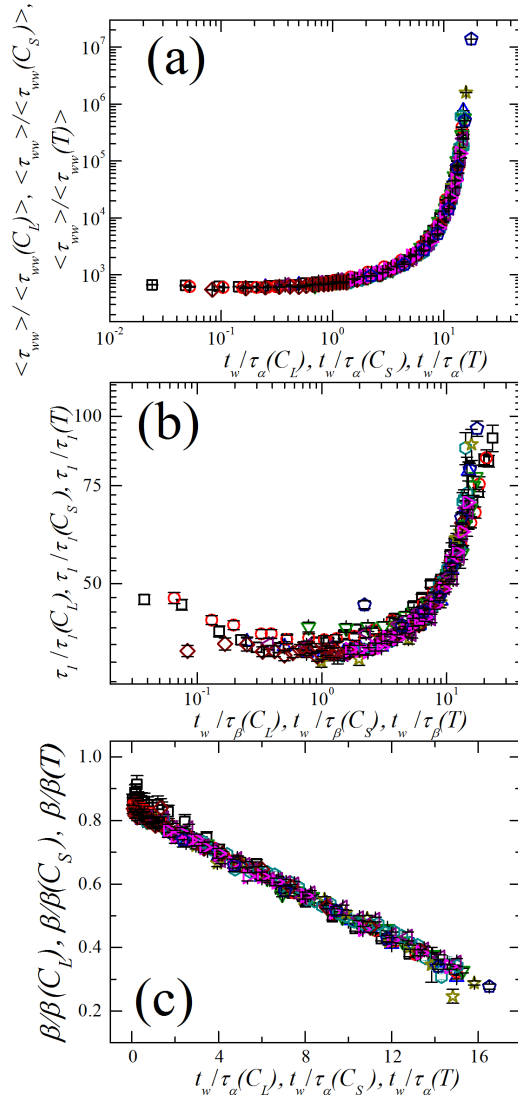


FIGURE 4.8: (a) The comprehensive superposition of the scaled mean slow relaxation times $\langle \tau_{ww} \rangle / \langle \tau_{ww}(C_L) \rangle, \langle \tau_{ww} \rangle / \langle \tau_{ww}(C_S) \rangle, \langle \tau_{ww} \rangle / \langle \tau_{ww}(T) \rangle$ is plotted vs. waiting time $t_w / \tau_\alpha(C_L), t_w / \tau_\alpha(C_S), t_w / \tau_\alpha(T)$. Here, $\langle \tau_{ww}(C_L) \rangle, \langle \tau_{ww}(C_S) \rangle$ and $\langle \tau_{ww}(T) \rangle$ are, respectively, the vertical shift factors for $\langle \tau_{ww} \rangle$ when C_L, C_S and T are changed and $\tau_\alpha(C_L), \tau_\alpha(C_S)$ and $\tau_\alpha(T)$ are the corresponding horizontal shift factors (plotted in figure 4.3 (b), (d) and (f)). (b) The comprehensive superposition of scaled fast relaxation times $\tau_1 / \tau_1(C_L), \tau_1 / \tau_1(C_S), \tau_1 / \tau_1(T)$ is plotted vs. scaled waiting time $t_w / \tau_\beta(C_L), t_w / \tau_\beta(C_S), t_w / \tau_\beta(T)$. Here, $\tau_1(C_L), \tau_1(C_S)$ and $\tau_1(T)$ are, respectively, the vertical shift factors for scaling τ_1 when C_L, C_S and T are changed and $\tau_\beta(C_L), \tau_\beta(C_S)$ and $\tau_\beta(T)$ are the corresponding horizontal shift factors (plotted in figure 4.6 (b), (d) and (f)). (c) The comprehensive superposition of scaled stretching exponents $\beta / \beta(C_L), \beta / \beta(C_S), \beta / \beta(T)$ is plotted vs. scaled waiting times $t_w / \tau_\alpha(C_L), t_w / \tau_\alpha(C_S), t_w / \tau_\alpha(T)$. Here, $\beta(C_L), \beta(C_S)$ and $\beta(T)$ are, respectively, the vertical shift factors for scaling β when C_L, C_S and T are changed and $\tau_\alpha(C_L), \tau_\alpha(C_S)$ and $\tau_\alpha(T)$ are the corresponding horizontal shift factors (plotted in figure 4.7 (b), (d) and (f)).

significantly old rejuvenated Laponite suspensions [5]. The results reported here therefore demonstrate that the time-evolutions of the relaxation processes remain similar in young and old Laponite samples. This is attributed to the fact that whatever the initial state of the sample, the process of structural build-up is dictated only by the interactions that the particles share among themselves.

Figure 4.8(b) clearly shows that τ_1 has a non-monotonic aging behavior with a minimum at small t_w . The initial decrease in τ_1 indicates the faster motion of the particle within its cage at short times. Interestingly, $\langle \tau_{ww} \rangle$ remains almost constant over the same duration. We believe that the decrease in τ_1 originates from the delamination of Laponite particles at early times, a scenario that has been reported earlier [13, 19]. It is seen from figure 4.8 that τ_1 and $\langle \tau_{ww} \rangle$ increase simultaneously before they eventually diverge. This observation suggests that the enhancements in both the relaxation timescales are correlated. For a material with purely repulsive interparticle interactions, the fast timescale is expected to remain finite, while the slow timescale diverges as the system approaches structural arrest. It is also seen in figure 4.5 that β decreases linearly with t_w and the decay becomes faster with increase in C_L , C_S and T . $\beta=1$ represents a simple exponential decay with a single dominating relaxation time, while $\beta < 1$ indicates a broadening of the distribution of relaxation times with t_w [18]. Usually, glasses formed by dominating repulsive interactions are known to preserve the shapes of the relaxation time distributions during aging. This has been confirmed for polymer glasses [20, 21], spin glasses [22], colloidal glasses with hard sphere interactions [23], microgel pastes [24] and concentrated emulsions [7]. On the other hand, chemical gels with covalent bonds between the polymeric chains and attractive colloidal gels are known to undergo broadening of their relaxation time distributions as a function of time [25–28]. Clearly, the spontaneously evolving young Laponite suspensions studied here show features that can be identified with colloidal gelation. Hence, the observations from our DLS experiments indicate an influence of attractive interactions. The correlation between τ_1 and $\langle \tau_{ww} \rangle$ and the decrease in β with t_w also remarkably corroborate the rheological observations reported earlier [29, 30].

It is necessary to quantify the interaction potentials between Laponite particles to verify the influence of attractive interactions postulated from the DLS experiments. We next estimate the concentrations of Na^+ present in the aging Laponite suspensions of different C_L , C_S and T . Na^+ in the suspensions can originate from the externally added NaCl and from the dissociation of Na^+ from the faces of Laponite particles into the bulk aqueous medium. Since concentration of externally added NaCl (C_S) is known, an estimation of the time-evolution of Na^+ ions can yield important information about the dissociation of Na^+ from the faces of the Laponite platelets. An estimation of the concentration of the dissociated Na^+ can be used to predict the amount of negative charges on the faces of the Laponite particles. The electronegativity of the Laponite particles, and hence the range of the electrostatic potential associated with the faces of these particles, can be then quantified by estimating the surface charge densities σ and the Debye screening lengths κ^{-1} . σ can be obtained by estimating the number of Na^+ dissociated per face of each Laponite particle and is given by $\sigma = e(n - n_0)/(2A_L n_p)$, where n_0 is the number density of ions due to the added salt, A_L is the area of the face of a Laponite particle ($=625 \text{ nm}^2$) and n_p is the number density of Laponite particles. κ^{-1} is given by $\kappa^{-1} = (\epsilon_0 \epsilon_r k_B T / \sum_i (z_i e)^2 n_i)^{1/2}$ [2], where ϵ_0 is the permittivity of free space, ϵ_r is the relative permittivity of the medium, k_B is the Boltzmann constant, T is the temperature of the suspension, e is the charge of an electron and z_i is the valence of the i th species of ions of concentration n_i . In aqueous suspensions of Laponite, two types of ions, Na^+ and Cl^- , influence κ^{-1} . The concentration of Na^+ in suspension is obtained using an ion meter, while the concentration of Cl^- ions is known *a priori* as C_S is fixed in every experiment.

The concentrations of Na^+ , measured for Laponite suspensions at different C_L , C_S and T , are used to extract σ and κ^{-1} values associated with the Laponite particles. Interestingly, for all Laponite suspensions, the concentrations of Na^+ progressively increase as a function of time (figure 4.9). This indicates a continuous dissociation of Na^+ from the faces of Laponite particles with increasing t_w . This results in a continuous temporal change in σ and κ^{-1} with change in C_L , C_S and T (figure 4.10). For a given t_w , the Na^+

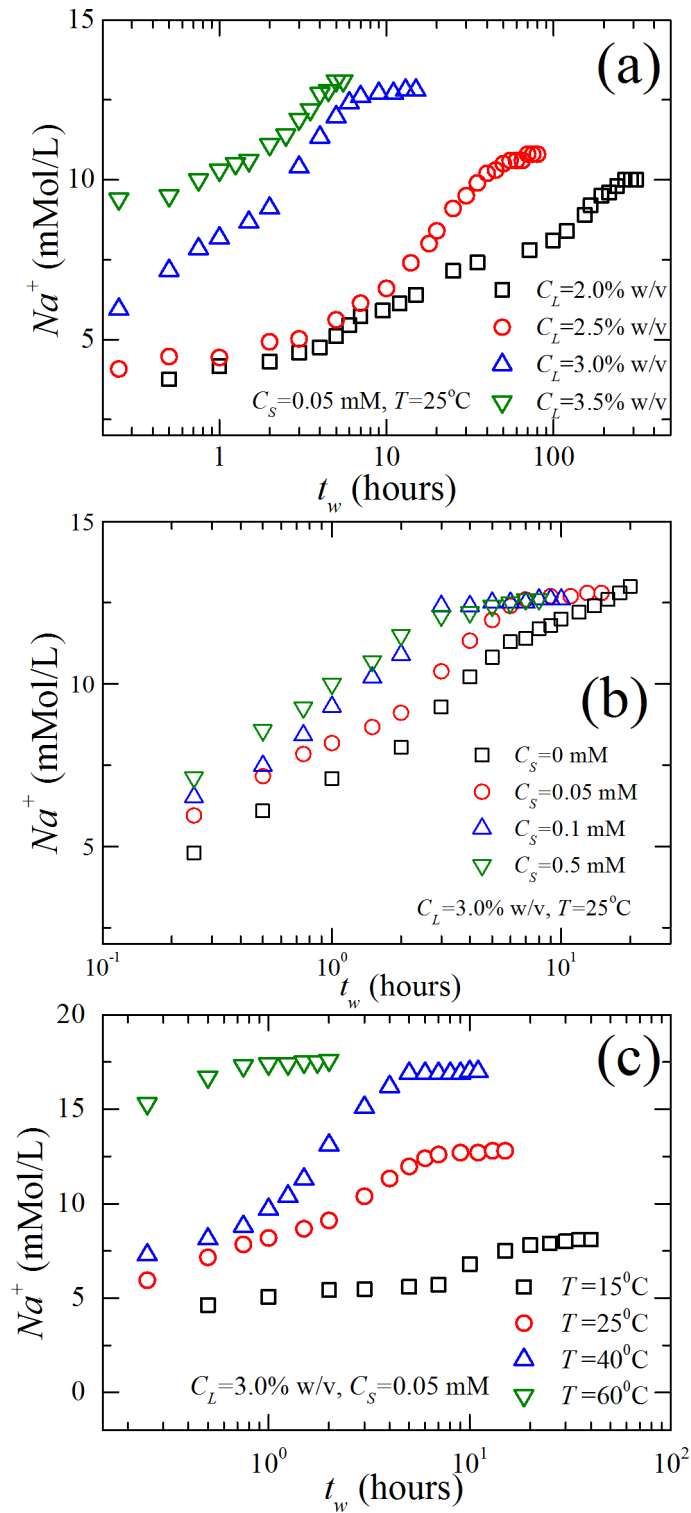


FIGURE 4.9: The Na^+ ion concentration vs. waiting time (t_w) for different C_L , C_S and T values in (a)-(c).

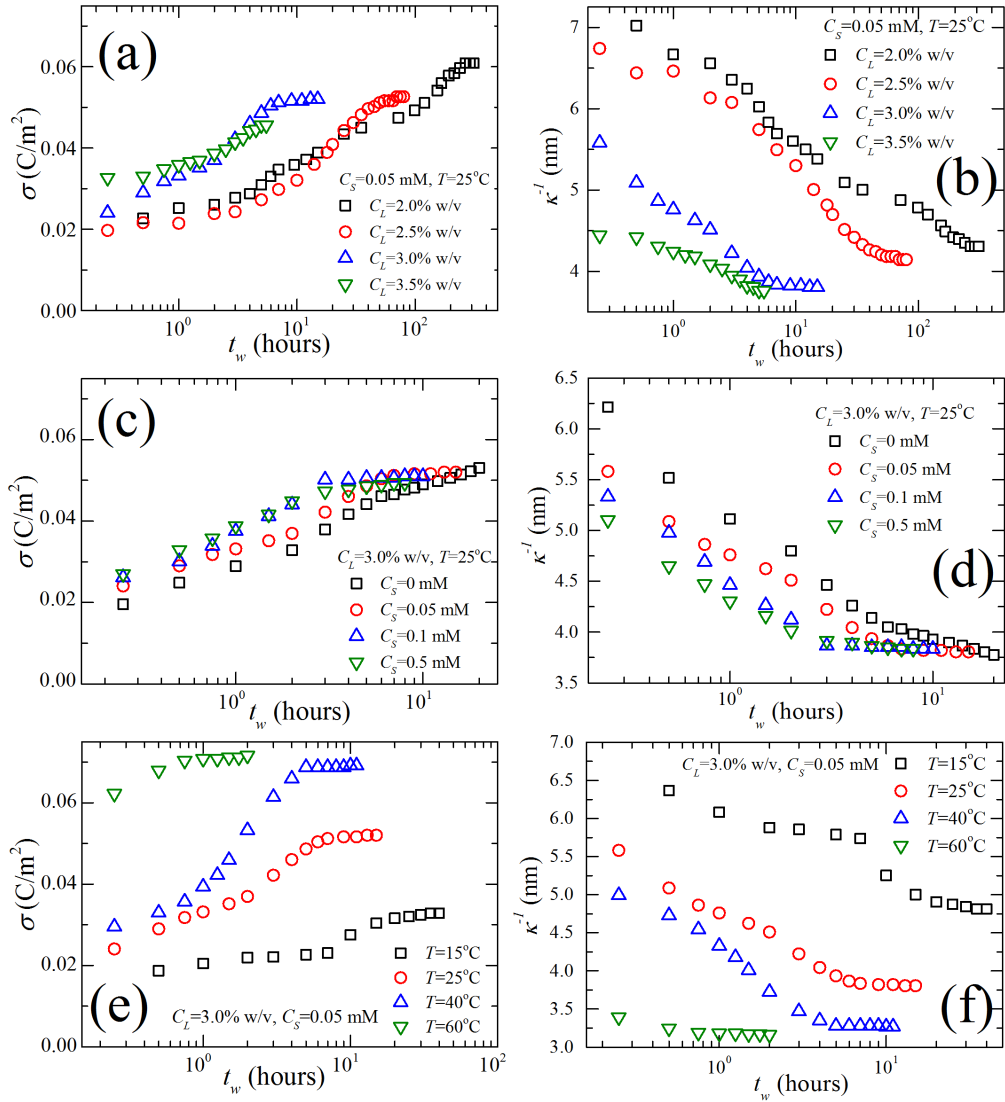


FIGURE 4.10: Surface charge density (σ) and Debye screening length (κ^{-1}) are plotted vs. t_w for different C_L , C_S and T values in (a)-(f).

concentration is higher for greater C_L , C_S and T (figure 4.9). Increasing C_L , C_S and T , therefore, all result in increased dissociation of Na^+ and enhancement of the surface electronegativity of the Laponite particles. A larger number of Na^+ in suspension enhances the screening and decreases the values of κ^{-1} , as observed in figures 4.10(b), (d) and (f).

To understand the effects of the enhanced electronegativity of the faces of Laponite

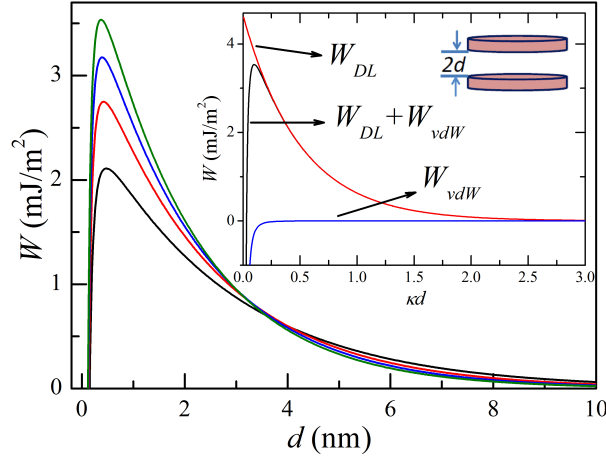


FIGURE 4.11: Free energy per unit area (W) between two layers of 2:1 Laponite clay (planar surfaces) calculated from DLVO theory and plotted as a function of half the distance, d , between Laponite platelets for a 3.0% w/v Laponite suspension with 0.1 mM salt at 25°C at different waiting times t_w (from top to bottom 10.0 hour, 5.0 hour, 1.5 hour and 0.25 hour). In the inset, the free energy per unit area for the double layer repulsive interaction W_{DL} , attractive van der Waals interaction (W_{vdW}) and the combined interaction $W_{DL} + W_{vdW}$ are plotted vs. κd for the same sample at $t_w = 10.0$ hour.

particles with increasing C_L , C_S and T and the observed decrease in the Debye screening lengths, we solve the DLVO model for a scenario in which two plates approach each other in a parallel fashion. The total free energy per unit area, due to van der Waals attraction (W_{vdW}) and double layer repulsion (W_{DL}) between the two layers of a 2:1 layer clay for weak interactions (*i.e.* κd large), is given by [3]:

$$W(d) = W_{vdW} + W_{DL} = -\frac{A_H}{48\pi} \left[\frac{1}{d^2} + \frac{1}{(d + \Delta)^2} - \frac{2}{(d + \Delta/2)^2} \right] + \left(\frac{64nk_B T}{\kappa} \right) \gamma^2 e^{-2\kappa d} \quad (4.2)$$

Here, A_H is the Hamaker constant (1.06×10^{-20} J), d is the half-distance between two Laponite platelets as shown in the inset of figure 4.11, Δ is the thickness of unit layers measured between the same planes (6.6 Å) [3], $\gamma = \tanh(ze\Phi_0/4k_B T)$, Φ_0 is the surface electric potential. Φ_0 is related to σ by $\sigma = e(n - n_0)/A_L n_p = \sqrt{8\epsilon_0 \epsilon_r k_B T n} \sinh(ze\Phi_0/2k_B T)$ [3].

In figure 4.11, we plot the total free energy of interaction $W(d)$ vs. the half-distance

d between the Laponite platelets for a 3.0% w/v Laponite suspension with 0.1 mM salt at 25°C for different t_w . It can be seen that the height of the repulsive barrier increases with the passage of time. However, it can be simultaneously observed that the width of the repulsive barrier decreases with t_w . In the inset, we have shown the contributions from the different parts (repulsive (W_{DL}), attractive (W_{vdW}) and combined ($W_{DL} + W_{vdW}$)) to the total free energy. Clearly, the effect of the van der Waals interaction is negligible except in the limit of $d \ll \kappa^{-1}$.

For a Laponite suspension of fixed C_L and C_S , an increase in T leads to an increase in the concentration of dissociated Na^+ counter-ions. Therefore, the predictions of the DLVO theory for different temperatures will also be qualitatively similar to the results plotted in figure 4.11, with t_w replaced by T [13]. Consequently, an increase in T is expected to cause an increase in the repulsive energy barrier, while simultaneously decreasing the barrier width. Unlike temperature T and waiting time t_w , a change in the concentration of salt, C_S , keeps the value of γ unaffected. However, since $1/\kappa \approx 1/\sqrt{n}$, the coefficient $nk_B T/\kappa$ in equation 4.2 increases with increase in concentration of salt according to $nk_B T/\kappa \approx \sqrt{n}$. Consequently, the qualitative behavior of the free energy per unit area calculated using DLVO theory with increase in C_S will be the same as that shown in figure 4.11, but with t_w replaced by C_S . Similarly, an increase in C_L , the concentration of Laponite, causes an increase in n , and since $nk_B T/\kappa \approx \sqrt{n}$, the qualitative behavior of the interparticle potential is again expected to remain the same as that shown in figure 4.11, but with t_w replaced by C_L .

Microscopically, aqueous suspensions of Laponite consist of randomly-oriented disk like particles that interact *via* face-to-face repulsive interactions, edge-to-face attractive interactions and van der Waals interactions. The physical cages in which the individual particles are arrested can be represented as energy wells. The complex interparticle interaction between the anisotropic particles results in a distribution of well depths in the sample's free-energy landscape. As the suspension is not in the lowest free energy state, Laponite particles continue to undergo microscopic motions as t_w increases. This gives rise to structural rearrangements, or physical aging, and results

in the eventual occupation of those states that have lower energy. If E is the mean energy well depth, the cage diffusion or the slow timescale can simply be represented by $\langle \tau_{ww} \rangle = \langle \tau_{ww} \rangle_0 \exp(E/k_B T)$. Consequently, the increase in $\langle \tau_{ww} \rangle$, which represents an increase in the mean energy well depth, is a manifestation of a physical aging process. In this process, the timescale associated with the microscopic dynamics, which sets a unit timescale for the physical aging process, is represented by a microscopic timescale τ_m [31]. The time dependence of the mean energy well depth can then be represented by: $E = E(t_w/\tau_m)$. The microscopic timescale τ_m , which is a measure of the rate of the evolution of $\langle \tau_{ww} \rangle$, can also be considered to have an Arrhenius temperature dependence given by $\tau_m = \tau_{m0} \exp(U/k_B T)$ [5]. Here, U , the activation energy barrier associated with microscopic motion, sets the aging timescale τ_m and is distinct from E , the average depth of the energy well in which the particles reside [5]. As reported earlier, the self-similar evolution of $\langle \tau_{ww} \rangle$ shifts to lower waiting times with increase in C_L , C_S and T . Therefore, the shift factors associated with the time axis shown in figures 4.2 and 4.8(a) can be related to microscopic timescale as: $\tau_m = \tau_m(C_L, C_S, T)$. Consequently, as per dependencies described in figures 4.3(b), (d) and (f), it can be concluded that τ_m decreases with increase in these variables. A decrease in τ_m indicates that the activation barrier U for microscopic motion decreases with increase in C_L and C_S . As already noted, the aging behavior of Laponite suspensions gets affected by T even more strongly. First, τ_m decreases with increase in T through the Arrhenius relationship cited earlier [5]. Increase in T also results in an increase in the concentration of Na^+ in suspension. Therefore, any change in T is expected to strongly affect the activation barrier U .

The results of our light scattering study and DLVO analysis, therefore, present a very interesting scenario. The light scattering study clearly suggests that the activation energy U , associated with the microscopic motion of the particles, sets a timescale τ_m for structural reorganization events, which determines the rate of aging. This timescale (τ_m) decreases with increasing C_L , C_S and T as mentioned before, accelerating the aging dynamics. A decrease in τ_m , in turn, indicates a decrease in U . Furthermore, due to

its Arrhenius temperature dependence, τ_m is expected to decrease with increase in T . However, the DLVO analysis shows that C_L , C_S and T not only cause an enhancement in the height of the repulsive potential, but also lead to a shrinkage in the width of the repulsive potential. Therefore, as increasing C_L , C_S and T results in a decrease in the width of the repulsive barrier leading to accelerated structure formation (or a decrease in U), it is concluded that the formed structure cannot be only repulsion dominated.

We note that the predictions of the DLVO theory are applicable strictly to the case when two Laponite particles approach each other in a parallel fashion as shown in the inset of figure 4.11. The DLVO interaction in the present case can only be solved for two parallel plates approaching each other. However, if the particles approach non-parallelly, then the edge-to-face attraction will increase. Therefore, for such non-parallel orientations, increase in C_L , C_S and T will give rise to an enhanced decrease in the energy barrier U associated with structure formation. Hence, for all orientations of Laponite particles, attractive interaction will have an important influence on the low energy structures.

4.4 Conclusions

In this work, we use dynamic light scattering to study the fast and slow relaxation timescales of young Laponite suspensions as a function of the aging or waiting times t_w . The time-evolutions of the relaxation processes of young Laponite suspensions under various physicochemical conditions are investigated systematically by changing the Laponite concentration C_L , the salt concentration C_S and the suspension temperature T using both DLS and Na^+ measurements. Our data shows that both the fast and slow relaxation processes are self-similar upon changing C_L , C_S and T . The stretching exponents β , associated with the slow relaxation timescales, also show self-similarity. The Laponite concentration-salt concentration-temperature-time superpositions obtained here highlight the self-similar nature of the energy landscapes of Laponite suspensions when these physicochemical variables are changed. We also see

signatures of a delamination effect of Laponite particles at early time when all these variables are changed.

For aqueous suspensions of Laponite without externally added salt, small angle X-ray scattering has established the presence of a repulsive glass at Laponite concentrations above 2 wt% [32] where the particles do not touch each other and remain self-suspended. Also, dissolution [8] and rheological studies [5] showed that young Laponite suspensions ($t_w < 2$ -3 days) are primarily repulsion dominated, while attractive interactions strongly influence the structures of old samples (3 days $< t_w < 7$ days). The present study combines DLS, Na^+ measurements and a DLVO analysis to show that even in young suspensions ($t_w < 2$ days), the effect of attractive interactions is not negligible. However, it is extremely likely that the attractive interactions in young Laponite suspensions are weaker than the solvation forces that are likely to have dominated in the dissolution experiments mentioned above [8]. While this work gives unique insight into the possible structure of the arrested state, it still cannot give direct structural information. In any case, we believe that the present study complements several previous reports on the aging of aqueous suspensions of Laponite by suggesting that in an overall repulsive environment, the attractive interactions between Laponite particles in aqueous suspension play an extremely influential role in exploring low energy structures.

References

- [1] D. F. Evans and H. Wennerstrom, *The Colloidal Domain*; Wiley VCH: New York, 1994.
- [2] J. N. Israelachvili, *Intermolecular and Surface Forces*; Academic Press: New York, 2010.
- [3] H. V. Olphen, *An Introduction to Clay Colloid Chemistry*; Wiley: New York, 1977.
- [4] G. L. Hunter and E. R. Weeks, *Rep. Prog. Phys.*, **75**, 066501 (2012).
- [5] A. Shahin and Y. M. Joshi, *Langmuir*, **28**, 15674-15686 (2012).
- [6] A. Shahin and Y. M. Joshi, *Langmuir*, **26**, 4219-4225 (2010).
- [7] A. Shahin and Y. M. Joshi, *Phys. Rev. Lett.*, **106**, 038302 (2011).
- [8] B. Ruzicka, L. Zulian, E. Zaccarelli, R. Angelini, M. Sztucki, A. Moussaïd and G. Ruocco, *Phys. Rev. Lett.*, **104**, 085701 (2010).
- [9] C. A. Angell, K. L. Ngai, G. B. McKenna, P. F. McMillan and S. W. Martin, *J. Appl. Phys.*, **88**, 3113-3157 (2000).
- [10] K. L. Ngai, *J. Chem. Phys.*, **109**, 6982 (1998).

-
- [11] P. Debenedetti and F. H. Stillinger, *Nature*, **410**, 259-267 (2001).
- [12] A. Kudlik, C. Tschirwitz, S. Benkhof, T. Blochowicz and E. Rössler, *Europhys. Lett.*, **40 (6)**, 649-654 (1997).
- [13] D. Saha, Y. M. Joshi and R. Bandyopadhyay, *Soft Matter*, **10**, 3292-3300 (2014).
- [14] B. Ruzicka, L. Zulian and G. Ruocco, *J. Phys.: Condens. Matter*, **16**, S4993-S5002 (2004).
- [15] B. Ruzicka, L. Zulian and G. Ruocco, *Phys. Rev. Lett.*, **93**, 258301 (2004).
- [16] W. Gotze and L. Sjogren, *Rep. Prog. Phys.*, **55**, 241-376 (1992).
- [17] B. Abou, D. Bonn and J. Meunier, *Phys. Rev. E*, **64**, 215101-215106 (2001).
- [18] C. P. Lindsey and G. Patterson, *J. Chem. Phys.*, **73**, 3348-3357 (1980).
- [19] S. Ali and R. Bandyopadhyay, *Langmuir*, **29(41)**, 12663-12669 (2013).
- [20] L. C. E. Struik, *Physical aging in amorphous polymers and other materials*; Elsevier: Houston, 1978.
- [21] Y. M. Joshi, *Rheologica Acta*, **53**, 477-488 (2014).
- [22] G. F. Rodriguez, G. G. Kenning and R. Orbach, *Phys. Rev. Lett.*, **91**, 037203 (2003).
- [23] C. Derec, G. Ducouret, A. Ajdari and F. Lequeux, *Phys. Rev. E*, **67**, 061403 (2003).
- [24] M. Cloitre, R. Borrega and L. Leibler, *Phys. Rev. Lett.*, **85**, 4819 (2000).
- [25] H. H. Winter, *Macromolecules*, **46**, 2425-2432 (2013).
- [26] D. F. Hodgson and E. J. Amis, *J. Non-Cryst. Solids*, **131**, 913-920 (1991).
- [27] J. H. Choi, S. W. Ko, B. C. Kim, J. Blackwell and W. S. Lyoo, *Macromolecules*, **34**, 2964-2972 (2001).

- [28] A. Ponton, A. Bee, D. Talbot and R. Perzynski, *J. Phys.: Condens. Matter*, **17**, 821-836 (2005).
- [29] S. Jatav and Y. M. Joshi, *Journal of Rheology*, **58**, 1535 (2014).
- [30] A. Shahin and Y. M. Joshi, *Langmuir*, **28**, 5826 (2012).
- [31] S. M. Fielding, P. Sollich and M. E. Cates, *Journal of Rheology*, **44**, 323-369 (2000).
- [32] B. Ruzicka, L. Zulian, R. Angelini, M. Sztucki, A. Moussaid and G. Ruocco, *Phys. Rev. E*, **77**, 020402-020404 (2008).

5

Kinetics of the glass transition of fragile soft colloidal suspensions

5.1 Introduction

The dependence of transport properties (diffusivity, viscosity etc.) and structural relaxation times near the glass transition are of crucial importance in understanding glass formers. A few key observations, like the rapid increase of viscosity near the glass transition temperature T_g , the heat-capacity jump at T_g , the Kauzmann entropy catastrophe, the super-Arrhenius temperature dependence of the structural relaxation processes, and fragile behavior are common to many glass formers [1–3]. An enormous increase in viscosity and relaxation time (14 decades and more) is observed as a molecular glass former is quenched towards its glass transition temperature [4]. Specific heat measurements show a jump in the heat-capacity at T_g and the extent of the jump, in general, is

larger for a fragile glass [2]. Fragile glasses show super-Arrhenius temperature dependence and exhibit an extremely steep increase in viscosity η which can be expressed by the Vogel-Fulcher-Tammann (VFT) relation, i.e., $\eta = \eta_0 \exp [DT_0/(T - T_0)]$. Here, T_0 is the Vogel temperature at which η diverges. The fragility parameter D quantifies the deviation from Arrhenius behavior. D is a material specific quantity [5], whose magnitude is small (typically <10) for fragile supercooled liquids and can change to very large values for strong glass formers. It is very difficult to differentiate between an Arrhenius temperature dependence and a super-Arrhenius temperature dependence for $D > 100$ [5, 6].

The relation between the fragility parameter D and the structural properties of a material is still not completely understood despite many theoretical and experimental studies. A correlation is drawn between the fragility of a material and its physical properties, i.e. its Poissons ratio or the relative strength of its shear and bulk moduli [7]. The relation between the nature of the interaction potential and fragility has also been studied for model binary mixture glass formers [8] and colloidal glass formers [9]. In the supercooled liquids literature, T_g is the temperature at which the mean α -relaxation time ($\langle \tau_\alpha \rangle$) is 100 sec [5, 6]. It is to be noted that T_g depends on the heating or cooling rate [10].

The phenomenology of glass formers have often described by a potential energy landscape (PEL) [11, 12] which can be visualized in terms of a multi-dimensional surface describing the dependence of the potential energy of the system as a function of the particle coordinates [13]. If N is the number of particles, then the dimension of the hyperspace is $3N + 1$, with the system represented by a point evolving temporally in this complex potential hyperspace [13]. In this topographic description, the minima of the PEL correspond to mechanically stable arrangement of particles [13]. A correlation is drawn between the fragility of a glass former and the density of minima in the PEL. Fragile glass formers are observed to have more density of minima than strong glass formers [5]. Interestingly, the PEL is particularly useful to calculate another important quantity, the configurational entropy (S_c) of a supercooled liquid [14]. In the

supercooled regime, S_c is the excess entropy of the liquid over its crystalline phase. At a hypothetical temperature known as Kauzmann temperature T_K , S_c vanishes and the system is postulated to go through a thermodynamic transition to avoid a catastrophe (the Kauzmann catastrophe) which would require the entropy of the crystalline state to be greater than that of the liquid state. The resultant ‘ideal glass’ state corresponds to the global minimum of the PEL [11].

Even after decades of research, a proper understanding of the ideal glass state and the link between the thermodynamics and kinetics of glass formers remains elusive. However, it is seen that for most fragile supercooled liquids, T_K is approximately equal to T_0 , indicating a possible relation between its thermodynamics and kinetics [6]. The random first order transition theory of the glass transition predicts a possible relation between the stretching exponent β of the non-Debye α -relaxation and T_K [15]. It is believed that β is temperature dependent and vanishes at T_K which corresponds to the divergence of the width w of the α -relaxation spectrum [15, 16].

This chapter describes further analysis of the microscopic relaxation processes of colloidal suspensions of Laponite approaching the jamming transition and discussed earlier in chapters 3 and 4. The evolution of microscopic relaxation timescales are studied for Laponite suspensions with different concentrations (C_L), added salt concentrations (C_S) and temperatures (T) to observe the effects of these variables on the fragility parameter D . It has been confirmed in chapters 3 and 4 that the evolutions of relaxation timescales of Laponite for all C_L , C_S and T can be compared with molecular glass formers if the waiting time (t_w) of the former is mapped with the inverse of thermodynamic temperature ($1/T$) of the latter [17]. The stretching exponent β , associated with the non-Debye structural relaxation processes, is also extracted for different waiting times t_w for samples of different C_L , C_S and T . A hypothetical timescale t_k at which the width of the distribution of structural relaxation times diverges is defined by extrapolating $\beta \rightarrow 0$. It is shown here that this timescale is correlated to the timescale t_α^∞ at which the mean structural relaxation time diverges. This remarkable correlation between these two hypothetical timescales is reminiscent of the correlation

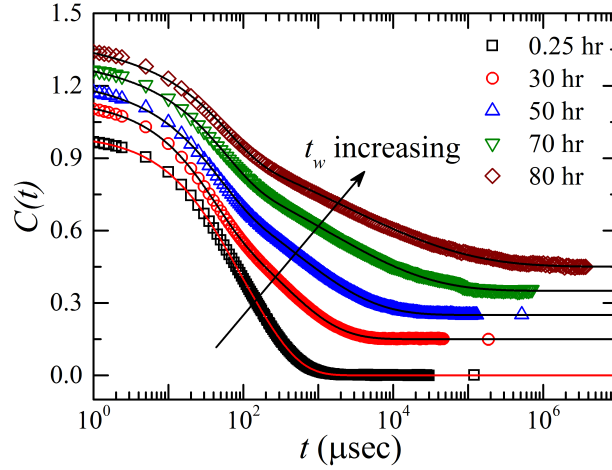


FIGURE 5.1: The normalized intensity autocorrelation functions $C(t)$, vs. the delay time t , at 25°C and scattering angle $\theta = 90^\circ$, for 2.5% w/v Laponite suspension with 0.05 mM salt at several t_w . The solid lines are fits to equation 5.1. Data are shifted by an additive constant for better visibility.

of two hypothetical temperatures, the Kauzmann and Vogel temperatures, seen previously in extremely fragile molecular glass formers. We explain this correlation by appropriately modifying the coupling model for molecular glass formers and by analyzing the observed waiting time dependence of the stretching exponent associated with the primary relaxation process of Laponite particles in suspension.

5.2 Sample preparation and experimental methods

All the experiments are done with aqueous suspensions of Laponite RD[®]. Details of the experimental techniques and sample preparation are given in chapters 2 and 4 respectively.

5.3 Results and discussions

Intensity autocorrelation functions $g^{(2)}(t)$ are obtained as a function of the waiting time t_w . In figure 5.1, the normalized intensity autocorrelation function, $C(t) = g^{(2)}(t) - 1$,

for a 2.5% w/v Laponite suspension with 0.05 mM salt at 25°C, is plotted as a function of delay time t for several t_w values. Similar to the data of chapters 3 and 4, two-step relaxation processes, with the two steps becoming more distinguishable as t_w increases, are observed in $C(t)$. It is also seen that the decay of $C(t)$ slows down with t_w and can be expressed by a sum of an exponential and a stretched exponential decay in the following way [17–19].

$$C(t) = [a \exp\{-t/\tau_1\} + (1 - a) \exp\{-(t/\tau_{ww})^\beta\}]^2 \quad (5.1)$$

The data in figure 5.1 are fitted to equation 5.1, with τ_1 , τ_{ww} , a and β being the fitting parameters. The fast decay, expressed by an exponential function, describes a relaxation time quantified by a timescale τ_1 , the fast relaxation time. Similarly, the slow decay is represented by a stretched exponential function, where τ_{ww} and β are the slow relaxation time and the stretching exponent respectively [18]. The mean slow relaxation time is given by $\langle \tau_{ww} \rangle = (\tau_{ww}/\beta)\Gamma(1/\beta)$ [20].

As noted earlier, two-step decays are often seen in glass formers [21–23]. In supercooled liquids and in the present system, the faster decay involves diffusion of a particle within a cage formed by its neighbors [24], while the slower decay (the α -relaxation process) is connected to structural or orientational rearrangements [6]. The mean slow relaxation time $\langle \tau \rangle$ is very sensitive to changes in temperature and can be expressed by the Vogel-Fulcher-Tammann relation $\langle \tau \rangle = \tau_{VF} \exp[B/(T - T_0)]$ [6], where the fitting parameter $\tau_{VF} = \langle \tau \rangle (T \rightarrow \infty)$. B and T_0 are identified as the fragility index and the Vogel temperature respectively. For quantifying the deviation from Arrhenius behavior, i.e. $\langle \tau \rangle = \tau \exp(E/k_B T)$, one can define $B = DT_0$, where D is the strength or fragility parameter [2, 5, 6].

It has been already shown in chapter 3 that the mean slow relaxation time $\langle \tau_{ww} \rangle$ shows a VFT-type dependence on t_w given by the following expression [17]:

$$\langle \tau_{ww} \rangle = \langle \tau_{ww} \rangle^0 \exp(Dt_w/(t_\alpha^\infty - t_w)) \quad (5.2)$$

In equation 5.2, D is the fragility parameter and t_α^∞ is identified with the Vogel time or the waiting time at which $\langle \tau_{ww} \rangle$ diverges.

In figure 5.2(a), $\langle \tau_{ww} \rangle$ and the corresponding fits to equation 5.2, discussed in our recent work [25] and in chapter 4, are plotted for different values of C_L with $C_S=0.05$ mM and $T=25^\circ\text{C}$. It is seen from the plots that the evolution of $\langle \tau_{ww} \rangle$ becomes faster with increase in C_L . The fragility parameters D (\bullet) and the Vogel times t_α^∞ (\square) obtained from the fits are plotted in figure 5.2(b). Recent simulation results suggest that the kinetic fragility K_{VFT} ($K_{VFT} = 1/D$), calculated from the α -relaxation time for Kob-Anderson (KA) model glass formers, has a very weak dependence on density [26]. In the Laponite suspensions studied here, the suspension density changed from 1020 Kg m^{-3} to 1035 Kg m^{-3} when C_L is varied between 2.0% w/v and 3.5% w/v. Since the change in the density of the Laponite suspensions studied here is very small, D can be expected to be constant. Remarkably, our experimental observation, as demonstrated in figure 5.2(b), nicely supports this observation for molecular glass formers.

It is to be noted that although the bulk suspension density does not change appreciably within the range of C_L studied here, the number density of particles increases with C_L . The subsequent decrease in the interparticle distance in Laponite suspensions for higher C_L therefore translates to an increase in pressure as more particles are now packed in the same volume of the suspension. The apparent independence of D on number density in the Laponite suspensions studied here is therefore reminiscent of recent results for many molecular glass formers for which the isochoric fragility is independent of pressure [27]. It is also seen from figure 5.2(b) that t_α^∞ decreases monotonically with C_L , thereby indicating a faster approach to an arrested state with increasing Laponite concentration. Since the number density of Laponite particles in suspension is directly proportional to C_L , multi-body interactions are enhanced with increasing C_L , thereby shifting the onset of the glass transition to earlier times (figure 5.2(a)). This feature is reminiscent of a previous observation in dense colloidal suspensions [28] and has been also discussed earlier in the context of the aging of Laponite suspensions in chapters 3 and 4 [17, 25].

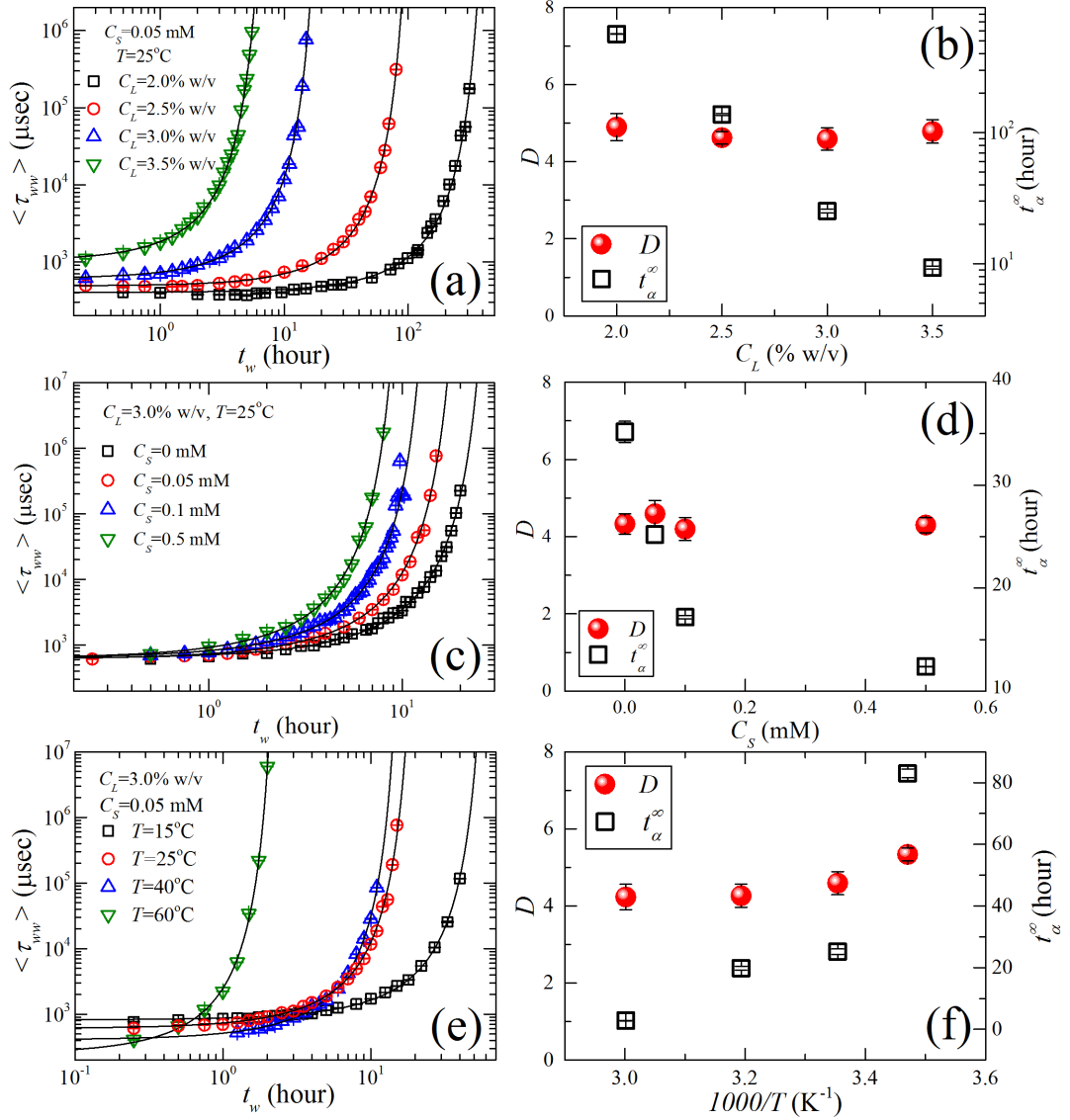


FIGURE 5.2: Mean slow relaxation times $\langle \tau_{ww} \rangle$, obtained by fitting $C(t)$ data to equation 5.1, are plotted vs. t_w for different C_L , C_S and T in (a), (c) and (e) respectively. Fragility D (●) and Vogel time t_α^∞ (□), measured by fitting $\langle \tau_{ww} \rangle$ data to equation 5.2, are plotted for different C_L , C_S and T in (b), (d) and (f) respectively.

In figure 5.2(c), $\langle \tau_{ww} \rangle$ is plotted for different values of C_S with $C_L=3.0\%$ w/v and $T=25^\circ\text{C}$ [25]. D (\bullet) and t_α^∞ (\square) are obtained from the fits of the data to equation 5.2 and are plotted in figure 5.2(d). D is almost constant for the entire range of salt concentrations C_S . DLVO calculations for Laponite suspensions reported in chapter 4 have revealed that the height of the repulsive barrier increases and the width of the barrier decreases with increase in C_S [25]. This is due to the enhancement of the screening of the interparticle repulsive interactions and the increasingly important role that interparticle attractions play in spontaneously evolving Laponite suspensions. The addition of salt and the development of interparticle attractions clearly increase the rate of structure formation, as it is seen in figure 5.2(d), when t_α^∞ decreases rapidly with increase in C_S [25]. This verifies our earlier observation in chapter 4 that the arrested state is approached at a faster rate due to stronger interparticle interactions when the concentration of salt in the system is enhanced. However, an almost constant value of D (figure 5.2(d)) with increasing C_S indicates that the fragility parameter is independent of the screening effects on the interparticle interaction within the range of salt concentrations studied here.

Simulation results for binary mixtures of soft spheres have shown that fragility is independent of the softness of the repulsive interaction [29]. However, recent computer simulation results on binary mixture glass formers with a modified Lennard-Jones type potential show that the kinetic fragility increases with increasing softness [8]. Experiments on soft colloidal systems show that soft (more compressible) particles form stronger glasses than hard (less compressible) colloidal particles [9]. In our experiment, it is to be noted that while relative magnitudes of the attractive and repulsive interaction changes with C_S , the softness of interparticle interactions and the compressibility of the Laponite particles do not change. This is established from the observed self-similarity of the potential energy landscape with C_S reported in chapter 4. Hence, the apparent insensitivity of D to changes in C_S confirms several earlier simulations and experimental results on colloidal and molecular glass formers [8, 9, 29].

It has been noted in chapter 4 that temperature has a strong effect on the evolution of relaxation processes in Laponite suspensions [25, 30]. $\langle \tau_{ww} \rangle$ is plotted for different values of T with $C_L=3.0\%$ w/v and $C_S=0.05$ mM in figure 5.2(e). It is seen that increase in T accelerates the time-evolution of $\langle \tau_{ww} \rangle$ [25, 30]. In figure 5.2(f), D (\bullet) and t_α^∞ (\square) are plotted for the data shown in figure 5.2(e). Like C_L and C_S , T has a negligible effect on D except at the lowest temperature. However, t_α^∞ is seen to increase with decrease in temperature, thereby indicating that the glass transition is achieved at earlier times with increase in T . Increase in T is therefore equivalent to increasing the apparent cooling rate q' , with the system being driven towards the glass transition at faster rates at higher temperatures. For bulk metallic glass formers, i.e. $Zr_{57}Cu_{15.4}Ni_{12.6}Al_{10}Nb_5$ and $Zr_{58.5}Cu_{15.6}Ni_{12.8}Al_{10.3}Nb_{2.8}$, there is an apparent increase in D at slower cooling rates [31], while the Vogel temperature T_0 increases with cooling rate. The small increase in D with $1000/T$ at the slowest cooling rate seen in figure 5.2(f) therefore, is in accordance with the observations in [31]. Since an inverse relation exists between T_0 and t_α^∞ (i.e. $T_0 \leftrightarrow 1/t_\alpha^\infty$) [17], the decrease of t_α^∞ with increase in T or q' is remarkably consistent with the observations in metallic glass formers [31].

As discussed in the introduction of this chapter, strong glass formers have a lower density of minima in the potential energy landscape compared to fragile glass formers [5]. The very small changes in D (figure 5.2) reported in this chapter indicate that the underlying energy landscapes are self-similar for the ranges of C_L , C_S and T studied here. This is in agreement with the conclusion from chapter 4 where it was shown that the time-evolutions of the microscopic relaxation times scales and the stretching exponents β associated with the slow relaxation process show comprehensive Laponite concentration-salt concentration-temperature-waiting time superpositions, thereby indicating the self-similarity of the underlying energy landscapes [25].

In figure 5.3, the stretching exponent β , obtained by fitting the $C(t)$ data to equation 5.1, is plotted vs. t_w for different C_L , C_S and T . It is seen that for all

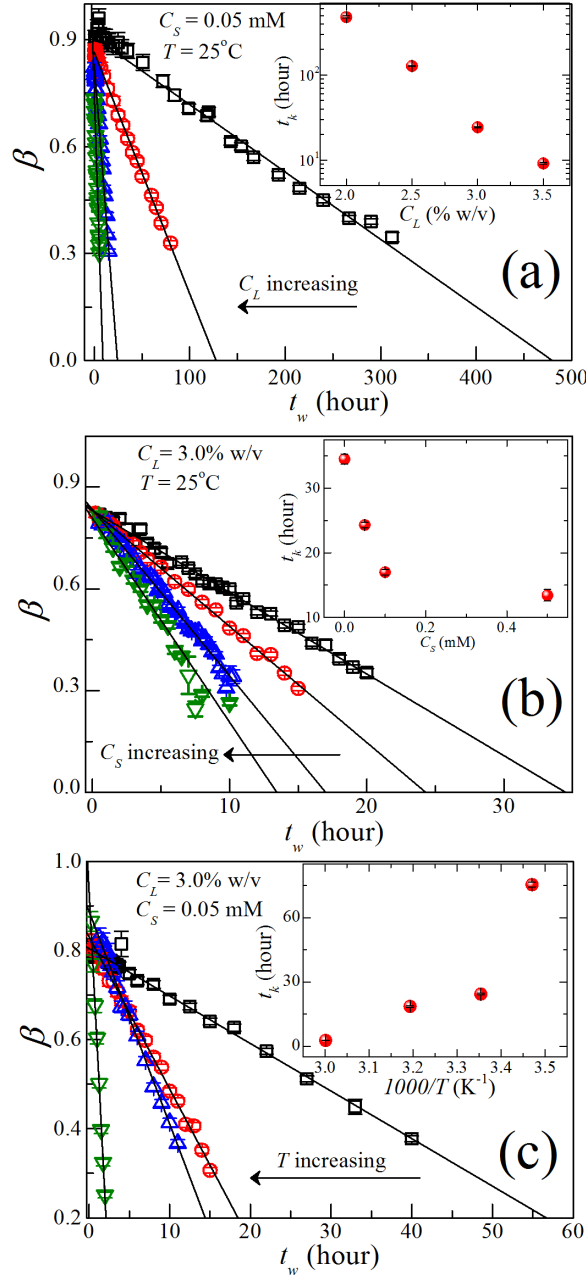


FIGURE 5.3: (a) Stretching exponents β are plotted vs. t_w for $C_S=0.05$ mM and $T=25^\circ\text{C}$ at different C_L (from right to left, 2.0% w/v (\square), 2.5% w/v (\circ), 3.0% w/v (\triangle), 3.5% w/v (∇)). (b) β vs. t_w for $C_L=3.0\%$ w/v and $T=25^\circ\text{C}$ at different C_S (from right to left, 0 mM (\square), 0.05 mM (\circ), 0.1 mM (\triangle), 0.5 mM (∇)). (c) β vs. t_w for $C_L=3.0\%$ w/v and $C_S=0.05$ mM at different T (from right to left, 15°C (\square), 25°C (\circ), 40°C (\triangle), 60°C (∇)). t_k (\bullet), the waiting time at which $\beta \rightarrow 0$, measured by extrapolation of β , are plotted for different C_L , C_S and T in the insets of (a), (b) and (c) respectively.

C_L , C_S and T , β decreases linearly with t_w . For many supercooled liquids, β depends on temperature and decreases linearly with $1/T$ [16]. As discussed earlier, a non-Arrhenius stretched exponential decay of the $C(t)$ data can arise due to the well-known Kohlrausch-Williams-Watts distribution of the slow relaxation timescales given by $\rho_{ww}(\tau) = -\frac{\tau_{ww}}{\pi\tau^2} \sum_{k=0}^{\infty} \frac{(-1)^k}{k!} \sin(\pi\beta k) \Gamma(\beta k + 1) \left(\frac{\tau}{\tau_{ww}}\right)^{\beta k + 1}$ [20]. The width w of the distribution can be written as $w = \frac{\langle \tau_{ww}^2 \rangle}{\langle \tau_{ww} \rangle^2} - 1 = \frac{\beta \Gamma(2/\beta)}{(\Gamma(1/\beta))^2} - 1$. Here $\beta \leq 1$, with a lower value of β indicating a broader distribution of relaxation timescales, with the width w of the distribution $\rho_{ww}(\tau)$ diverging at $\beta \rightarrow 0$ [20]. We define a time t_k as the waiting time at which $\beta \rightarrow 0$. This definition of a hypothetical divergence time t_k is similar to the definition of the Kauzmann temperature T_K for molecular glass formers where it is seen that w diverges with a vanishing β at T_K [15, 16, 32, 33]. From the data plotted in figure 5.3, t_k is measured by extrapolating β to 0 for different C_L , C_S and T . It is seen from the insets of figures 5.3(a)-(c) that the extrapolated values of t_k decrease with the increase of C_L , C_S and T .

The temperature T_K corresponding to a vanishing β in fragile supercooled liquids [32, 33], which is typically calculated from the extrapolation of the temperature dependent β data, is seen to be correlated to T_0 [15, 16], i.e. $T_0 \approx T_K$. Given the many similarities between supercooled liquids and aging Laponite suspensions, it is interesting to investigate if t_k has a connection with t_α^∞ , the analogous Vogel time. In figure 5.4, we plot t_α^∞ vs. t_k . Remarkably, it is seen that t_k is correlated with t_α^∞ , i.e. $t_\alpha^\infty \approx t_k$. We further note that for all Laponite suspensions studied here, $4 \leq D \leq 5.5$ (inset of figure 5.4). It is to be noted that values of D for sorbitol, toluene, *o*-terphenyl, propylene carbonate, triphenyl phosphite and sucrose, for example, are 8.6, 5.6, 5.0, 2.9, 2.9 and 0.154 respectively [3, 34]. The obtained values of D for Laponite suspensions therefore compare very well with the D -values for these fragile molecular glass formers, thereby indicating that Laponite suspensions are excellent candidates for the study of the glass transition [35].

In the supercooled liquids literature, the Kauzmann temperature T_K is also known

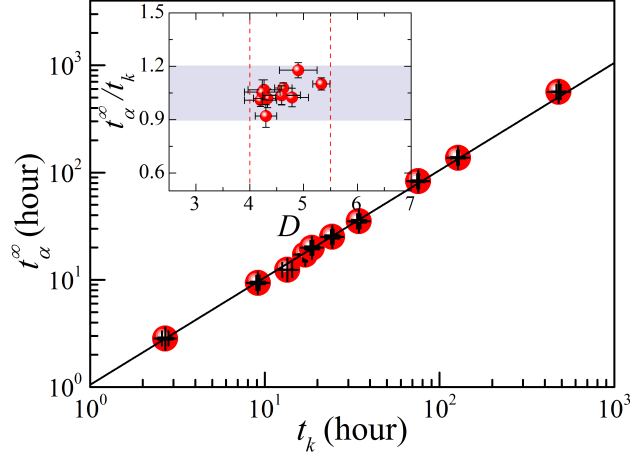


FIGURE 5.4: Analogous Vogel time t_α^∞ is plotted vs. t_k , the waiting time at which $\beta \rightarrow 0$ for all the samples studied here. Solid line is the linear fit with a slope 1.02 ± 0.025 . In the inset, the ratio t_α^∞ / t_k is plotted vs. D .

as the equilibrium glass transition temperature [36]. According to this theory, the system in the supercooled regime relaxes by exploring possible configurations available in the energy landscape via activated processes. However, it is not completely clear that a simple relation between the kinetics and the thermodynamics of a glass former (*i.e.* $T_0 \approx T_K$) always exists, as a systematic increase of T_k/T_0 from unity was observed for increasing values of D [34]. It was reported in an earlier work that the ratio T_k/T_0 lies between 0.9 to 1.2 for $D < 20$ [34]. In the inset of figure 5.4 we have plotted the ratio t_α^∞ / t_k vs. D for data acquired for all the Laponite suspensions of different C_L , C_S and T studied here. It is seen that $0.9 \leq t_\alpha^\infty / t_k \leq 1.2$ for all the samples. As discussed earlier, it was shown in a previous study that T_K/T_0 starts increasing from unity for fragile glass formers and attains higher values for strong supercooled liquids [34]. Although there is an apparent similarity between the results plotted in figure 5.4 and T_k/T_0 ratios reported earlier [34], we note here that t_k , the time at which $w \rightarrow \infty$, for the colloidal suspensions of Laponite studied here, has a very different physical origin when compared to T_K in supercooled liquids.

We now explain the simultaneous divergence of the two hypothetical times, t_α^∞

and t_k in terms of the Vogel-Fulcher behavior of the relaxation times, the stretched-exponential nature of the slow relaxation process and the linear decrease of β with t_w [37]. The observed stretched exponential dependence of the slow relaxation process can be rewritten for aging colloidal suspensions as:

$$\exp\left\{-\left(t/\tau\right)^{\beta(t_w)}\right\} = \exp\left\{-t/L(t_w, t)\right\} \quad (5.3)$$

Here, $L(t_w, t)$ can be interpreted as the time-dependent relaxation time and has a similar physical origin as for supercooled liquids [37]. Following the coupling model proposed by Ngai *et al.* [38–40], we relate $L(t_w, t)$ to the time-dependent relaxation rate $W(t)$ by $W(t) = \beta/L(t_w, t)$, where $\beta = \beta(t_w)$ [41]. This model of relaxation indicates that each relaxation unit of the system relaxes independently with a primitive rate W_0 at timescales that are short when compared to the characteristic timescale $t_0 \equiv 1/\omega_c$ associated with the coupling of the relaxing molecular units. At longer times, i.e. $\omega_c t > 1$, the primitive relaxation rate slows down and can be expressed as, $W(t) = W_0(\omega_c t)^{-n}$, $0 < n < 1$ and $n = 1 - \beta$ [41]. If $L(t_w, t) = L_0(t_w)(t/t_0)^{1-\beta}$ [37], where $L_0 = \beta/W_0$ [41], it follows from equation 5.3 that $\exp\left[-\left(t/\tau\right)^\beta\right] = \exp\left[-\frac{t}{L_0(t_w)(t/t_0)^{1-\beta}}\right] = \exp\left[-\left(\frac{t}{t_0[L_0(t_w)/t_0]^{1/\beta}}\right)^\beta\right]$. Hence, τ can be rewritten as, $\tau = t_0[L_0(t_w)/t_0]^{1/\beta}$ [37]. For colloidal suspensions of Laponite, the secondary relaxation process is related to the microscopic motion of a single relaxation unit (a Laponite particle) and has the following Arrhenius dependence on t_w as discussed earlier in chapter 3: $\tau_1 = \tau_1^0 \exp(t_w/t_\beta^\infty)$ [17]. As $L_0(t_w)$ is related to the single relaxation unit [41], we assume an Arrhenius dependence of $L_0(t_w)$ on t_w for the colloidal suspension of Laponite, $L_0(t_w) = L \exp(t_w/t_\beta^\infty)$, where L is a constant. We have already seen from figure 5.3 that β decreases linearly with t_w , i.e. $\beta(t_w) = \beta_0(t_k - t_w)$. Substituting the t_w -dependence of β along with the Arrhenius dependence of $L_0(t_w)$ in the expression for τ yields a VFT equation,

$$\tau = t_0 \left[\frac{L \exp(t_w/t_\beta^\infty)}{t_0} \right]^{1/\beta} = L^{1/\beta} t_0^{(\beta-1)/\beta} \exp(t_w/t_\beta^\infty) = C \exp\left(\frac{t_w}{t_\beta^\infty \beta_0(t_k - t_w)}\right) \quad (5.4)$$

where $C = L^{1/\beta} t_0^{(\beta-1)/\beta}$. Equation 5.4 has an identical form as equation 5.2, when $t_k \approx t_\alpha^\infty$ with τ diverging at $t_w \rightarrow t_\alpha^\infty$ and the width w of the distribution $\rho_{ww}(\tau)$ diverging at t_k . This explains the correlation between t_k and t_α^∞ observed in figure 5.4.

This successful adaptation of the coupling model to the present scenario of aging colloidal Laponite suspensions, which was previously proposed for molecular glass formers, clearly states the universal nature of the approach to a final arrested state in these two seemingly different glass formers. Additionally, the similar behavior of the fragility parameter D in these two glass formers, together with the explanation of the observed correlation between the two hypothetical divergence times t_α^∞ and t_k using the coupling model, indicate a remarkable similarity in these relaxation processes at the particle scale.

5.4 Conclusions

In this chapter, the time evolutions of the relaxation processes of colloidal suspensions of Laponite are studied by dynamic light scattering (DLS). The fragility parameter D is obtained by fitting the autocorrelation data $C(t)$ for Laponite suspensions of different concentrations (C_L), added salt concentrations (C_S) and temperatures (T). It is seen that the value of D is approximately constant for the entire range of Laponite concentrations and salt concentrations investigated here. These results are reminiscent of the observed independence of the isochoric fragilities of supercooled liquids on pressure. Furthermore, D is independent of the screening effects of the repulsive interparticle interactions due to the addition of salt. Finally, it is seen that T determines the rate at which system approaches the glass transition (or the apparent cooling rate) and that D is weakly dependent on T . This result is reminiscent of the dependence of the kinetic fragility on the cooling rate for metallic glass formers [31].

The stretching exponent β for Laponite suspensions with different C_L , C_S and T is seen to decrease linearly with waiting time, indicating a divergence of the width of the relaxation time distribution at even higher waiting times. This observation is similar

to the decrease of β with $1/T$ in many fragile molecular glass formers. We next define a timescale t_k at which the width of the distribution of the slow relaxation timescale diverges. We report a correlation between t_k and t_α^∞ , where t_α^∞ is the hypothetical Vogel time at which the average slow relaxation time diverges. This correlation corroborates analogous observations in fragile molecular glass formers for which it was reported that the Kauzmann and Vogel temperature are approximately equal ($T_K \approx T_0$). We next calculate the ratio t_α^∞/t_k and plot it vs. D . This ratio is found to be approximately 1 for all the D values reported here. This observation is reminiscent of the ratio T_K/T_0 with fragility parameter D for several supercooled liquids [34].

Our results therefore clearly agree very well with existing results for fragile glass formers. Interestingly, in the case of Laponite which is a colloidal system, t_k is measured from the kinetics of the relaxation process. In contrast, T_K for supercooled liquids is a thermodynamic quantity and generally calculated from calorimetric data. Finally, the correlation between the two hypothetical diverging time scales for Laponite suspensions, t_k and t_α^∞ , demonstrates that the average value and the width of the distribution of slow relaxation times diverge simultaneously. This result is explained using the coupling model proposed for molecular glass formers [38] and the t_w -dependence of the stretching exponent β observed in our experiments.

References

- [1] C. A. Angell, *Science*, **267**, 1924 (1995).
- [2] V. Lubchenko and P. G. Wolynes, *Annu. Rev. Phys. Chem.* **58**, 235 (2007).
- [3] C. A. Angell, *J. Res. Natl. Inst. Stand. Technol.*, **102**, 171 (1997).
- [4] M. D. Ediger, C. A. Angell and S. R. Nagel, *J. Phys. Chem.*, **100**, 13200-13212 (1996).
- [5] C. A. Angell, *J. Non-Cryst. Solids*, **131-133**, 13-31 (1991).
- [6] R. Böhmer, K. L. Ngai, C. A. Angell and D. J. Plazek, *J. Chem. Phys.* **99**, 4201 (1993).
- [7] V. N. Novikov and A. P. Sokolov, *Nature*, **431**, 961-963 (2004).
- [8] S. Sengupta, F. Vasconcelos, F. Affouard and S. Sastry, *J. Chem. Phys.*, **135**, 194503 (2011).
- [9] J. Mattsson, H. M. Wyss, A. Fernandez-Nieves, K. Miyazaki, Z. Hu, D. R. Reichman and D. A. Weitz, *Nature*, **462**, 83-86, (2009).
- [10] C. T. Moynihan, A. J. Eastal and J. Wilder, *J. Phys. Chem.*, **78**, 2673 (1974).

-
- [11] P. G. Debenedetti and F. H. Stillinger, *Nature (London)*, **410**, 259-267 (2001).
- [12] A. Heuer, *J. Phys.: Condens. Matter*, **20**, 373101 (2008).
- [13] F. H. Stillinger, *Science*, **267**, 1935 (1995).
- [14] S. Sastry, *Nature*, **409**, 164-167 (2001).
- [15] X. Xia and P. G. Wolynes, *Phys. Rev. Lett.*, **86**, 5526 (2001).
- [16] P. K. Dixon and S. R. Nagel, *Phys. Rev. Lett.*, **61**, 341 (1988).
- [17] D. Saha, Y. M. Joshi and R. Bandyopadhyay, *Soft Matter* **10**, 3292 (2014).
- [18] B. Ruzicka, L. Zulian and G. Ruocco, *J. Phys.: Condens. Matter* **16**, S4993-S5002 (2004).
- [19] B. Ruzicka, L. Zulian and G. Ruocco, *Phys. Rev. Lett.* **93**, 258301 (2004).
- [20] C. P. Lindsey and G. Patterson, *J. Chem. Phys.* **73**, 3348-3357 (1980).
- [21] C. A. Angell, K. L. Ngai, G. B. McKenna, P. F. McMillan and S. W. Martin, *J. Appl. Phys.*, **88**, 3113 (2000).
- [22] F. Mezei, W. Knaak and B. Farago, *Phys. Rev. Lett.* **58**, 571 (1987).
- [23] D. Sidebottom, R. Bergman, L. Börjesson and L. M. Torell, *Phys. Rev. Lett.* **71**, 2260 (1993).
- [24] W. Gotze and L. Sjogren, *Rep. Prog. Phys.*, **55**, 241-376 (1992).
- [25] D. Saha, R. Bandyopadhyay and Y. M. Joshi, *Langmuir*, **31** (10), 3012-3020 (2015).
- [26] S. Sengupta, T. B. Schrøder and S. Sastry, *Eur. Phys. J. E.* **36**, 141 (2013).
- [27] R. Casalini and C. M. Roland, *Phys. Rev. B*, **71**, 014210 (2005).
- [28] J. J. Stickel and R. L. Powell, *Annu. Rev. Fluid Mech.*, **37**, 129-149 (2005).

-
- [29] C. D. Michele, F. Sciortino and A. Coniglio, *J. Phys.: Condens. Matter*, **16**, L489-L494 (2004).
- [30] A. Shahin and Y. M. Joshi, *Langmuir*, **28**, 15674-15686 (2012).
- [31] Z. Evenson, I. Gallino and Ralf Busch, *J. Appl. Phys.*, **107**, 123529 (2010).
- [32] P. K. Dixon, *Phys. Rev. B*, **42**, 8179 (1990).
- [33] M. Papoular, *Phil. Mag. Lett.*, **64**, 421 (1991).
- [34] H. Tanaka, *Phys. Rev. Lett.*, **90**, 055701 (2003).
- [35] S. A. Kivelson and G. Tarjus, *Nature Materials*, **7**, 831-833 (2008).
- [36] G. Adams and J. H. Gibbs, *J. Chem. Phys.*, **43**, 139 (1965).
- [37] S. R. Nagel and P. K. Dixon, *J. Chem. Phys.*, **90**, 3885 (1989).
- [38] K. L. Ngai, R. W. Rendell, A. K. Rajagopal and S. Teitler, *Ann. New York Acad. Sci.*, **484**, 150 (1986).
- [39] K. L. Ngai, A. K. Rajagopal and S. Teitler, *J. Chem. Phys.*, **88**, 5086 (1988).
- [40] A. K. Rajagopal, S. Teitler and K. L. Ngai, *J. Phys. C:Solid State Phys.*, **17**, 6611 (1984).
- [41] K. L. Ngai, R. W. Rendell, A. K. Rajagopal and S. Teitler, *J. Chem. Phys.*, **91**, 8002 (1989).

6

Characteristics of the secondary relaxation process in soft glassy colloidal suspensions

6.1 Introduction

The study of the relaxation processes in complex, disordered and out-of-equilibrium systems is one of the many unsolved problems in non-equilibrium statistical mechanics. The plethora of non-equilibrium systems around us, supply several opportunities to observe diverse fascinating phenomena. The physics of relaxation processes in glasses or glassy systems has been meticulously pursued during the last century, but is yet unsolved. It has been noted that glasses comprise a disordered state of matter which is structurally like a liquid but whose dynamics are characterized by extremely slow

relaxation. These systems fail to relax within timescales accessible in the laboratory. At the particulate scale, many types of relaxation processes are possible that can involve an atom, a molecule, a part of molecule, a group of molecules or particles. It is important to study how these microscopic relaxation processes slow down as glass-forming materials are quenched below their glass transition temperatures, with their relaxation time scales exceeding the observation time scales as the system falls out of equilibrium.

As discussed earlier, the different types of relaxation processes in glass formers can be classified in two categories- the primary and the secondary relaxation processes [1, 2]. The former is involved with the orientational or structural rearrangements of the molecules or particles and is considered to be the main process leading to structural relaxation. This type of structural relaxation process in molecular glasses or supercooled liquids, metallic glasses, polymer glasses and other glass formers, is generally known as the α -relaxation process [1]. The latter relaxation process, known as the β -relaxation process, involves the motion of a molecule or a part of a molecule and is generally believed to have no connection with the glass transition process [3]. These secondary relaxation processes are much faster than the α -relaxation process. However, many experimental results have shown that some β -relaxation processes are closely related to the structural relaxation process. Very recent molecular dynamics simulation results on asymmetric diatomic molecular glass formers demonstrate that the α -relaxation process has a close relationship with a particular secondary relaxation process known as the Johari-Goldstein β -relaxation (J-G) process [4–7]. This type of secondary relaxation process is generally considered to be universal in nature as it appears in a variety of glass formers such as supercooled liquids, metallic glasses, polymeric glasses and plastic crystals. It involves all the parts of the molecule or particle and is particularly important in glassy systems because of its very close relationship with the α -relaxation process. However, the absence of any experimentally reported result detecting a J-G β -relaxation mode in the colloidal glasses has raised questions regarding its universality.

After decades of research, a general route is used to classify the secondary relaxation processes in glass formers based on their dynamic properties [3] and to determine whether it is related to its structural relaxation process. These include a through characterization of the nature of the glass former in terms of the following:

- Molecule with or without internal degrees of freedom.
- Involvement of the whole molecule or part of a molecule in the secondary relaxation process.
- The temperature and pressure dependencies of the secondary relaxation time τ_β .
- The separation between τ_β and τ_α , the primary or structural relaxation times.
- The relationship between τ_β and τ_0 , with τ_0 being the independent primitive relaxation time according to the coupling model.
- The pressure and temperature dependencies of τ_β and τ_0 .
- The temperature dependence of the secondary relaxation strength $\Delta\epsilon_\beta$ (measured from dielectric spectroscopy) across the glass transition temperature T_g .
- The aging behavior of τ_β and $\Delta\epsilon_\beta$ below T_g .
- Merging of τ_β with the primary relaxation time τ_α at very high temperatures.

In this chapter, we study the microscopic relaxation processes for Laponite suspensions by dynamic light scattering (DLS) experiments. The α and β -relaxation timescales are estimated from the autocorrelation functions obtained by DLS measurements for Laponite suspensions with different concentrations (C_L), salt concentrations (C_S) and temperatures (T). We measure the primitive relaxation timescales from the α -relaxation time and the stretching exponent β by applying the coupling model for highly correlated systems. Our experimental results suggest that the β -relaxation process involves all the parts of a Laponite particle and is coupled with the primitive relaxation process. The glass transition time is also correlated with the activation energy of the β -relaxation

process for all Laponite concentrations, salt concentration and temperatures. Our studies indicate that the β -relaxation process of colloidal glasses of Laponite carries many similarities with the J-G β -relaxation processes and may, indeed, be a plausible candidate that requires further investigation.

6.2 Sample preparation and experimental methods

All the experiments reported in this chapter are performed with aqueous suspension of Laponite RD ®. Details of the sample preparation is given in chapter 4 (section 4.2). Details of the experimental techniques are given in chapter 2 (section 2.2.1).

6.3 Results and discussions

Intensity autocorrelation functions $g^{(2)}(t)$ are acquired in dynamic light scattering experiments (DLS) as a function of the waiting time t_w of aging Laponite suspensions. In figure 6.1, we plot the normalized intensity autocorrelation function, $C(t) = g^{(2)}(t) - 1$ as function of delay time t for several waiting times for a 2.5% w/v Laponite suspension at 25°C and at a scattering angle $\theta=60^\circ$. It is seen from this figure that the $C(t)$ data show two-step relaxations and that the slow relaxation process progressively slow down with t_w . The two-step relaxation process in $C(t)$ can be expressed by a sum of an exponential and a stretched exponential decay [8–10].

$$C(t) = [a \exp \{-t/\tau_1\} + (1 - a) \exp \{-(t/\tau_{ww})^\beta\}]^2 \quad (6.1)$$

In equation 6.1, a , τ_1 , τ_{ww} and β are the four fitting parameters corresponding to the relaxation strength, the fast relaxation time, the slow relaxation time and the stretching exponent respectively. $C(t)$ is a second order autocorrelation function with the two terms within the brackets of equation 6.1 giving the first order autocorrelation function $g^{(1)}(t)$. It is to be noted that in most molecular glass formers, dielectric spectroscopy,

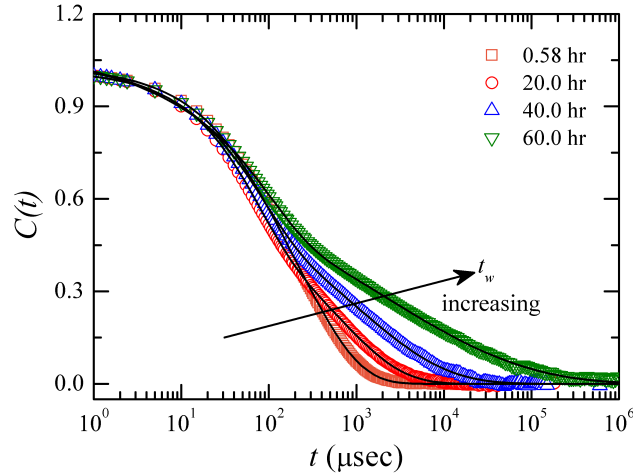


FIGURE 6.1: The normalized intensity autocorrelation functions $C(t)$ vs. the delay time t at 25°C and at a scattering angle $\theta=60^\circ$ for 2.5% w/v Laponite suspension at several different waiting times t_w (from left to right: 0.58 hour (\square), 20.0 hour (\circ), 40.0 hour (\triangle) and 60.0 hour (∇)). The solid lines are fits to equation 6.1.

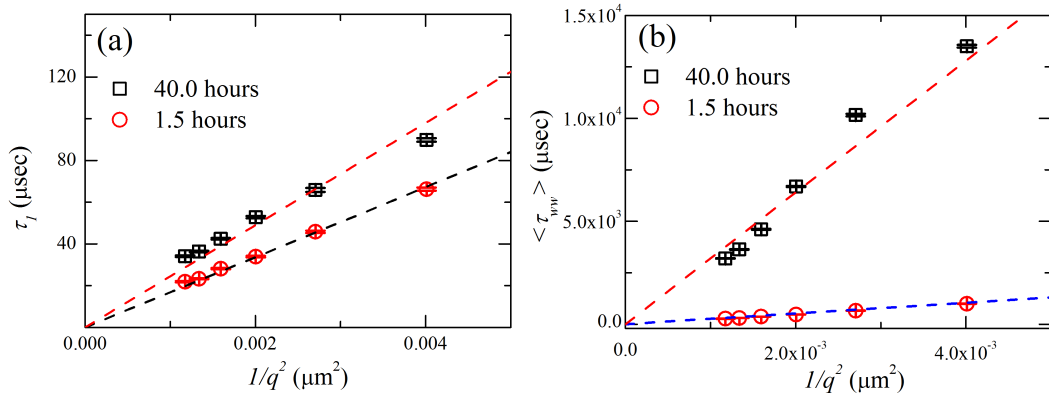


FIGURE 6.2: The diffusive dynamics of the fast relaxation time (τ_1) and the mean slow relaxation time ($\langle \tau_{ww} \rangle$) are shown in (a) and (b) respectively for a 2.5% w/v Laponite sample for two different waiting times t_w . The dashed lines are linear fits passing through the origin.

which yields a first order correlation function due to dipole-dipole correlation, has been often used to study relaxation processes.

We plot τ_1 and τ_{ww} vs. $1/q^2$ in figures 6.2(a) and (b), where q is the scattering wave vector for two different waiting times ($t_w = 40$ hour and 1.5 hour) for a 2.5% w/v Laponite suspension. A straight line passing through the origin indicates that both

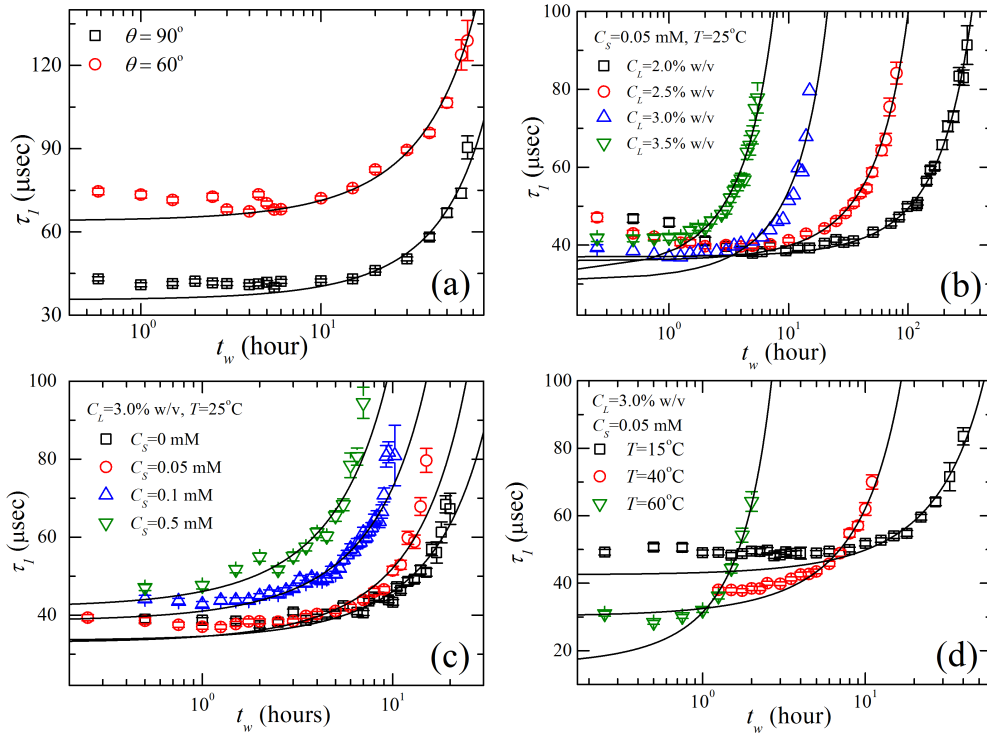


FIGURE 6.3: (a) Fast relaxation time τ_1 vs. waiting time t_w for $C_L = 2.5\%$ w/v Laponite suspension ($C_S = 0$ mM and $T = 25^\circ\text{C}$) at two different scattering angles ($\theta = 90^\circ$ (\square) and $\theta = 60^\circ$ (\circ)). Solid lines are fits to the equation 6.2. τ_1 is plotted vs. t_w for different (b) C_L (2.0% w/v (\square), 2.5% w/v (\circ), 3.0% w/v (\triangle) and 3.5% w/v (∇)), (c) C_S (0 mM (\square), 0.05 mM (\circ), 0.1 mM (\triangle) and 0.5 mM (∇)), and (d) T (15°C (\square), 40°C (\circ) and 60°C (∇)) values at scattering angle $\theta = 90^\circ$.

the relaxation processes at 25°C are diffusive i.e. $\tau_1 = 1/D_1 q^2$ and $\langle \tau_{ww} \rangle = 1/D_2 q^2$, where D_1 and D_2 are the diffusion coefficient corresponding to the fast and slow relaxation processes respectively. Another important observation is that both τ_1 and $\langle \tau_{ww} \rangle$ slow down with t_w .

It was seen in chapter 3 that the aging dynamics of a spontaneously evolving Laponite suspension and its approach to a kinetically arrested state can be compared to molecular glasses which achieve glass transition upon rapid cooling to avoid the crystalline state. It has been demonstrated in chapter 3 that Arrhenius and super-Arrhenius dependencies of the fast and slow relaxation times on waiting time are obtained if the waiting time of a spontaneously evolving Laponite suspension is mapped with the inverse of the thermodynamic temperature $1/T$ of molecular glasses [10]. It was also

demonstrated that the t_w -dependence of τ_1 and $\langle \tau_{ww} \rangle$ are given in the following equations:

$$\tau_1 = \tau_1^0 \exp\left[\frac{t_w}{t_\beta^\infty}\right] \quad (6.2)$$

and,

$$\langle \tau_{ww} \rangle = \langle \tau_{ww} \rangle^0 \exp\left[\frac{Dt_w}{t_\alpha^\infty - t_w}\right] \quad (6.3)$$

In equation 6.2, the fitting parameter $\tau_1^0 = \tau_1(t_w \rightarrow 0)$ while t_β^∞ is the characteristic timescale associated with the slowdown of the secondary relaxation process. In equation 6.3, D , $\langle \tau_{ww} \rangle^0$ and t_α^∞ are the three fitting parameters. D is called the fragility or strength parameter which quantifies the deviation from an Arrhenius behavior, $\langle \tau_{ww} \rangle^0 = \langle \tau_{ww} \rangle(t_w \rightarrow 0)$ and t_α^∞ is the Vogel time, or the hypothetical waiting time at which $\langle \tau_{ww} \rangle \rightarrow \infty$ [10].

In figure 6.3(a), the time-evolutions of τ_1 is plotted *vs.* t_w for two scattering angles ($\theta = 60^\circ$ and 90°) for a 2.5% Laponite suspension. It is seen from figure 6.3 that τ_1 decreases with t_w at smaller t_w , while at higher t_w , τ_1 increases with t_w for all the Laponite suspensions with different C_L , C_S and T investigated here. It is known that Laponite particles can form tactoids or rigid aggregates consisting of more than one platelet in aqueous suspension [11]. At the early stage of dispersion, these tactoids exfoliate and the rate of exfoliation decreases with time as the intertactoid Coulombic repulsion increases rapidly with time [11]. This tactoid fragmentation process results in the speeding up of the dynamics and gives rise to the non-monotonicity of the τ_1 *vs.* t_w plot at small t_w . It is seen from figure 6.3 that the later increasing part of τ_1 can be fitted to equation 6.2 and the rate of increase becomes faster for higher values of C_L , C_S and T .

The diffusion coefficient D_1 of a sphere is related to its relaxation time τ_1 by the relation $\tau_1 = 1/D_1 q^2$ [12]. D_1 can be estimated for a dilute suspension of monodisperse sphere from the Stokes-Einstein relation, $D_1 = k_B T / 6\pi\eta r_h$ [12], where k_B , η and r_h are the Boltzmann constant, viscosity of the medium (0.89 mPa.s at 25°C) and hydrodynamic radius of the particle respectively. It follows, therefore, that $\tau =$

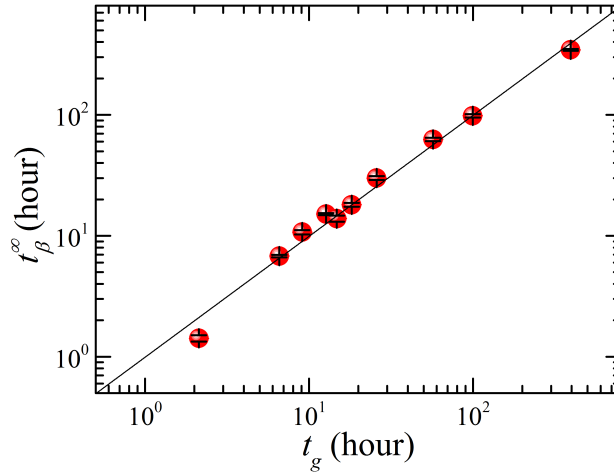


FIGURE 6.4: The characteristic timescale associated with the secondary relaxation process t_{β}^{∞} vs. the glass transition time t_g for different C_L , C_S and T . The solid line ($t_{\beta}^{\infty} \approx (0.99 \pm 0.05)t_g$) is a linear fit passing through the origin.

$1/D_1 q^2 = 6\pi\eta r_h/k_B T q^2$. However, the Laponite platelet is a disk shaped particle (diameter $d = 25\text{-}30$ nm and thickness $t = 1$ nm approximately [13]). For these anisotropic platelets, the equivalent spherical diameter (ESD) is given by the Jennings-Parslow relation, $d_s = d \left(\frac{3 \arctan \sqrt{(d/t)^2 - 1}}{2 \sqrt{(d/t)^2 - 1}} \right)^{1/2}$ [14]. From the Jennings-Parslow relation the estimated value of d_s for Laponite is 7.5-8.3 nm. Using the value of $d_s = 7.5 - 8.3$ nm for the Laponite particle, the estimated value of diffusion timescale of the particle τ is 30-34 μsec and 62-68 μsec at $q = 0.0223 \text{ nm}^{-1}$ ($\theta = 90^\circ$) and $q = 0.0157 \text{ nm}^{-1}$ ($\theta = 60^\circ$) respectively. It is seen from figure 6.3(a) that the values of τ_1^0 , i.e. $\tau_1(t_w \rightarrow 0)$, is 34 μsec and 63 μsec for $\theta = 90^\circ$ and $\theta = 60^\circ$ and agrees well with the estimated values of τ_1 at smaller t_w . Therefore, τ_1 is associated with a relaxation process that involves all parts of the Laponite platelet.

In chapter 5, it was seen that $\langle \tau_{ww} \rangle$ increases with t_w for all C_L , C_S and T . It is also seen that the time-evolution of $\langle \tau_{ww} \rangle$ can be fitted to equation 6.3 very well. Similar to chapter 3, we define the glass transition time t_g as the waiting time at which $\langle \tau_{ww} \rangle = 100$ sec for all Laponite suspensions [15]. In figure 6.4, the characteristic

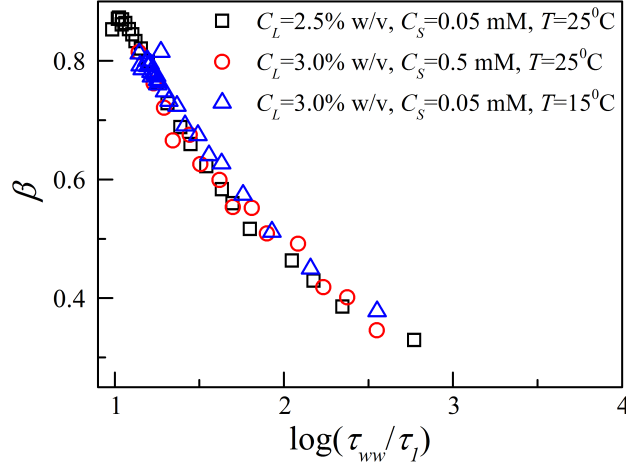


FIGURE 6.5: Stretching exponent β vs. $\log(\tau_{ww}/\tau_1)$ for Laponite suspensions with different C_L , C_S and T .

timescale t_β^∞ associated with fast relaxation process is plotted vs. t_g for Laponite suspensions with different C_L , C_S and T studied in this work. It is seen from the figure that $t_\beta^\infty \propto t_g$ indicating a possible coupling between the fast and slow relaxation processes. A linear fit to the data (solid line) yields $t_\beta^\infty = (0.99 \pm 0.05)t_g$. This is reminiscent of an empirical observation for many supercooled liquids where it was seen that the glass transition temperature T_g is proportional to the activation energy E_β of the slow secondary β -relaxation process [16, 17].

The α -relaxation process is a non-exponential process which can be given by a stretched exponential function (equation 6.1). As discussed in chapters 1 and 3, the non-exponential decay arise due to the distribution of relaxation timescales given by the well-known Kohlrausch-Williams-Watts distribution (equation 3.4): $\rho_{ww}(\tau) = -\frac{\tau_{ww}}{\pi\tau^2} \sum_{k=0}^{\infty} \frac{(-1)^k}{k!} \sin(\pi\beta k) \Gamma(\beta k + 1) \left(\frac{\tau}{\tau_{ww}}\right)^{\beta k + 1}$ [18]. The width w of the distribution is related to stretching exponent β and given by $w = \frac{\langle \tau_{ww}^2 \rangle}{\langle \tau_{ww} \rangle^2} - 1 = \frac{\beta\Gamma(2/\beta)}{(\Gamma(1/\beta))^2} - 1$. In figure 6.5, we plot β vs. $\log(\tau_{ww}/\tau_1)$. It is seen that β decreases with $\log(\tau_{ww}/\tau_1)$ indicating that the width of the α -relaxation process is coupled with the secondary relaxation time [5]. This coincides well with an empirical observation in supercooled liquids that the width of the α -relaxation process is coupled with the J-G relaxation timescale, with β

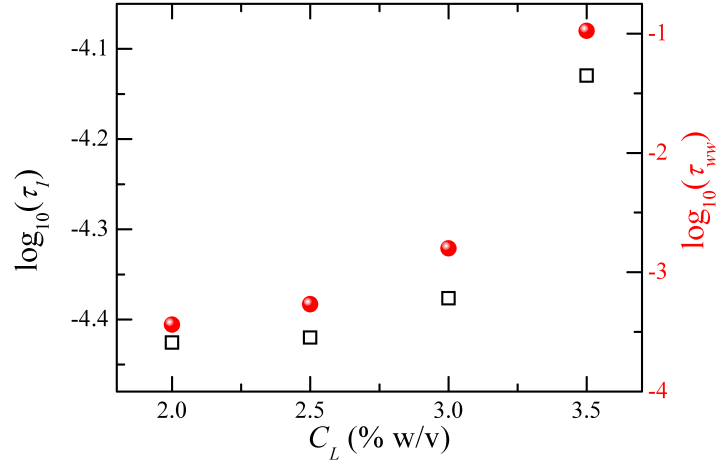


FIGURE 6.6: Relaxation times τ_1 (□) and τ_{ww} (●) vs. C_L for $t_w=5.5$ hour.

decreasing monotonically with $\log(\tau_\alpha/\tau_\beta)$ [5, 19].

In figure 6.6, we plot $\log(\tau_1)$ and $\log(\tau_{ww})$ for different C_L for a fixed waiting time $t_w=5.5$ hour. It is seen from figure that both τ_1 and τ_{ww} increase with C_L . In chapter 5, we had pointed out that increasing C_L is analogous to increasing pressure on the system as a larger number of particles are packed in a fixed volume. So, both the relaxation processes of Laponite suspensions are sensitive to pressure or concentration. It must be pointed out here that in the context of supercooled liquids, the slow secondary relaxation process or the J-G relaxation process is very sensitive to pressure [19]. For example, it was seen from the dielectric measurement of sorbitol and xylitol that the separation between the α and β relaxation peaks is greater at elevated pressure confirming the sensitivity of the β relaxation process to high pressures [20].

We have calculated the primitive relaxation time τ^* from the coupling model [21–23] which is discussed in chapter 5. The two coupled equations which follow from this model are given by:

$$\phi(t) = \exp \left[- \left(\frac{t}{\tau_{ww}} \right)^{1-n} \right] \quad (6.4)$$

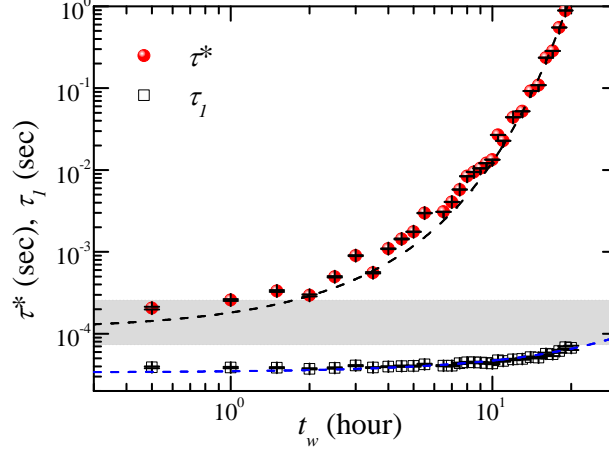


FIGURE 6.7: The secondary relaxation times τ_1 (\square) and the primitive relaxation times τ^* (\bullet) vs. t_w for 3.0% w/v Laponite suspension ($C_S = 0$ mM, $T = 25^\circ\text{C}$). Dashed lines are exponential fits.

and,

$$\tau_{ww} = \left[(1-n)\omega_c^n W_0^{-1} \right]^{1/1-n} \quad (6.5)$$

In the above two equations $\phi(t)$ is the slow relaxation process, n is the coupling parameter and it is related to the stretching exponent β by $n = 1 - \beta$. As discussed in chapter 5, W_0 is the primitive rate (i.e. $W_0 = 1/\tau^*$) and the characteristic timescale $t_0 = 2\pi/\omega_c$. It follows from equation 6.5 that τ^* can be calculated from the following relation [3, 24].

$$\tau_{ww} = \left[\beta \left(\frac{2\pi}{t_0} \right)^{1-\beta} W_0^{-1} \right]^{1/\beta} = \left[\beta \left(\frac{2\pi}{t_0} \right)^{1-\beta} \tau^* \right]^{1/\beta} \quad (6.6)$$

Here, it is reasonable to assume that $t_0 = 300 \mu\text{sec}$ as $\tau_1 < t_0 < \tau_{ww}$ at all t_w . In figure 6.7, we plot the evolution of τ_1 and τ^* for a 3.0% w/v Laponite suspension ($C_S = 0$ mM, $T = 25^\circ\text{C}$). It is seen that both relaxation timescales grow exponentially with increase in t_w as the Laponite suspension approaches the glass transition. This indicates that the secondary relaxation process is correlated with the primitive relaxation process. From the extrapolation of τ_1 at higher t_w , it is seen that τ_1 approaches τ_0^* which is

the value of τ^* at $t_w = 0$ (shaded region in figure 6.7). A similar correlation is observed between τ^* and the JG β -relaxation time τ_β in case of molecular glass formers [3, 19].

6.4 Conclusions

In this chapter, we have extracted the primary and secondary relaxation timescales of Laponite suspensions with different Laponite concentrations (C_L), salt concentrations (C_S) and temperatures (T) from the intensity autocorrelation functions obtained from dynamic light scattering (DLS) measurements. A well-known route is followed to characterize the secondary relaxation process [3]. It is seen that the secondary relaxation process of aging Laponite suspensions involves all parts of a Laponite particle. Furthermore, it is coupled with the primary relaxation process as it is seen that its glass transition time t_g is coupled with its characteristic time t_β^∞ . It is also demonstrated that the width w is correlated with the β -relaxation timescale. Both τ_1 and τ_{ww} are found to be very sensitive to concentration even within the narrow range explored here. Finally, a correlation is observed between the primitive relaxation time τ^* and τ_1 as τ_1 approaches τ_0^* at longer waiting times. Our experimental observations suggest that the β -relaxation process of colloidal glasses of Laponite show many characteristics of the J-G β -relaxation processes that are seen in molecular glass formers.

References

- [1] W. Gotze and L. Sjogren, Rep. Prog. Phys., **55**, 241-376 (1992).
- [2] P. G. Debenedetti and F. H. Stillinger, Nature (London), **410**, 259-267 (2001).
- [3] K. L. Ngai and M. Paluch, J. Chem. Phys., **120**, 857-873 (2004).
- [4] D. Fragiadakis and C. M. Roland, Phys. Rev. E, Phys. Rev. E, **86**, 020501(R) (2012).
- [5] D. Fragiadakis and C. M. Roland, Phys. Rev. E, **88**, 042307 (2013).
- [6] D. Fragiadakis and C. M. Roland, Phys. Rev. E, **89**, 052304 (2014).
- [7] D. Fragiadakis and C. M. Roland, Phys. Rev. E, **91**, 022310 (2015).
- [8] B. Ruzicka, L. Zulian and G. Ruocco, J. Phys.: Condens. Matter **16**, S4993-S5002 (2004).
- [9] B. Ruzicka, L. Zulian and G. Ruocco, Phys. Rev. Lett. **93**, 258301 (2004).
- [10] D. Saha, Y. M. Joshi and R. Bandyopadhyay, Soft Matter **10**, 3292 (2014).
- [11] S. Ali and R. Bandyopadhyay, Langmuir, **29**, 12663-12669 (2013).

-
- [12] B. J. Berne and R. Pecora, *Dynamic Light Scattering: With Applications to Chemistry, Biology, and Physics*, Wiley-Interscience, New York, 1976.
- [13] M. Kroon, G. H. Wegdam and R. Sprik, *Phys. Rev. E*, **54**, 6541-6550 (1996).
- [14] B. R. Jennings and K. Parslow, *Proc. R. Soc. Lond. A*, **419**, 137-149 (1988).
- [15] C. A. Angell, *J. Non-Cryst. Solids*, **131-133**, 13-31 (1991).
- [16] A. Kudlik, C. Tschirwitz, S. Benkhof, T. Blochowicz and E. Rössler, *Europhys. Lett.*, **40**, 649-654 (1997).
- [17] D. Prevosto, S. Capaccioli, M. Lucchesi, S. Sharifi, K. Kessairi and K.L. Ngai, *Phil. Mag.*, **88**, 4063-4069 (2008).
- [18] C. P. Lindsey and G. D. Patterson, *J. Chem. Phys.*, **73**, 3348-3357 (1980).
- [19] K. L. Ngai, *J. Chem. Phys.*, **109**, 6982 (1998).
- [20] M. Paluch, C. M. Roland, S. Pawlus, J. Ziolo, and K. L. Ngai, *Phys. Rev. Lett.*, **91**, 115701 (2003).
- [21] K. L. Ngai, R. W. Rendell, A. K. Rajagopal and S. Teitler, *Ann. New York Acad. Sci.*, **484**, 150 (1986).
- [22] K. L. Ngai, A. K. Rajagopal and S. Teitler, *J. Chem. Phys.*, **88**, 5086 (1988).
- [23] A. K. Rajagopal, S. Teitler and K. L. Ngai, *J. Phys. C:Solid State Phys.*, **17**, 6611 (1984).
- [24] K. L. Ngai, J. Colmenero, A. Alegria, and A. Arbe, *Macromolecules*, **25**, 6727-6729 (1992).

7

Fragile behavior of a soft glassy colloidal suspension in the presence of probe particles

7.1 Introduction

The nature of the glass transition in supercooled liquids is one of the oldest unsolved problems in condensed matter physics [1, 2]. Supercooled liquids, in general, show increase in their viscosities and structural relaxation times when quenched rapidly towards their glass transition temperatures to avoid crystallization. As discussed earlier in chapter 1, this change in viscosity or structural relaxation time has a super-Arrhenius dependence on temperature for many supercooled liquids and is expressed by the Vogel-Fulcher-Tammann (VFT) relation, $\tau = \tau_0 \exp\left(\frac{DT_0}{T-T_0}\right)$ [3–5]. The fragility

or strength parameter D is a measure of the deviation from the Arrhenius temperature dependence and T_0 is a hypothetical divergence temperature or Vogel temperature. The super-Arrhenius dependence of viscosity and transport quantities is characteristic of a fragile glass former that is approaching its glass transition.

Even after decades of research, there is no general theory which can explain all the features of the glass transition. There is also no consensus on whether the glass transition is a thermodynamic transition or a purely kinetic phenomenon. In order to develop a better theory, it is necessary to find an analytically and numerically tractable model system for an extremely fragile liquid [6]. A model system with tunable fragility could be invaluable for experiments as well as theory to understand several concepts related to the glass transition. It should be noted here that fragility is believed to be a solely material dependent quantity [3], though what determines fragility is still an enigma.

Experiments and simulations on glass formers report several correlations between fragility and other material parameters as discussed in previous chapters. Simulation results reveal that the softness of the interparticle potential is correlated to the fragility of glass forming binary mixtures [7]. It was shown experimentally for supercooled liquids that a correlation exists between Poisson's ratio and fragility [8] while for colloidal glasses, soft i.e. compressible colloid particles were seen to form stronger glasses [9]. Recent experiments on metallic glass formers have correlated the material fragility to the rate of its structural ordering with decreasing temperature, thus revealing a fundamental link between its structure and dynamics [10].

In the last few decades, a different class of glass formers i.e. spin glasses have been studied extensively [11–13]. These glass formers, that are formed in magnetic systems due to the disordered freezing of spins upon decreasing temperature [14], are extremely fragile and are relatively better-understood when compared to molecular glass formers. However, spin glasses have some basic differences when compared to molecular glass formers. The presence of quenched disorder in spin glasses is so ubiquitous that it is necessary to introduce quenched disorder in model molecular glass formers to compare these two systems properly. In practice, these kinds of systems

are commonly described by the random pinning glass model, where some parts of the system are frozen in space and therefore always out of equilibrium [15, 16]. It is a challenge to verify the results of the random pinning glass model experimentally as it requires an external field in most of the cases to drive parts of a system out of equilibrium. A comparatively easy approach could be the introduction of less mobile regions comprising larger probe particles in the form of impurities. Exploring the possibility of tunable fragility in these systems due to the addition of such less mobile regions is an extremely interesting problem.

Another aspect of any glass or glassy system is that in spite of its liquid-like structure, it is kinetically totally different from a liquid as its microscopic dynamics are frozen [17]. Many experimental techniques, for example video microscopy, confocal microscopy, static and dynamic light scattering, rheology etc., are available to study both the dynamics and structure of colloidal glass formers [17]. These measurements are extremely important as they offer opportunities to justify or falsify the fundamental connection between the structure and dynamics of disordered systems. In this context, colloidal glass formers could be particularly important, as visualization at the particulate level is easily possible because of their large sizes when compared to the constituents of molecular systems.

In this chapter, we report dynamic light scattering (DLS) experiments on fragile glasses formed by colloidal suspensions of Laponite RD[®], a model glass former. Polystyrene beads, of sizes larger than the Laponite particle, are dispersed in the Laponite suspensions and constitute the less mobile regions. Dynamic light scattering (DLS) experiments are performed to study the time evolution of the microscopic dynamics. The primary or α -relaxation timescales (τ_{ww}) are extracted from the intensity autocorrelation functions of light scattered by the less mobile regions dispersed in the Laponite suspensions. It is seen that the secondary β -relaxation timescale (τ_1) arise due to the diffusion of Laponite particles. The fragility parameter D is calculated with different concentrations and sizes of polystyrene beads. Our experimental results are compared with existing simulation results on model glass-forming binary mixtures in

the presence of random pinning.

7.2 Sample preparation and experimental methods

All experiments reported in this chapter are performed using Laponite RD[®]. As discussed in chapter 1, Laponite is a disk shaped particle with diameter $d = 25\text{-}30$ nm and thickness $t = 1$ nm approximately [18]. The equivalent spherical diameter (ESD) can be estimated for these anisotropic platelets using the Jennings-Parslow relation, $d_s = d \left(\frac{3 \arctan \sqrt{(d/t)^2 - 1}}{2 \sqrt{(d/t)^2 - 1}} \right)^{1/2}$ [19]. The estimated value of d_s for Laponite is 7.5-8.3 nm. The details of preparation and filtration of Laponite suspensions have been discussed in chapter 3. Polystyrene NanosphereTM (refractive index $n=1.595$ at wavelength $\lambda=532$ nm [20]) of sizes 95.6 nm, 208 nm, 390 nm and 588 nm were bought from Thermo Scientific and Bangs Laboratories, Inc. To study the effect of bead sizes on the Laponite medium, polystyrene beads of different sizes (95.6 nm, 208 nm, 390 nm and 588 nm) at a fixed volume fraction ($\phi = 4.75 \times 10^{-5}$) are added separately in the cuvettes loaded with Laponite suspensions (concentration of Laponite 2.0% w/v i.e. volume fraction of Laponite $\phi_L = 7.9 \times 10^{-3}$, and refractive index $n \approx 1.335$ at a wavelength $\lambda=589.3$ nm [21]) and are sealed immediately. The concentration of Laponite expressed in % w/v refers to the weight of Laponite in grams that is dispersed in 100 ml MilliQ water. Polystyrene beads (208 nm) of different volume fractions ($\phi=1.9 \times 10^{-5}$, 2.85×10^{-5} , 3.8×10^{-5} , 4.75×10^{-5} and 5.7×10^{-5}) are also added separately to the cuvettes loaded with Laponite suspensions for experiments with different polystyrene concentrations. Each cuvette is gently moved upside down several times to mixed the polystyrene beads uniformly. The waiting time (i.e. $t_w = 0$) is measured from the moment when the mixing of the polystyrene beads in the Laponite suspension is complete. The cuvettes are kept at a constant temperature by water circulation using a Polyscience Digital Inc. water circulator. The Dynamic Light Scattering (DLS) experiments are done using a Brookhaven Instruments Corporation (BIC) BI-200SM spectrometer. Details of the experimental set-up are described in chapter 2. Rheological measurements are done by

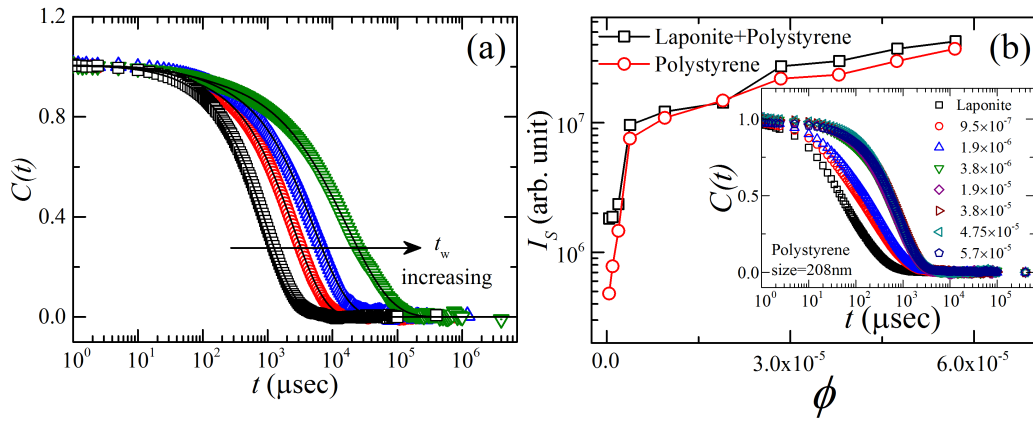


FIGURE 7.1: (a) The normalized intensity autocorrelation functions $C(t)$ vs. the delay time t at 25°C and scattering angle $\theta=90^\circ$ for 2.0% w/v Laponite suspensions ($\phi_L = 7.9 \times 10^{-3}$) with 208 nm polystyrene probe particles embedded at a volume fraction $\phi = 4.75 \times 10^{-5}$ at several different waiting times t_w (from left to right) 16 hour (\square), 102 hour (\circ), 150 hour (\triangle), 207 hour (∇). The solid lines are fits to equation 7.1.(b) The scattered intensity I_s vs. ϕ for 208 nm polystyrene beads dispersed in 2.0% w/v Laponite suspension (\square) and dispersed in MilliQ water (\circ) at $t_w = 1$ hour, $T = 25^\circ\text{C}$ and $\theta = 90^\circ$. In the inset, $C(t)$ vs. t at 25°C and $\theta = 90^\circ$ for 2.0% w/v Laponite suspension with 208 nm polystyrene beads of different ϕ values (from left to right, no polystyrene (\square), 9.5×10^{-7} (\circ), 1.9×10^{-6} (\triangle), 3.8×10^{-6} (∇), 1.9×10^{-5} (\diamond), 3.8×10^{-5} (\triangleright), 4.75×10^{-5} (\triangleleft), 5.7×10^{-5} (\diamond)).

an Anton Paar MCR 501 Rheometer. Laponite suspensions are filled in a concentric cylinder geometry (Anton Paar CC17) and the complex viscosity is measured with t_w by applying an oscillatory strain with amplitude 0.1% at an angular frequency $\omega = 1$ rad s^{-1} . Details of the rheometer and the measuring geometry are given in chapter 2.

7.3 Results and discussions

As discussed in chapters 1 and 2, colloidal suspensions of Laponite evolve spontaneously with time and the system approaches kinetic arrest with increasing waiting time t_w [25–27]. In spontaneously evolving Laponite suspensions, the microscopic relaxation processes slow down with t_w in a manner that is reminiscent of the dynamical slow down observed in molecular glass formers when the latter is driven out of equilibrium as the temperature is decreased rapidly [22]. In order to compare these two systems, the waiting time t_w of aging Laponite suspensions can be mapped with the inverse

of the thermodynamic temperature $1/T$ of a supercooled liquid (chapter 3 and [22]). In figure 7.1(a), we plot $C(t)$, the normalized intensity autocorrelation function, vs. the delay time t for a 2.0% w/v Laponite suspension with 208 nm polystyrene particles that comprise the less mobile regions at several different waiting times t_w . Similar to the data presented in the earlier chapters of this thesis, two-step relaxation processes are observed, with α and β -relaxation processes becoming more distinguishable at higher waiting times. As discussed earlier, this kind of two-step decay in autocorrelation function is ubiquitous in glass formers [28]. The $C(t)$ data acquired experimentally in this work can be represented by the following equation.

$$C(t) = g^{(2)}(t) - 1 = [a \exp\{-t/\tau_1\} + (1 - a) \exp\{-(t/\tau_{ww})^\beta\}]^2 \quad (7.1)$$

In the above equation, τ_1 , τ_{ww} , β and a are the fitting parameters. τ_1 is the fast relaxation time due to the diffusion of a particle within the cage formed by its neighbors. The slow relaxation time τ_{ww} is associated with diffusion of the scatters out of the cage leading to structural rearrangements. This is a non-Debye relaxation process and can occur due to a distribution of relaxation times, with β being the stretching exponent associated with this slow relaxation process. The mean slow relaxation time $\langle \tau_{ww} \rangle$ can be obtained by $\langle \tau_{ww} \rangle = (\tau_{ww}/\beta)\Gamma(1/\beta)$ [29]. In equation 7.1, a and $(1 - a)$ are the relaxation strengths of the fast and slow relaxation processes respectively.

In figure 7.1(b), we plot the scattered intensity from 2.0% w/v Laponite suspensions with increasing concentration of polystyrene beads (\square) and compare these data with the scattered intensity of polystyrene beads dispersed in water (\circ). It is seen from this figure that polystyrene is a strong scatterer of light and that the scattering from the Laponite suspension is insignificant when the volume fraction of polystyrene beads $\phi > 0.5 \times 10^{-5}$. It is seen from the inset of figure 7.1(b) that the shape of the auto-correlation function for a pure Laponite suspension changes significantly even when very small amounts ($\phi = 4.0 \times 10^{-6}$) of polystyrene is added. The higher scattering contrast of polystyrene arises from its refractive index mismatch with respect to the

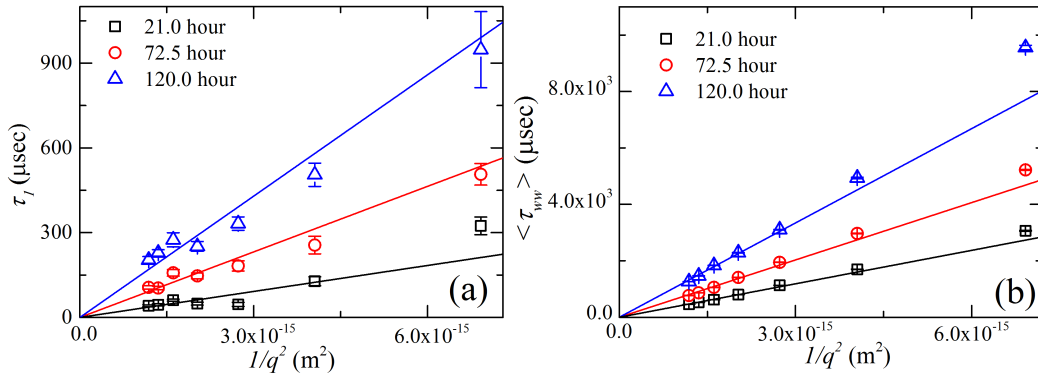


FIGURE 7.2: The diffusive nature of (a) the fast relaxation time (τ_1) and (b) mean slow relaxation time ($\langle \tau_{ww} \rangle$) are shown for a 2.0% w/v Laponite suspension with 95.6 nm polystyrene beads (volume fraction $\phi=4.75 \times 10^{-5}$) at different waiting times. The solid lines are linear fits passing through the origin.

Laponite suspension ($\Delta n = 1.595 - 1.335 = 0.260$). Since the Laponite particles have a much smaller ESD= 7.5-8.3 nm in comparison to the polystyrene particles used here (95.6-588 nm), the polystyrene beads dispersed in Laponite suspension scatter light more strongly when compared to the Laponite particles.

In figure 7.2, both τ_1 and $\langle \tau_{ww} \rangle$ are plotted vs. $1/q^2$ for a 2.0% w/v Laponite suspension with 95.6 nm polystyrene beads (volume fraction $\phi=4.75 \times 10^{-5}$) at different waiting times. Straight line fits passing through the origin indicate the diffusive natures of τ_1 and $\langle \tau_{ww} \rangle$. The diffusive behaviors of both these relaxation processes are also seen for all the samples used here with different sizes of embedded polystyrene beads. In figure 7.3(a), we plot the fast relaxation time τ_1 , obtained from the fits of equation 7.1 to $C(t)$ vs. t for 2.0% w/v Laponite suspension (volume fraction $\phi_L = 7.9 \times 10^{-3}$) with 208 nm polystyrene beads dispersed at volume fractions ϕ between 1.9×10^{-5} - 5.7×10^{-5} . τ_1 is seen to increase from 30 μsec to 100 μsec for the range of t_w investigated. For a Laponite suspension without beads, an increase in τ_1 is also seen with t_w [22, 23]. The relaxation time (τ) of a spherical particle is related to its diffusion coefficient D_1 by: $\tau = 1/D_1 q^2$ [24]. According to the Stokes-Einstein relation, $D_1 = k_B T / 6\pi\eta r_h$ for a dilute suspension of spherical monodisperse particles, where k_B , η and r_h are the Boltzmann constant, viscosity of the medium (0.89 mPa.s at 25°C) and hydrodynamic radius of the particle respectively. Furthermore, as shown

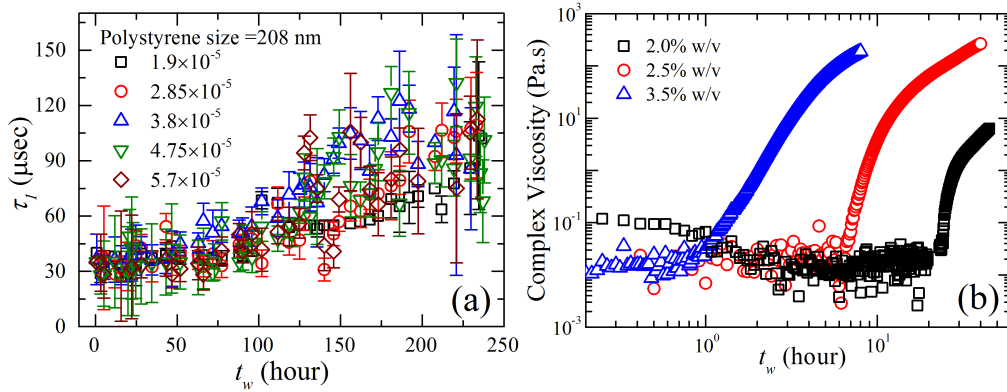


FIGURE 7.3: (a) Fast relaxation time $\langle \tau_1 \rangle$ vs. waiting time t_w for 2.0% w/v Laponite suspension with 208 nm polystyrene beads of volume fractions (ϕ) 1.9×10^{-5} (\square), 2.85×10^{-5} (\circ), 3.8×10^{-5} (\triangle), 4.75×10^{-5} (∇), 5.7×10^{-5} (\diamond) at 25 °C and at a scattering angle $\theta = 90^\circ$. (b) Complex viscosity vs. t_w for 2.0% w/v (\square), 2.5% w/v (\circ) and 3.5% w/v (\triangle) Laponite suspensions at 25 °C.

in figure 7.2(a), $\tau = 1/D_1 q^2 = 6\pi\eta r_h/k_B T q^2$ ($q = 0.0223 \text{ nm}^{-1}$), which gives us $\tau \approx 30 - 34 \text{ } \mu\text{sec}$ for $d_s = 7.5\text{-}8.3 \text{ nm}$, the ESD of Laponite particle. It is seen from figure 7.3(a) that for suspensions of very low t_w where the constituents may be assumed to diffuse freely, the average value of τ_1 is approximately $30 \text{ } \mu\text{sec}$ and agrees well with the estimated values of τ_1 at very small t_w . As the Laponite suspension ages, the viscosity increases with t_w (figure 7.3(b)) which results in increased viscous drag on the polystyrene particles at large t_w . The corresponding growth in relaxation timescales is seen in figure 7.3(a) and agrees well with the previously reported results [22, 23, 26]. The large scatter in the data in figure 7.3(a) can be attributed to fitting errors that arise due to the limited dynamical extent of the fast relaxation process in our experiments and to the fact that Laponite particles are very weak scatterers of light (figure 7.1(b)).

The autocorrelation function for polystyrene dispersed in water has a single exponential decay (figure 7.4). In contrast to this, the data in figure 7.5, the autocorrelation function for polystyrene beads dispersed in a Laponite suspension cannot be fit to a single exponential decay. However, a functional form that is a sum of an exponential and a stretched exponential decay shows good fits. In figure 7.5(a), we also see that the decay of the autocorrelation function is significantly slower when polystyrene beads

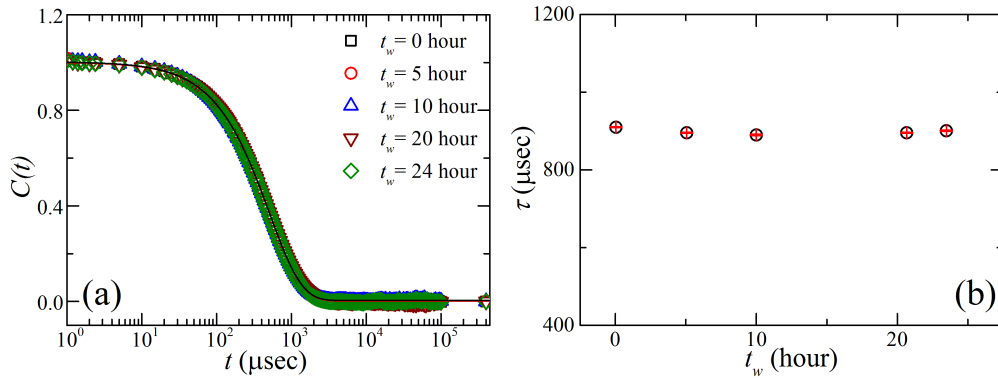


FIGURE 7.4: (a) The normalized intensity autocorrelation functions $C(t)$ vs. the delay time t at 25°C and at a scattering angle $\theta = 90^\circ$ for polystyrene (size=208 nm, volume fraction $\phi=4.75 \times 10^{-5}$) in MilliQ water at different waiting times t_w . The solid lines are fits to the exponential function. (b) The relaxation time τ vs. t_w are extracted from the $C(t)$ data plotted in (a). The size of the scatterers is extracted from the relation $2r_h = k_B T \tau q^2 / 3\pi\eta$ which yields the size 215.6 ± 0.9 nm.

are dispersed in Laponite suspensions rather than in water. This is because in the former samples, the polystyrene beads are confined and diffuse inside cages formed by the Laponite particles. The slower non-exponential decay in $C(t)$ is therefore mainly dominated by the diffusion of these polystyrene beads out of their cages. In contrast, the polystyrene beads dispersed in water show only Brownian motion without any aging (figure 7.4(b)). The slow-down seen in figure 7.1, can therefore be attributed to the aging of the Laponite suspension which in turn results in the slowing down of the polystyrene particle dispersed in it.

We plot the mean slow relaxation time $\langle \tau_{ww} \rangle$ vs. t_w for 2.0% w/v Laponite suspension with different concentrations of 208 nm polystyrene beads in figure 7.6(a). It is seen from this figure that $\langle \tau_{ww} \rangle$ remains almost constant at earlier times and increases rapidly at longer t_w . For an aging Laponite suspension, $\langle \tau_{ww} \rangle$ shows a Vogel-Fulcher-Tammann like dependence on t_w given by [22]:

$$\langle \tau_{ww} \rangle = \langle \tau_{ww} \rangle^0 \exp(Dt_w / (t_w^\infty - t_w)) \quad (7.2)$$

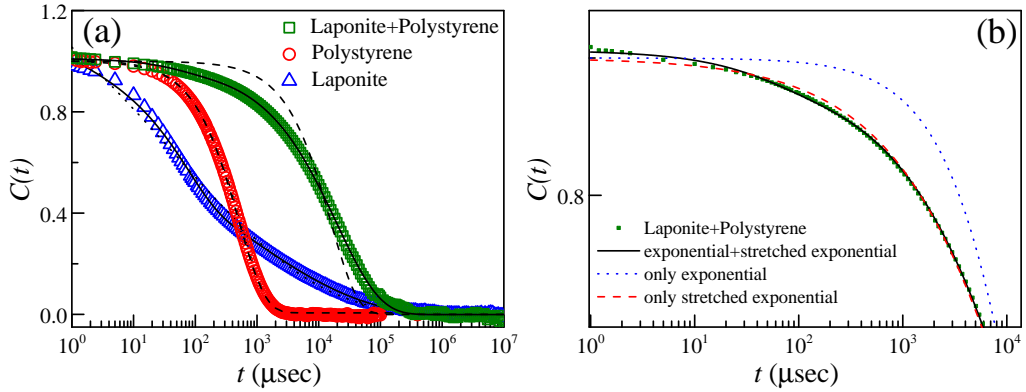


FIGURE 7.5: (a) The normalized intensity autocorrelation functions $C(t)$ vs. the delay time t at 25°C and $\theta = 90^\circ$ for polystyrene beads (size=208 nm, volume fraction $\phi = 4.75 \times 10^{-5}$) dispersed in water (\circ), polystyrene beads dispersed in 2.0% w/v Laponite suspension (\square) and 2.0% w/v Laponite suspension without any bead (Δ), at $t_w = 212$ hour. Dashed and solid lines are fits to an exponential function and to equation 7.1 respectively. (b) $C(t)$ vs. t for polystyrene beads dispersed in 2.0% w/v Laponite suspension (\square) plotted in (a). Dotted, solid and dashed lines are fits to an exponential function, equation 7.1 and a stretched exponential function respectively. It is seen from the plot that equation 7.1 yields the best fit.

Here, D , t_α^∞ and $\langle \tau_{ww} \rangle^0$ are the fragility parameter, Vogel time and $\langle \tau_{ww} \rangle$ at $t_w \rightarrow 0$, respectively. As already discussed, the aging process in Laponite suspensions results in a dynamical slowing down of the slow relaxation process obtained from the $C(t)$ data for polystyrene particles embedded in the Laponite suspension. We fit equation 7.2 to the data plotted in figure 7.6(a). It is seen that equation 7.2 fits extremely well to the slow relaxation time data. This validates our assumption that the slowing down of the relaxation timescales of polystyrene is due to the slowing down of the relaxation dynamics of the Laponite suspension. In figure 7.6(b), we plot $\langle \tau_{ww} \rangle$ vs. t_w for different sizes of polystyrene beads ($\phi = 4.75 \times 10^{-3}$) dispersed in 2.0% w/v Laponite suspensions. It is seen from the plot that $\langle \tau_{ww} \rangle$ is longer for larger particle sizes as the relaxation time is proportional to the hydrodynamic radius of the particle in dilute suspension i.e. $\tau = 1/Dq^2 = 6\pi\eta r_h/k_B T q^2$. We see that the rate of increase of the relaxation time at higher t_w is also size-dependent. It has been reported earlier that the polystyrene beads show size-dependent diffusion in Laponite suspensions [30].

It is evident from figure 7.6 that the relaxation timescale increases as the size

Size (nm)	$\mu = \frac{1}{3\pi\eta d}$ (Kg ⁻¹ s)
8	1.49×10^{10}
95.6	1.25×10^9
208	5.73×10^9
390	3.06×10^8
588	2.03×10^8

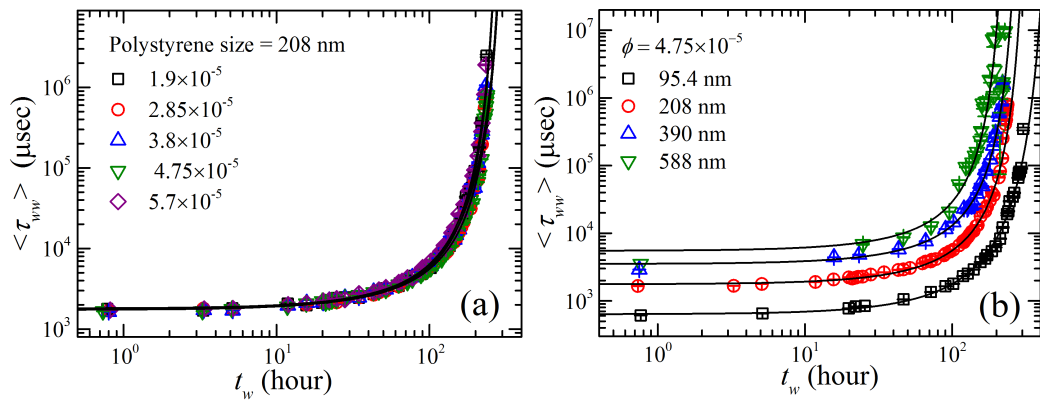
Table 7.1: Mobility of Laponite particle (ESD \approx 8 nm) and polystyrene beads.

FIGURE 7.6: (a) Mean slow relaxation time $\langle \tau_{ww} \rangle$ vs. waiting time t_w at different concentrations of 208 nm polystyrene beads dispersed in 2.0% w/v Laponite suspension. (b) $\langle \tau_{ww} \rangle$ vs. t_w at different sizes of polystyrene beads at volume fraction (ϕ) 4.75×10^{-5} dispersed in 2.0% w/v Laponite suspension. Solid lines are fits to equation 7.2.

(d) or the mass of the embedded polystyrene particle increases. Mobility $\mu = \frac{1}{3\pi\eta d}$ decreases as the size of the particle increases (table 7.1). Polystyrene particles therefore behave as less mobile regions in the Laponite suspension which are diffusing inside and out of the cages formed by the neighboring Laponite particles.

In order to see the effects of the concentration and the size of the polystyrene particles on the aging dynamics of the Laponite medium, we plot the fragility parameter D and Vogel time t_α^∞ , calculated by fitting equation 7.2 to $\langle \tau_{ww} \rangle$ data, vs. the concentration (figure 7.7(a)) and size (figure 7.7(b)) of the polystyrene beads respectively. It is seen from the figure 7.7(a) that D increases by a very small amount with polystyrene concentration while t_α^∞ remains almost independent of concentration. Such a dependence of D and t_α^∞ on polystyrene concentration is reminiscent of the results in recent molecular dynamics simulations of supercooled liquids with random pinning

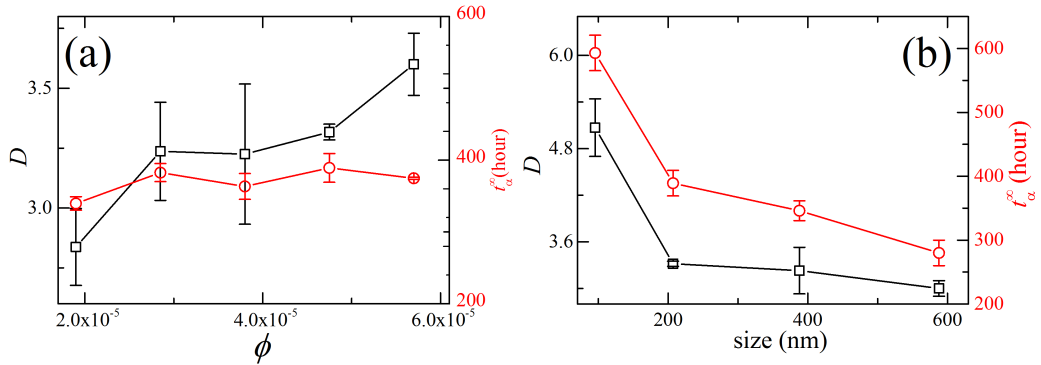


FIGURE 7.7: (a) Fragility parameter D (\square) and Vogel time t_α^∞ (\circ) vs. volume fraction ϕ of 208 nm polystyrene bead dispersed in Laponite suspension of volume fraction (ϕ_L)= 7.9×10^{-3} . (b) D (\square) and t_α^∞ (\circ) vs. size of polystyrene beads for a fixed $\phi = 4.75 \times 10^{-5}$.

[31] which revealed that the kinetic fragility parameter, $K_{VFT} = 1/D$, decreases as the pinning concentration increases, while the hypothetical divergence temperature (T_0) is independent of the pinning concentration. We further note that in our experimental range of ϕ , D is very weakly dependent on ϕ . In figure 7.7(b), we plot D and t_α^∞ for different sizes of the embedded polystyrene beads at the same volume fraction ($\phi = 4.75 \times 10^{-5}$). It is seen that both D and t_α^∞ decrease rapidly as the size of the bead increases.

7.4 Conclusions

We have studied the relaxation dynamics of aqueous Laponite suspensions in the presence of less mobile regions, introduced by adding larger polystyrene beads. The α -relaxation timescales (τ_{ww}) are extracted from the intensity autocorrelation functions of light scattered by the less mobile regions dispersed in the Laponite suspensions. It is seen that the secondary β -relaxation timescale (τ_1) originates due to the diffusion of Laponite particles. It is seen that both fragility parameter D and the hypothetical divergence time t_α^∞ decrease with the size of the polystyrene bead. The fragility parameter D

increases by a very small amount but t_{α}^{∞} remains almost unchanged in the narrow concentration range of the beads investigated here. These observations are reminiscent of simulation results obtained for supercooled liquids with random pinning [31]. However, in the simulation results, the pinned sites are always out of equilibrium and are therefore truly quenched. In the present case, polystyrene beads have finite mobilities even though the sizes of polystyrene beads are much bigger than Laponite particles. Therefore, the polystyrene beads behave as regions of sparse mobility and can only be compared qualitatively to the simulation results for very low pinning concentrations [31].

References

- [1] P. W. Anderson, *Science* 267, 1615 (1995).
- [2] A. J. Liu and S. R. Nagel in *Jamming and Rheology: Constrained Dynamics on Microscopic and Macroscopic Scales* (eds A. J. Liu & S. R. Nagel) 1-6 (Taylor and Francis, 2001).
- [3] C. A. Angell, *J. Non-Cryst. Solids*, **131-133**, 13-31 (1991).
- [4] R. Böhmer, K. L. Ngai, C. A. Angell and D. J. Plazek, *J. Chem. Phys.* **99**, 4201 (1993).
- [5] P. G. Debenedetti and F. H. Stillinger, *Nature*, **410**, 259-267 (2001).
- [6] S. A. Kivelson and G. Tarjus, *Nature Materials* **7**, 831-833 (2008).
- [7] S. Sengupta, F. Vasconcelos, F. Affouard and S. Sastry, *J. Chem. Phys.*, **135**, 194503 (2011).
- [8] V. N. Novikov and A. P. Sokolov, *Nature*, **431**, 961-963 (2004).
- [9] J. Mattsson, H. M. Wyss, A. Fernandez-Nieves, K. Miyazaki, Z. Hu, D. R. Reichman and D. A. Weitz, *Nature*, **462**, 83-86, (2009).

-
- [10] N. A. Mauro, M. Bloggett, M. L. Johnson, A. J. Vogt and K. F. Kelton, *Nature Communications*, **5**:4616 (2014), doi:10.1038/ncomms5616.
- [11] S. F. Edwards and P. W. Anderson, *J. Phys. F: Metal Phys.*, **5**, 965 (1975).
- [12] K. Binder and A. P. Young, *Rev. Mod. Phys.*, **58**, 801 (1986).
- [13] L. Berthier and G. Biroli, *Rev. Mod. Phys.*, **83**, 587 (2011).
- [14] D. L. Stein and C. M. Newman, *Spin Glasses: Old and New Complexity*, Princeton University Press, Princeton, New Jersey 08540, 2013.
- [15] S. Karmakar and G. Parisi, *Proc. Nat. Acad. Sci.*, **110**, 2752-2757 (2013).
- [16] K. Kim, *Europhys. Lett.*, **61**, 790-795 (2003).
- [17] G. L. Hunter and E. R. Weeks, *Rep. Prog. Phys.*, **75**, 066501 (2012).
- [18] M. Kroon, G. H. Wegdam and R. Sprik, *Phys. Rev. E*, **54**, 6541-6550 (1996).
- [19] B. R. Jennings and K. Parslow, *Proc. R. Soc. Lond. A*, **419**, 137-149 (1988).
- [20] S. H. Jones, M. D. King and A. D. Ward, *Phys. Chem. Chem. Phys.*, **15**, 20735-20741 (2013).
- [21] N. Ravi Kumar, K. Muralidhar and Y. M. Joshi, *App. Clay Sci.*, **42** (1-2), 326 (2008).
- [22] D. Saha, Y. M. Joshi and R. Bandyopadhyay, *Soft Matter*, **10**, 3292 (2014).
- [23] D. Saha, R. Bandyopadhyay and Y. M. Joshi, *Langmuir*, **31** (10), 3012-3020 (2015).
- [24] B. J. Berne and R. Pecora, *Dynamic light scattering: With applications to Chemistry, Biology, and Physics*; John Wiley & Sons: New York, 1975.
- [25] B. Abou, D. Bonn and J. Meunier, *Phys. Rev. E*, **64**, 021510 (2001).

- [26] B. Ruzicka, L. Zulian and G. Ruocco, *J. Phys.: Condens. Matter*, **16**, S4993-S5002 (2004).
- [27] B. Ruzicka, L. Zulian and G. Ruocco, *Phys. Rev. Lett.*, **93**, 258301 (2004).
- [28] W. Gotze and L. Sjorgen, *Rep. Prog. Phys.*, **55**, 241-376 (1992).
- [29] C. P. Lindsey and G. D. Patterson, *J. Chem. Phys.*, **73**, 3348-3357 (1980).
- [30] D. R. Strachan, G. C. Kalur and S. R. Raghavan, *Phys. Rev. E*, **73**, 041509 (2006).
- [31] S. Chakrabarty, S. Karmakar and C. Dasgupta, *Phase Diagram of Glass Forming Liquids with Randomly Pinned Particles*, arXiv:1404.2701v3.

8

Falling ball experiments on aging colloidal suspensions

8.1 Introduction

The falling of an object through a non-Newtonian aging suspension leads to very interesting manifestations of Stokesian flows without any terminal velocity. Many industrial processes, for example chocolate and concrete preparation that involve the settling of solid objects through non-Newtonian pasty fluids, depend strongly on the settling behavior of these objects.

In a Newtonian fluid, the terminal velocity v of an object falling through it under the action of gravity arises because of the balance between the drag force of the fluid on the object and the buoyant weight of the object [1].

$$v = \frac{2(\rho_s - \rho)gR^2}{9\eta} \quad (8.1)$$

Here, ρ_s , ρ , η , g and R are the density of the object, fluid density, viscosity of the fluid, acceleration due to gravity and radius of the object respectively. However, the fall of an object through a non-Newtonian fluid may not achieve terminal velocity as the drag force depends on many factors like shear rate, preparation history and also on the initial structure. After decades of research, the complete understanding of the motion of an object in a fluid with structure (i.e. pasty fluids) remains elusive. Several experiments on the fall of an object through non-Newtonian fluids i.e. Laponite clay suspensions [2–4], polymer solutions [5] and concentrated suspensions [6] have been carried out during the last few decades and several models have been developed to explain the observed flow behaviors [7, 8]. It was seen that a sphere falling through a thixotropic medium (i.e. Laponite suspension) showed different types of motion depending on the age of the medium or its initial structure [9]. For example, the ball was seen to fall rapidly with almost constant velocity at smaller ages. This was followed by a slower fall with decreasing velocity at moderate ages and stoppage at higher ages. On the other hand, observations in bentonite clay suspensions show that the velocity of the fall increases as the object gets deeper into the fluid [10]. All these results indicate the important roles of the structure formation and rejuvenation processes during the motion of an object in aging clay suspensions.

In recent years, it was observed that the rheological behavior of aging Laponite suspensions have striking differences depending on whether they had evolved spontaneously or were rejuvenated suspensions. In shear melted experiments, the plateau value of the complex viscosity was reported to depend upon the idle time or the time elapsed after preparation. A partial irreversibility in aging behavior upon rejuvenation was also observed [11]. It was also seen that the permanent structures in Laponite suspensions that are preserved for a larger idle time cannot be destroyed even by applying very large shear deformations [12]. The microscopic dynamics of Laponite suspensions also show dichotomic aging behaviors [13], indicating a difference in structure between spontaneously evolved and rejuvenated suspensions. It must be noted here that the motion of an object falling in a Laponite suspension was studied extensively

for only rejuvenated suspensions in earlier works [2–4, 9]. Therefore, experiments on spontaneously evolving suspensions could be extremely interesting as the fall of the object could likely explore different conditions of structure formation.

In this chapter, we report our results of the fall of steel balls through spontaneously evolving colloidal suspensions of Laponite. Balls of different sizes are dropped into the suspensions having different initial states of structure. An increase of velocity of the ball as it gets deeper into the fluid is observed. This increment is more pronounced for larger balls and for lower aging or waiting times of the suspensions. A simple rheological model is discussed to explain the experimental results by taking into account (i) the restructuring and destructuring processes and (ii) the dependence of the viscosity of the suspensions on the structure parameter and shear rate [9].

8.2 Sample preparation and experimental methods

All experiments reported in this chapter are done using Laponite XLG[®] (BYK Additives). Laponite XLG is a high-purity grade of Laponite RD [14, 15] with similar size as Laponite RD (diameter 25–30 nm and thickness 1 nm approximately [16]), but with less heavy metal content than the RD grade. Laponite XLG is hygroscopic in nature. It is first heated in a hot air oven (Biovision Inc.) for 16 hours at 120°C before the experiment. Colloidal suspensions of Laponite XLG (concentration 3.5% w/v) are prepared by adding dried Laponite powder to MilliQ water (resistivity $\approx 18.2 \text{ M}\Omega\text{-cm}$). Here, the concentration (% w/v) is the weight of Laponite XLG powder in grams added to 100 ml MilliQ water. The Laponite suspension is vigorously stirred with a magnetic stirrer for 1 hour for complete dispersion of Laponite powder in the aqueous medium. After 1 hour, the suspension becomes optically clear. It is then filtered through a Millipore membrane filter (pore size = $0.45 \mu\text{m}$) with the help of a vacuum pump (Tarsons Rockyvac) in order to avoid large particle clusters. Proper care is taken to avoid any change of Laponite concentration during the filtration process. After filtration, the Laponite suspension (approximately 600 ml) is loaded into a falling ball viscometer

which consists of a cylindrical tube kept inside a water bath. Details of the design and working principle of the falling ball viscometer are given in chapter 2. Freshly prepared Laponite suspensions are used to fill the viscometer for each experiment. The temperature of the water bath is maintained at 25°C with the help of a temperature controller (Polyscience Digital Inc.). After loading, the top of the cylindrical tube is covered with a parafilm to keep it isolated from the atmosphere and the material is left to age so that its microstructure starts to develop. The waiting time t_w is calculated from the moment the Laponite suspension is completely loaded into the viscometer. After a waiting time t_w , the parafilm cover is removed from the top and the steel ball is dropped using a push-pull solenoid based release mechanism positioned at the center to avoid the rotation of the balls. A guide tube is used to ensure that the ball always falls through the center of the tube. The path followed by the ball is recorded with an IDT Motion Pro Y4-S2 high speed camera at 700-1500 frames per second. Details of the camera are given in chapter 2. The position of the ball during its fall is tracked from the images recorded by the camera using a LabView based tracking program [17] and the velocity of the ball is calculated from the position *vs.* time data.

8.3 Results and discussions

We have performed falling ball experiments with steel balls falling through spontaneously evolving Laponite suspensions. The experiments reported here are performed with freshly prepared Laponite suspension of $t_w < 100$ min. In figure 8.1(a), snapshots captured by the camera are shown for various stages of the fall of a 5 mm steel ball through a 3.5% w/v Laponite suspension at $t_w = 90$ min. In figure 8.1(b), displacement of the ball from the free surface of the suspension is plotted *vs.* the time of fall for the 5 mm steel ball for different t_w . As expected, the ball gets deeper into the fluid with time, with the velocity of fall depending strongly on t_w . The velocity of the falling ball, which is calculated from the displacement *vs.* time data, is plotted *vs.* x in figure 8.2 for the 5 mm steel ball for different waiting times t_w . It is seen from the figure that (i)

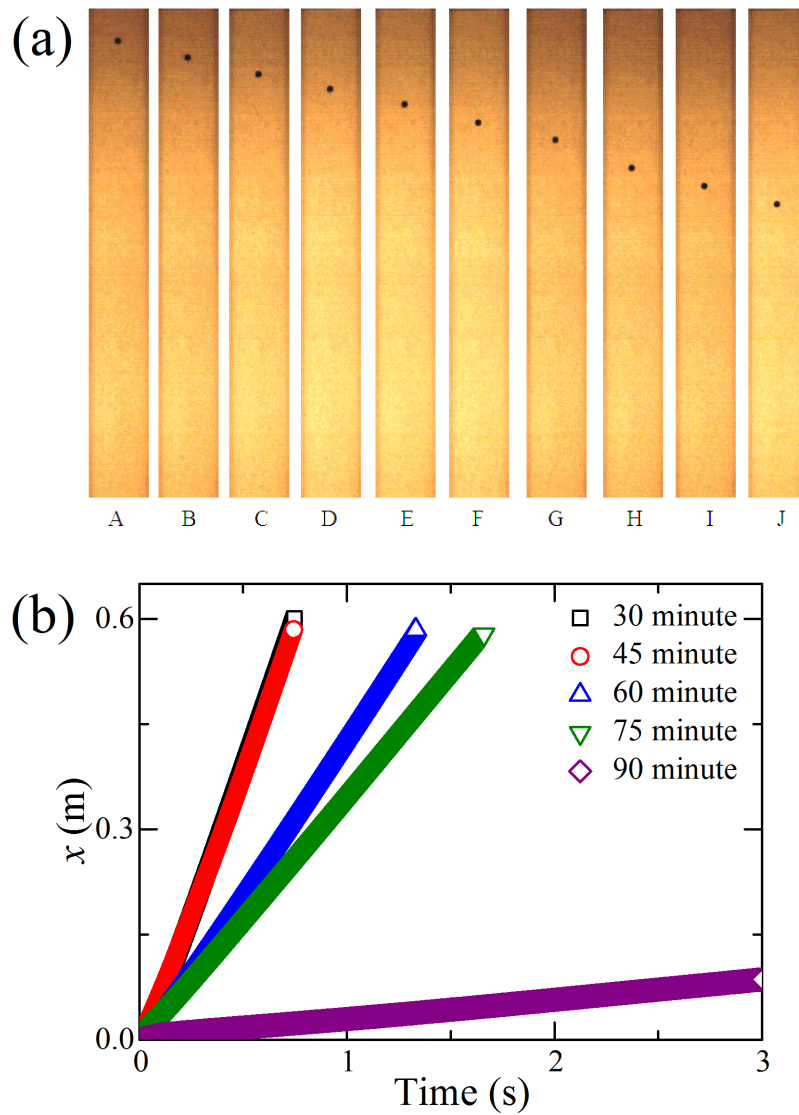


FIGURE 8.1: (a) Snapshots of a steel ball of 5 mm in diameter falling through a Laponite suspension of 3.5% (w/v) of waiting time $t_w=90$ minutes. (b) Displacement vs time of a steel ball of 5 mm in diameter falling through Laponite suspensions of 3.5% w/v characterized by several waiting times.

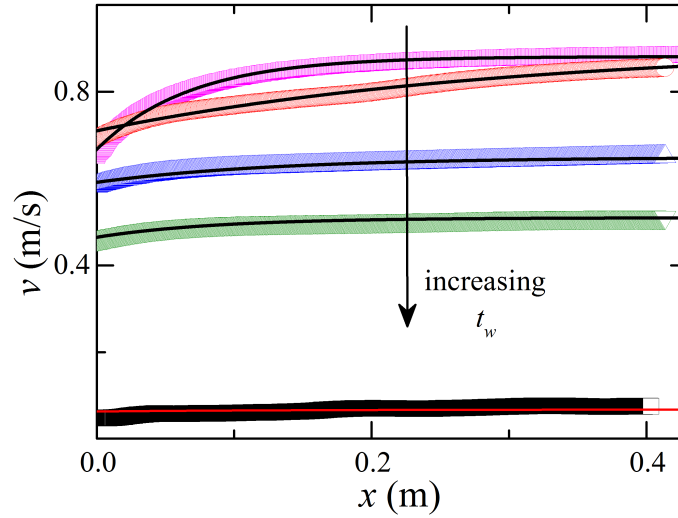


FIGURE 8.2: Velocity of a steel ball of 5 mm diameter falling through a Laponite suspension of 3.5% (w/v) at several different waiting times t_w (from top to bottom) 30 minutes (\square), 45 minutes (\circ), 60 minutes (\triangle), 75 minutes (∇), 90 minutes (\diamond) plotted as a function of the displacement from the free surface of the tube. The solid lines are fits to equations 8.14.

v decreases with increasing t_w and (ii) v increases monotonically with x for all t_w , with the increase of v being more prominent for smaller t_w . It is seen from equation 8.1 that the velocity of fall for Stokesian flow also depends on the size of the object. We plot v vs. x for steel balls of different sizes for $t_w = 30$ min in figure 8.3. It is seen from this figure that v is larger for the bigger balls. However, terminal velocity is not achieved in any of the runs. Instead, an increase in velocity, which is more prominent for larger balls, is observed.

We describe a simple rheological model proposed by Ferroir and coauthors [9] to explain our experimental observations i.e. the increase in velocity with depth of fall as seen in figures 8.2 and 8.3 for balls of different sizes and t_w of Laponite suspensions. This rheological model was originally proposed for thixotropic pasty fluids and accounts for the presence of structure of the fluid in the form of a structure parameter λ [8, 18–21]. The structure parameter λ has the following physical interpretation: $\lambda=0$ for a fully broken or destructured state of the thixotropic fluid or when the structure is yet to form at microscopic scale, while $\lambda=1$ for a fully structured fluid when the

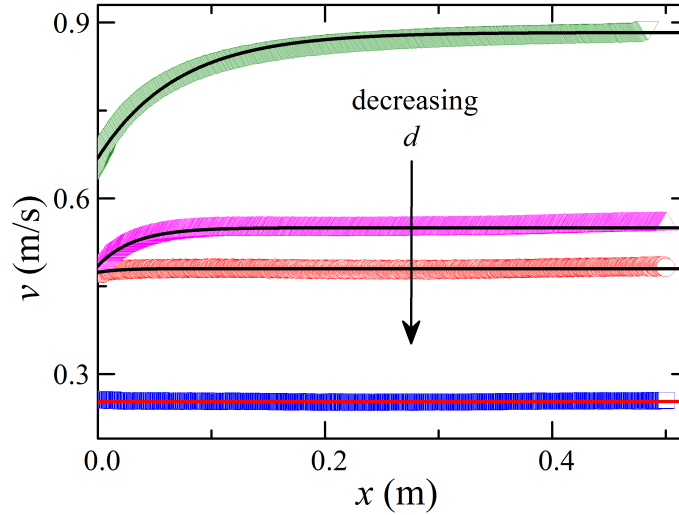


FIGURE 8.3: Velocity of steel balls of several different diameters (from bottom to top) 2 mm (\square), 3 mm (\circ), 4 mm (\triangle), 5 mm (∇), falling through a Laponite suspension of 3.5% (w/v) at waiting time $t_w=30$ minutes are plotted as a function of the displacement from the free surface of the tube. The solid lines are fits to equations 8.14.

recovery from a broken state is complete. The viscosity of these pasty materials is not only shear rate ($\dot{\gamma}$) dependent but also depends on the instantaneous state of the structure [22]. Hence, the kinetic equation which governs the time evolution of structure parameter λ has two terms due to (i) restructuring or structural recovery and (ii) structural break-down or destructuring processes and can be represented by the following equation [9]:

$$\frac{d\lambda}{dt} = F(\lambda) - G(\lambda)\dot{\gamma} \quad (8.2)$$

In the above equation, $F(\lambda)$ and $G(\lambda)$ are associated with the rates of the restructuring and destructuring processes of the internal structure respectively, and are generally functions of λ .

This above model is particularly useful for Laponite suspension as it is thixotropic in nature and shows structural recovery [23]. We further explore the role of destructuring and restructuring process by rheological and conductivity measurement. In figure 8.4, the evolution of conductivity σ and storage moduli G' are plotted for a 3.5%

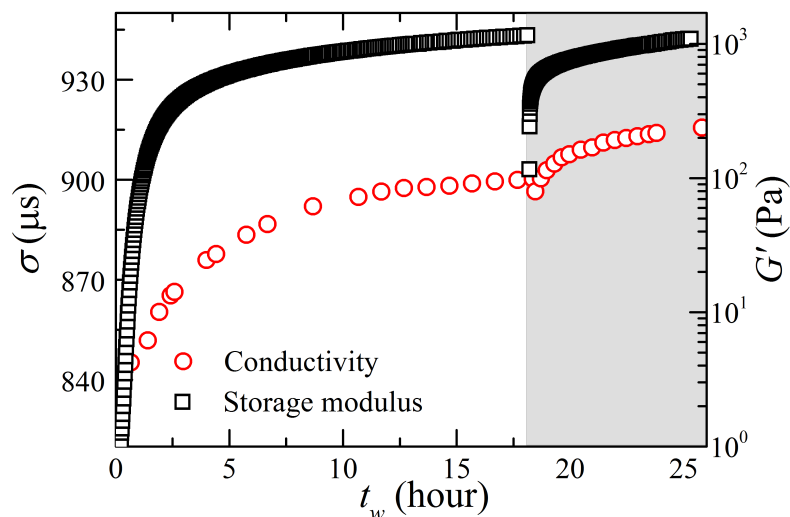


FIGURE 8.4: Conductivity σ (\circ) and storage modulus G' (\square) vs. waiting time t_w for a 3.5% w/v Laponite suspension. Shaded region in the evolution plots of σ and G' for the Laponite suspension highlights the evolution of both the quantities upon rejuvenation after 18 hours of preparation.

w/v Laponite suspension measured by a Eutech Instruments PC 2700 conductivity meter and Anton Paar MCR501 rheometer respectively. It is seen from the figure that both σ and G' are increasing with t_w . This indicates the presence of structure in Laponite suspension. A shear rejuvenation is applied to this Laponite suspension after 18 hours of preparation and both σ and G' are monitored to study the structural recovery (shaded region in figure 8.4). It is seen that G' increases from a very low value of approximately 1 Pa to a very high value ($G' > 10^3$ Pa) after 18 hours of aging. However, the value of G' decreases during the shear-melting process in which a very high shear rate (500/s) is applied for 5 minutes to break the structure. But unlike G' , the value of σ does not decrease in the shear rejuvenation process (applied shear rate approximately 500/s for 5 minutes using a syringe pump). Interestingly, G' shows a faster structural recovery for rejuvenated suspensions as G' increases to 10^3 Pa in only 7 hours. Therefore, the process of structure formation or restructuring is faster for higher sodium ion concentration or equivalently for higher conductivity. This has been indeed seen in chapters 4

where addition of salt to Laponite suspension accelerates the structure formation process. It is also seen from figure 8.4 that the structure of Laponite suspensions can be broken by the application of shear.

From the above discussion, it is evident that both the restructuring and the destructuring processes are likely to be important as the structures of Laponite suspensions are amenable to shear deformation when an object passes through it. The kinetic equation (equation 8.2) can be simplified by taking $F = 1/\theta$ and $G = \alpha\lambda$, where $1/\theta$ and α are two parameters related to the restructuring and destructuring rates respectively [9]. Therefore,

$$\frac{d\lambda}{dt} = \frac{1}{\theta} - \alpha\lambda\dot{\gamma} \quad (8.3)$$

Equation 8.2 can be further simplified if a simple expression of viscosity, $\eta = \eta_0(1+\lambda^n)$, often used for structured fluids, is assumed [9]. Here η_0 is the viscosity in the absence of any structure and $n \geq 1$. In this case, the terminal velocity of the ball falling through the fluid can be obtained from equation 8.1 by using the following expression [9]:

$$v = \frac{2}{9} \frac{(\rho_s - \rho)gR^2}{\eta_0} \frac{1}{1 + \lambda^n} = \frac{W_0}{1 + \lambda^n} \quad (8.4)$$

The parameter $W_0 = \frac{2}{9} \frac{(\rho_s - \rho)gR^2}{\eta_0}$ is the reference fall velocity of the ball through a completely destructured fluid ($\lambda = 0$). The expression for the velocity of the ball can be obtained from the equation 8.4 using the expression for λ from equation 8.3. The above equation can be further simplified by taking $n = 1$ [9]. In the equations 8.2 and 8.3, the presence of both restructuring and destructuring processes is assumed. However, in an earlier work by Ferroir and coauthors [9] it was seen that only the restructuring process is important (i.e. $G(\lambda) = 0$ in equation 8.2) for rejuvenated Laponite suspensions. In this case, we can write from equations 8.2 and 8.3,

$$\frac{d\lambda}{dt} = F(\lambda) = \frac{1}{\theta} \quad (8.5)$$

which yields,

$$\lambda = \lambda_0 + \frac{t}{\theta} \quad (8.6)$$

Here, λ_0 is the structural state of the material at $t=0$. Using equation 8.6 in equation 8.4 with $n = 1$, we have,

$$v = \frac{dx}{dt} = \frac{W_0}{1 + \lambda_0 + \frac{t}{\theta}} \quad (8.7)$$

Integrating both sides of the above equation,

$$x = \int_0^t \frac{W_0}{1 + \lambda_0 + \frac{t}{\theta}} dt = \theta W_0 \ln \left[\frac{1 + \lambda_0 + \frac{t}{\theta}}{1 + \lambda_0} \right] \quad (8.8)$$

Replacing the value of $\left(1 + \lambda_0 + \frac{t}{\theta}\right)$ from equation 8.7 in equation 8.8, we have the velocity as a function of depth x as following:

$$v = \frac{W_0}{1 + \lambda_0} \exp \left[\frac{-x}{\theta W_0} \right] = \frac{W_0}{1 + \lambda_0} \exp \left[\frac{-x}{x_0} \right] \quad (8.9)$$

Here $x_0 = \theta W_0$. It is clear from equation 8.9 that velocity of the ball decreases as it gets deeper into the fluid. This is the original solution used in [9]. Equation 8.9 is a very good approximation when the Laponite suspension is left undisturbed for a long time after preparation, such that it evolves to a vitreous state, and is eventually rejuvenated to break the structure before the experiment. As already seen in figure 8.4, for such Laponite suspensions, the recovery process is faster than in a spontaneously evolving Laponite suspension. Ferroir and coauthors had, indeed, seen a decrease in velocity with the depth for rejuvenated Laponite suspensions [9].

Equation 8.9 clearly fails to explain the increase in velocity with depth seen in figures 8.2 and 8.3. This feature arises as the destructuring process is dominant for spontaneously evolving Laponite suspensions. We solve equations 8.2 and 8.3 taking

into account only the destructuring process (i.e. $F(\lambda) = 0$).

$$\frac{d\lambda}{dt} = -G(\lambda)\dot{\gamma} = -\alpha\dot{\gamma}\lambda \quad (8.10)$$

Solving the above equation, we have,

$$\lambda = \lambda_0 \exp[-\alpha\dot{\gamma}t] \quad (8.11)$$

Using the expression of λ from equation 8.11, we have from equation 8.4 for $n = 1$,

$$v = \frac{dx}{dt} = \frac{W_0}{[1 + \lambda_0 e^{-\alpha\dot{\gamma}t}]} = \frac{W_0}{[1 + \lambda_0 e^{-\beta t}]} \quad (8.12)$$

Here, $\beta = \alpha\dot{\gamma}$. Integrating both sides of the above equation, we have,

$$x = \int_0^t \frac{W_0}{1 + \lambda_0 e^{-\beta t}} dt = -\frac{W_0}{\beta} \ln \left[\frac{(1 + \lambda_0)e^{-\beta t}}{1 + \lambda_0 e^{-\beta t}} \right] \quad (8.13)$$

Substituting the value of $e^{-\beta t}$ from equation 8.12 in equation 8.13, we have the following expression for the velocity of a ball falling through a destructuring medium with depth x :

$$v = W_0 \left[1 - \frac{\lambda_0}{1 + \lambda_0} \exp \{-x/x_1\} \right] \quad (8.14)$$

Here $x_1 = W_0/\beta = W_0/\alpha\dot{\gamma}$. The above equation predicts an increase in velocity of the ball with x .

We fit the data shown in figures 8.2 and 8.3 to equation 8.14. It is seen from these figures that equation 8.14 fits the data extremely well. In the tables 8.1 and 8.2, the fitting parameters are shown for different waiting times t_w and sizes d of the ball respectively. From the tables 8.1 and 8.2, it is seen that the characteristic length associated with the destructuring process, x_1 , is always less than the length L ($L \approx 0.5$ m) of the viscometer. It was reported in chapter 4 and also seen in figure 8.4 that

Only destructuring			
t_w	$W_0 \text{ ms}^{-1}$	λ_0	$x_1 \text{ m}$
30 min	0.8812 ± 0.0002	0.3206 ± 0.0001	0.0676 ± 0.0003
45 min	0.9069 ± 0.0028	0.2769 ± 0.0034	0.3021 ± 0.0079
60 min	0.6491 ± 0.0003	0.0974 ± 0.0006	0.1332 ± 0.0024
75 min	0.5098 ± 0.0001	0.0965 ± 0.0006	0.0890 ± 0.0012
90 min	0.0676 ± 0.0003	0.0700 ± 0.0001	0.1499 ± 0.0406

Table 8.1: Fitting parameters from figure 8.2 for a 5 mm steel ball falling through 3.5% w/v Laponite suspensions at different t_w .

the concentration of sodium ions (or conductivity) increases with t_w for spontaneously evolving Laponite suspensions. At earlier times, interparticle interactions are weak and amenable to breakage, which results in a very slow restructuring process of Laponite suspension around the ball during its motion. Therefore, the destructuring process dominates for spontaneously evolving Laponite suspensions at smaller t_w as our experiments and data analysis demonstrate. Given the several approximations in the model (for example, $n = 1$ for pasty fluid) and the assumption that restructuring is not at all influencing our Laponite suspensions (i.e. $F(\lambda) = 0$), we clearly need to improve the model to obtain better quantitative fits.

Only destructuring			
d	$W_0 \text{ ms}^{-1}$	λ_0	$x_1 \text{ m}$
5 mm	0.8812 ± 0.0002	0.3206 ± 0.0010	0.0676 ± 0.0004
4 mm	0.5499 ± 0.0007	0.1357 ± 0.0010	0.0314 ± 0.0004
3 mm	0.4799 ± 0.0005	0.0134 ± 0.0010	0.0188 ± 0.0022
2 mm	0.2530 ± 0.0002	0.0100 ± 0.0001	0.0002 ± 0.0001

Table 8.2: Fitting parameters from figure 8.3 for steel balls of different sizes d falling through 3.5% w/v Laponite suspension of $t_w = 30 \text{ min}$.

8.4 Conclusions

We have shown that the motion of solid objects (steel balls) through spontaneously evolving aging colloidal suspensions of Laponite is very different from the motion of a solid object in a Newtonian fluid. It is observed that there is a net increase in the velocity of the balls over the period of the fall, as it gets deeper into the fluid. The increase in velocity is more prominent for smaller waiting times t_w of the suspension and for the larger balls. A simple model is discussed to explain the experimental results based on the structural kinetics of the thixotropic fluid [8, 9, 20, 21]. In this model, the restructuring and destructuring processes in thixotropic materials are taken into account. These two processes, which are functions of the viscosity of the suspension on structure parameter and shear rate, were previously used to explain the decreasing velocity of fall in rejuvenated Laponite suspensions [9]. We have seen that the same model could be used to explain all the experimental results. However, the conductivity and rheological data indicate a clear difference between spontaneously evolving and rejuvenated Laponite suspensions. The structural recovery is faster for rejuvenated suspensions due to the higher amount of sodium ions. In the present experiments which are done only for spontaneously evolving Laponite suspensions, it is seen that restructuring process is very slow and only destructuring process is important over the period of fall.

References

- [1] G. K. Batchelor, *An Introduction to Fluid Dynamics*, Cambridge Mathematical Library, Cambridge, 2000.
- [2] B. Gueslin, L. Talini, B. Herzhaft, Y. Peysson and C. Allain, *Phys. Fluids*, **18**, 103101 (2006).
- [3] B. Gueslin, L. Talini, and Y. Peysson, *Rheol. Acta*, **48**, 961-970 (2009).
- [4] H. Tabuteau, F. K. Oppong, J. R. de Bruyn and P. Coussot, *Europhys. Lett.*, **78**, 68007 (2007).
- [5] A. M. V. Putz, T. I. Burghelea, I. A. Frigaard, and D. M. Martinez, *Phys. Fluids*, **20**, 594-601 (2008).
- [6] R. P. Chhabra, *Bubbles, Drops, And Particles in Non-Newtonian Fluids*, CRC, Boca Raton, FL, 1993.
- [7] C. F. Chan Man Fong, G. Turcotte, and D. De Kee, *J. Food. Eng.*, **27**, 63 (1996).
- [8] E. A. Toorman, *Rheol. Acta*, **36**, 56 (1997).
- [9] T. Ferroir, H. T. Huynh, X. Chateau, and P. Coussot, *Phys. Fluids*, **16**, 594-601 (2004).

-
- [10] B. J. Briscoe, M. Glaese, P. F. Luckham and S. Ren, *Colloids and Surfaces*, **65**, 69-75 (1992).
- [11] A. Shahin and Y. M. Joshi, *Langmuir*, **26**, 4219-4225 (2010).
- [12] A. Shahin and Y. M. Joshi, *Langmuir*, **28**, 15674-15686 (2012).
- [13] R. Angelini, L. Zulian, A. Fluerasu, A. Madsen, G. Ruocco, and B. Ruzicka, *Soft Matter*, **9**, 10955-10959 (2013).
- [14] Technical Information B-RI 21, LAPONITE: Performance Additives, BYK Additives and Instruments, <http://www.byk.com/>
- [15] H. Z. Cummins, *J. Non-Cryst. Solids*, **353**, 3891-3905 (2007).
- [16] B. Ruzicka, and E. Zaccarelli, *Soft Matter*, **7**, 1268-1286 (2011).
- [17] Particle Tracking Resource Page, <http://grahammilne.com/tracker.htm>.
- [18] J. Mewis, *J. Non-Newtonian Fluid Mech.*, **6**, 1-20 (1979).
- [19] P. Coussot, A. I. Leonov, and J. M. Piau, *J. Non-Newtonian Fluid Mech.*, **46**, 179 (1993).
- [20] D. C. H. Cheng and F. Evans, *Brit. J. Appl. Phys*, **16**, 1599 (1965).
- [21] F. Moore, *Trans. Brit. Ceramic Soc.*, **58**, 470-494 (1959).
- [22] C. W. Macosko, *Rheology: Principles, Measurements and Applications*, VCH Publishers, New York, 1993.
- [23] F. Pignon, A. Magnin, and J. M. Piau, *J. Rheol.*, **42**, 1349 (1998).

9

Instabilities at the interface between a Newtonian fluid and an aging non-Newtonian fluid in quasi-2D geometry

9.1 Introduction

Viscous fingering is a very challenging problem in the context of the displacement of fluids in a porous material and it generally refers to the onset and evolution of instabilities at the interface between two fluids [1]. This problem originates from the

petroleum industry. Tongues of water in oil are observed by petroleum engineers during enhanced secondary oil recovery. This particular problem is industrially so important that a meticulous study of interfacial instabilities was pursued to determine the optimal policy of oil recovery [2, 3]. Pioneering work by Saffman and Taylor revealed that the boundary between oil and a displacing fluid becomes unstable if the latter is less viscous than the former [4, 5]. This instability at the interface between two fluids is called the Saffman-Taylor instability and the resultant finger-like protrusions are known as the Saffman fingers. Typically, the study of viscous fingering is performed in a confined geometry. A thin linear channel or a Hele-Shaw cell are often preferred most as they facilitate laminar flow [6].

The physics of interfacial patterns in a constrained geometry is understood in terms of Laplacian growth, where the boundary of a two dimensional domain grows at a rate proportional to the gradient of a Laplacian field, i.e. pressure, [7]. It is a general practice to write Darcy's law to relate the velocity of the finger to the gradient of the pressure in a narrow channel or porous medium [8]. For Newtonian fluids with a parabolic velocity profile of the finger over the gap in a Hele-Shaw cell, the gap-averaged velocity v is proportional to the pressure gradient ∇p : $v = -(b^2/12\mu)\nabla p$, where b is width of the gap or the spacing between the plates and μ is the viscosity of the fluid. For non-Newtonian fluids, this relation can be further modified by taking into account a shear rate dependent viscosity $\mu(\dot{\gamma})$: $v = -(b^2/12\mu(\dot{\gamma}))\nabla p$ [9–11].

A sound understanding of the interfacial phenomena in a Hele-Shaw cell involving non-Newtonian fluids is relatively difficult due to the complex flow behaviors of the elasticity and viscosity at different shear rates [12, 13]. For example, yield stress fluids, which do not flow until the shear stress is above a critical value of the stress known as the yield stress, show thixotropic behavior including aging, shear rejuvenation and also shear banding [14]. It was demonstrated experimentally in yield stress fluids that the Saffman-Taylor instability is dramatically modified and gives rise to different regimes and pattern morphologies i.e. branched patterns at low velocities, a

single stable finger at moderately high velocities and the destabilization of finger propagation and side-branching instabilities at very high velocities [9]. This problem was also studied analytically and numerically to understand the morphological features of the fluid-fluid interface, the finger competition dynamics and the stability of the interface at different stages of pattern evolution [15, 16]. Such instabilities and pattern morphologies have been also explored when one of the phases is a viscoelastic clay suspension [17, 18]. It was seen that viscous fingering is obtained when an aqueous suspension of bentonite clay is displaced by water for low clay/water ratios [17]. Interestingly, a transition from viscous finger to viscoelastic fracturing is observed with increasing clay/water ratio [18].

In general, clay suspensions (eg. Laponite suspension) are thixotropic in nature [19] and exhibit aging properties (chapter 1). Understanding the pattern morphologies for such aging viscoelastic fluids and a Newtonian fluid is of utmost theoretical and experimental importance as many natural phenomena involve clay/water systems [17]. In the present experiment, the instabilities at the interface between aging colloidal suspensions of Laponite XLG and two different Newtonian fluids are studied in a radial Hele-shaw cell. The Laponite suspension is displaced by the Newtonian fluids carbon tetrachloride or water at different waiting times. The morphology of the patterns obtained when aging Laponite suspensions are displaced by an immiscible Newtonian fluid (carbon tetrachloride) are found to be dependent on waiting times. A dense branching finger pattern emerges due to the non-linear development of the interface arising out of the Saffman-Taylor instability at longer waiting times. A dependence of the patterns on waiting times is also observed when Laponite suspensions are displaced by a miscible Newtonian fluid (water). In this case, a transition from viscous fingering to viscoelastic fracturing is observed at very high waiting times. The observed results are explained qualitatively with the help of rheological data.

9.2 Sample preparation and experimental methods

All experiments reported in this chapter are done using Laponite XLG[®] (BYK additives). The concentration of the aqueous suspension is kept constant at 3.5% w/v for all experiments. Here, the concentration of Laponite expressed in % w/v refers to the weight of Laponite in grams that is dispersed in 100 ml MilliQ water. Details of the sample preparation are given in chapter 8. The Laponite suspension is loaded inside a Hele-Shaw cell just after preparation. Details of the Hele-Shaw cell and the experimental procedure are given in chapter 2 (section 2.2.6). The waiting time $t_w = 0$ is measured from the moment at which the loading process of the Laponite suspension is completed. The waiting time t_w is the time interval between the time of loading of the Laponite suspension into the Hele-Shaw cell and the time at which the second (Newtonian) fluid is injected. All the experiments reported in this chapter are done with spontaneously evolving Laponite suspensions, i.e. for each experiment, a freshly prepared Laponite suspension is loaded into the cell. Two different types of experiments are performed by displacing aqueous Laponite suspensions by two different Newtonian fluids, (i) water (a miscible phase) and (ii) CCl₄ (carbon-tetrachloride- an immiscible phase). A tiny amount of dye (KMnO₄/Sudan III) is added to the displacing phases (water/CCl₄) to improve the contrast of the images obtained by the high speed camera.

9.3 Results and discussions

9.3.1 Pattern formation when an aging Laponite suspension is displaced by CCl₄

In this section, we discuss the morphologies of the patterns obtained when aging Laponite suspensions at different stages of structural evolutions (i.e. different t_w) are displaced by an immiscible Newtonian fluid i.e. CCl₄ (viscosity $\eta_1 = 0.90$ mPa.s,

specific density $\rho_1 = 1.58$ and surface tension $\sigma_1 = 0.026 \text{ Nm}^{-1}$). In figure 9.1, a few representative patterns are shown when Laponite is displaced by CCl_4 (colored red with dye) at different waiting times t_w . It is seen that the interface between the fluids is not circular due to the Saffman-Taylor instability and finger-like protrusions are observed (figure 9.1). At smaller t_w , the protrusions are not clearly separated from each other and they avoid side-branching (figure 9.1(a)). However, a very branched pattern emerges when Laponite is displaced by CCl_4 after $t_w = 5$ hours (figure 9.1(b)). At even higher t_w (i.e. $t_w = 24$ hours), similar types of branched patterns are observed (figure 9.1(c)), but the widths of the branches appear to decrease. Patterns that are shown in this figure are typical fractal patterns that emerge when a more viscous fluid is displaced by a less viscous fluid in porous media due to the Saffman-Taylor instability [1]. We have plotted the fractal dimensions d_f of the patterns as a function of t_w of the Laponite suspension in figure 9.3.

It is well known that fractal patterns are not compact objects and the relation between the area and any characteristic length scale (i.e. average radius of the patterns) does not have any definite functional form. In contrast, a compact object will have a definite functional form. For example, the area A of a circle is related to its radius r by $A = \pi r^{d_f}$, where $d_f = 2$ is an integer. In the case of a fractal pattern which is embedded

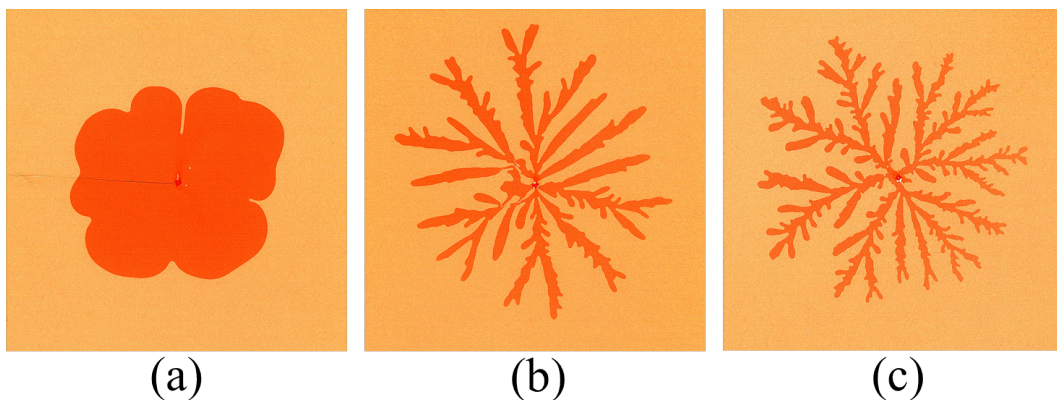


FIGURE 9.1: Interfacial patterns which are obtained when aging Laponite suspensions are displaced by CCl_4 at a constant flow rate of 5.25 ml/min in a Hele-Shaw cell (gap = 0.17 mm) at three waiting times: (a) $t_w = 1$ hour (b) $t_w = 5$ hours and (c) $t_w = 24$ hours.

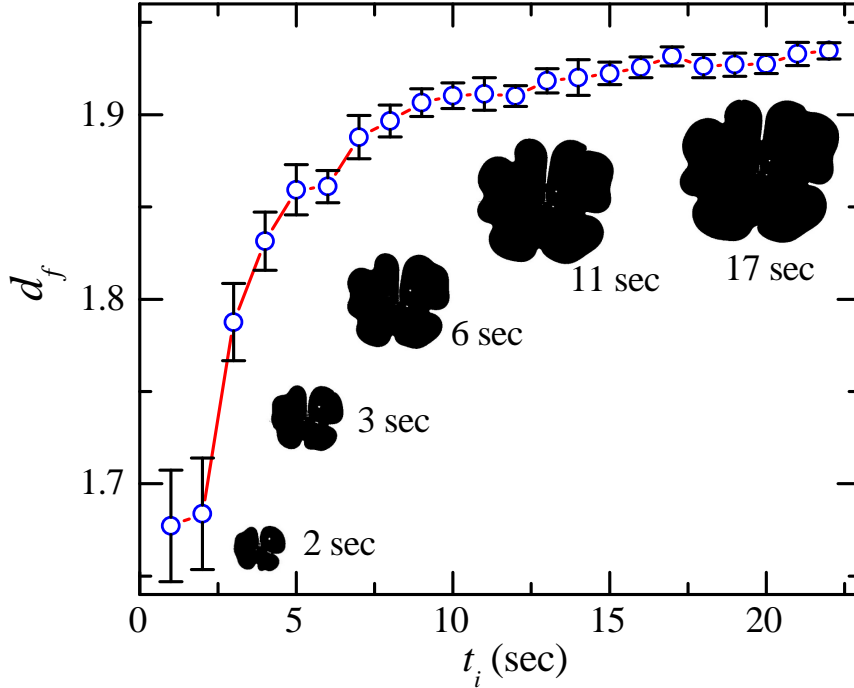


FIGURE 9.2: Fractal dimension d_f vs. injection time t_i for the patterns obtained when aging Laponite suspensions are displaced by CCl_4 at a constant flow rate of 5.25 ml/min in a Hele-Shaw cell (gap = 0.17 mm) at $t_w = 1$ hour.

in 2-dimensional space, d_f could be between 1 and 2. We use the fractal box counting method to calculate d_f for the patterns obtained in the experiments. In this method, the number of boxes N that are required to cover the whole area A of the fractal pattern is calculated. In general N depends on the size of the box l , i.e. $N(l)$ and the area can be written as $A = N(l)l^2$. Now the area is related to the characteristic length scale $A = cl^{d_f}$. Therefore, $\log A = 2 \log l + \log N(l) = d_f \log l + \log c$, where c is a constant. Next, d_f is estimated from the slope of $\log N$ vs. $\log l$ plot.

In figure 9.2, we plot d_f vs. the injection time t_i for a Laponite suspension that is displaced after $t_w = 1$ hour. The injection time $t_i = 0$ is measured from the moment when injection of the second fluid is commenced. t_i is always less than 3 minutes for our experiments and therefore, no significant aging happens during injection. It is seen from figure 9.2 that d_f increases with the increase in t_i and finally saturates above

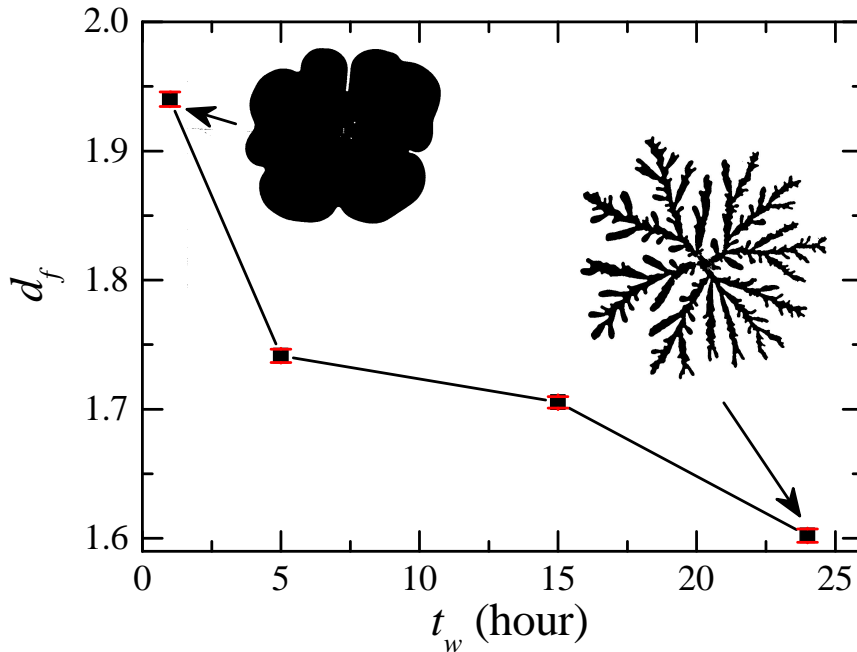


FIGURE 9.3: Fractal dimension d_f vs. waiting time t_w for aging Laponite suspensions that are displaced by CCl_4 at a constant flow rate of 5.25 ml/min in a Hele-Shaw cell (gap= 0.17 mm). The change in interfacial patterns at the two extreme values of t_w are also reproduced above.

$t_i = 10$ sec when the patterns becomes self-similar. It is also noted that errors in d_f are larger for smaller patterns as the statistics are poor (i.e. the number of boxes in the fractal box counting method is small). For the remainder of this chapter, we report only the values of d_f that are obtained for self-similar patterns when d_f does not depend on t_i .

In figure 9.3, we plot d_f vs. t_w to study the dependence of d_f on the aging or waiting times of Laponite suspensions. It is seen from the figure that d_f decreases from a value 1.94 ± 0.01 to 1.60 ± 0.01 with increasing t_w . As seen in figure 9.4 for a Laponite suspension of $t_w = 24$ hours that is displaced by CCl_4 , d_f also depends on the gap between the plates. It is seen that d_f increases with increasing gap between the plates.

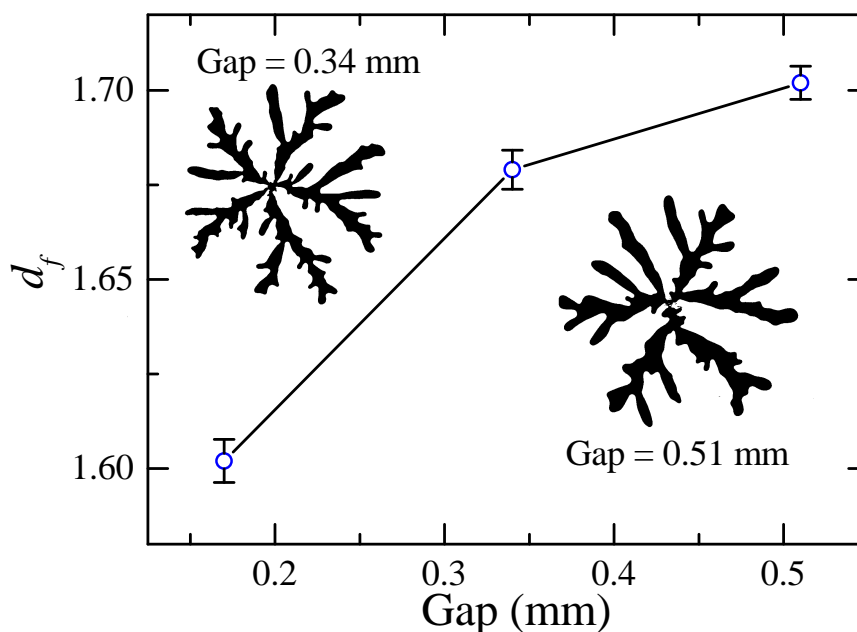


FIGURE 9.4: Fractal dimension d_f vs. the gap between the plates for aging Laponite suspensions that are displaced by CCl_4 at a constant flow rate of 5.25 ml/min in a Hele-Shaw cell at a fixed waiting time, $t_w = 24$ hours.

9.3.2 Pattern formation when an aging Laponite suspensions is displaced by water

Fractal patterns are also formed due to interfacial instabilities when aging aqueous Laponite suspensions are displaced by water, a miscible Newtonian fluid. In figure 9.5, patterns are shown for three different ages, t_w , of Laponite suspensions. Initially for $t_w = 1$ hour (figure 9.5), many closely spaced radially propagating fingers are observed. This is different from the pattern seen in figure 9.1(a), where the presence of only a few very broad fingers were observed.

A very dense dendritic pattern is observed when the Laponite suspension is displaced at a relatively higher waiting time $t_w = 5$ hours (figure 9.5(b)). Unlike in the immiscible case, the morphology of the patterns changes further when Laponite is displaced by water at even higher waiting times (figure 9.5(c)). Similar to our analysis

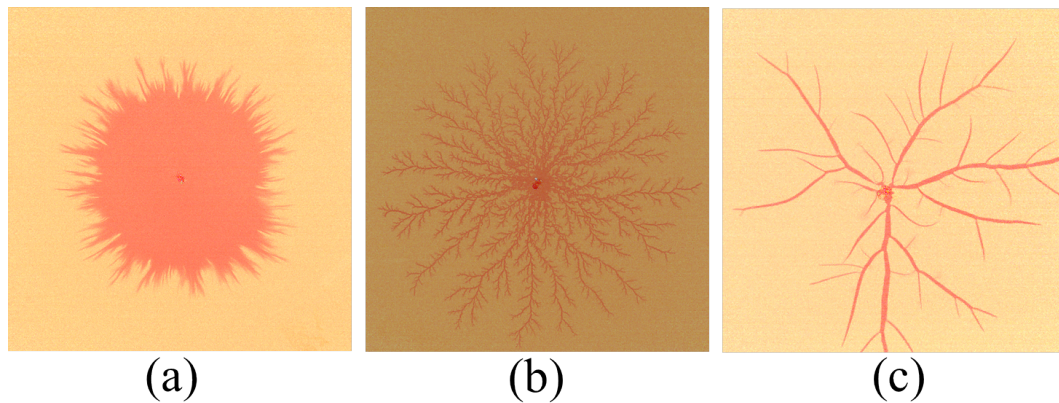


FIGURE 9.5: Fractal patterns that are obtained when aging Laponite suspensions are displaced by water at a constant flow rate of 5.25 ml/min in a Hele-Shaw cell (gap = 0.17 mm) at three waiting times t_w = (a) 1 hour (b) 5 hours and (c) 24 hours.

for the immiscible patterns, we have estimated the fractal dimension d_f of the patterns formed when Laponite suspension are displaced at different t_w . In figure 9.6, we plot d_f vs. injection time t_i . Similar to the data in figure 9.2, d_f increases with t_i initially, before saturating to a constant value 1.41 ± 0.01 . In figure 9.7, d_f is plotted vs. t_w . It is seen that the decrease in d_f is much more drastic in this plot than in figure 9.3. In the inset of figure 9.7, d_f is plotted vs. the gap between the plates for two different gaps. Similar to the case of the immiscible patterns, d_f increases with the increase in gap. For high waiting time $t_w = 28$ hours, $d_f = 1.32 \pm 0.01$ (figure 9.7) and the pattern looks similar to the viscoelastic fracturing patterns (figure 9.8) obtained for bentonite clay suspensions for very high clay/water ratios [17, 18]. The reported values of d_f for the viscoelastic fracturing pattern is below 1.50. It was also reported that in the viscoelastic fracturing regime, the fractures or cracks emerged at almost 90° relative to the primary branches [18]. The patterns seen in our experiments are very similar to the ones reported earlier [17, 18].

We next explore the morphology of the fracturing patterns for very high waiting times. In figure 9.8, the pattern which is obtained when aging Laponite suspensions are displaced by water at $t_w = 28$ hours are reproduced. It is seen from this figure that some cracks have emerged at almost 90° relative to the main branch (shown by

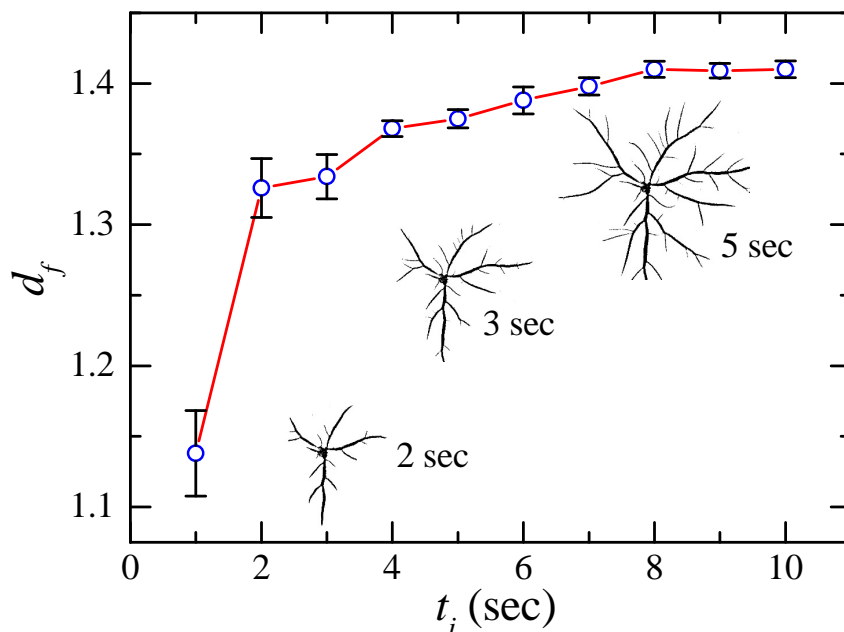


FIGURE 9.6: Fractal dimension d_f vs. injection time t_i for the pattern obtained when aging Laponite suspensions are displaced by water at a constant flow rate of 5.25 ml/min in a Hele-Shaw cell (gap = 0.17 mm) at $t_w = 24$ hours.

arrows). This is a typical features of viscoelastic fracturing [18] and is only seen when the age of the Laponite suspension is very high.

In figure 9.9, elastic G' and viscous G'' moduli and the complex viscosity η^* of a 3.5% w/v Laponite suspension are plotted vs. t_w . It is seen that at smaller t_w , the values of G' and G'' are comparable (shaded region in figure 9.9(a)) as the suspension is liquid-like. However, it is seen that both modulus and complex viscosity increase with t_w due to aging. At very high ages i.e. $t_w > 20$ hours, G' is almost two decades higher in magnitude than G'' . This indicates a development of elasticity and the emergence of soft solid-like behavior in the suspension. Since elasticity is more important at higher ages, it influences the morphology of the pattern and gives rise to a viscoelastic fracturing phenomenon reported in this chapter.

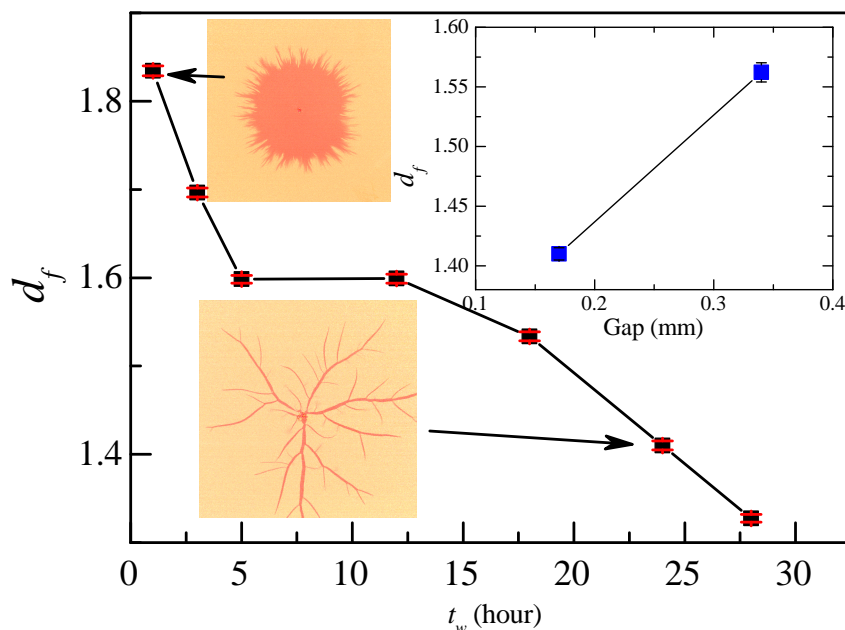


FIGURE 9.7: Fractal dimension d_f vs. waiting time t_w for the patterns obtained when aging aqueous suspensions of Laponite are displaced by water at a constant flow rate of 5.25 ml/min (gap = 0.17 mm). In the inset, d_f is plotted vs. the gap between the plates.

9.4 Conclusions

The elasticity of glassy colloidal suspensions builds up as the system ages, and the mechanical properties of soft glassy suspensions change dramatically as time progresses. Colloidal suspensions of Laponite are loaded into a quasi-2 dimensional cell consisting of two glass plates separated by a thin gap (a radial Hele-Shaw cell). A miscible and an immiscible Newtonian fluid, having low viscosity values compared to Laponite, are each injected in separate experiments at a constant flow rate through a hole in one of the glass plates of the cell to replace the aging Laponite suspension. The fractal behavior of the interfacial pattern is seen to have a strong dependence on the waiting time of the colloidal suspension of Laponite and on the surface tension between the two fluids. A transition from viscous to viscoelastic fracturing is observed when aging Laponite suspensions are displaced by water at higher waiting times due to the development of

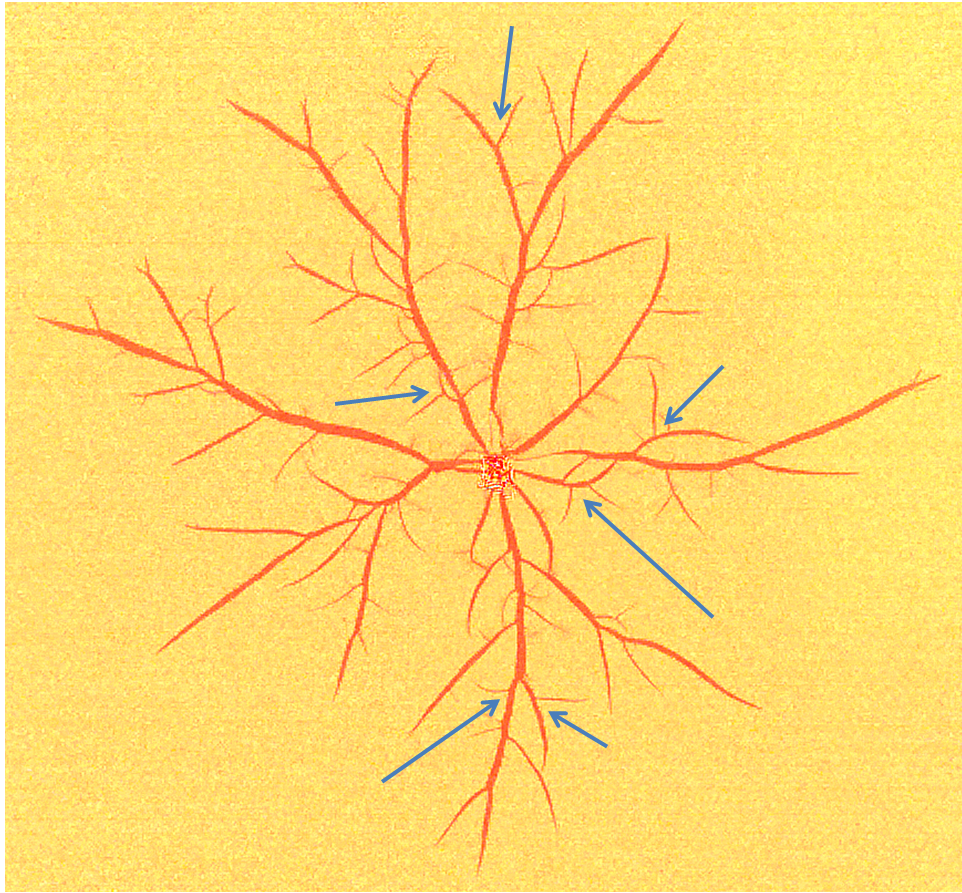


FIGURE 9.8: The viscoelastic fracturing pattern that is obtained when aging aqueous suspension of Laponite at $t_w = 28$ hours, is displaced by water (gap = 0.17 mm, flow rate = 5.25 ml/min). Arrows indicate that the fractures occur at an angle of approximately 90° .

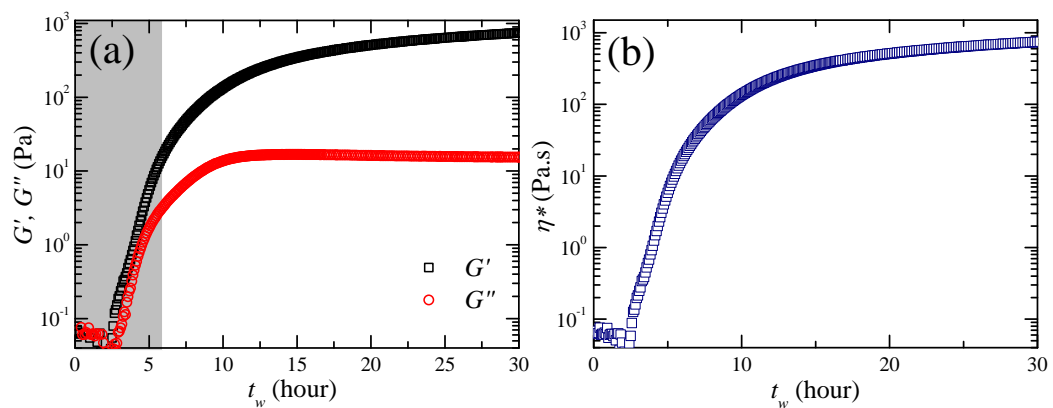


FIGURE 9.9: (a) Elastic or storage G' (\square) and viscous or loss G'' (\circ) moduli vs. waiting time t_w for a 3.5% w/v Laponite suspension at 25°C . (b) Complex viscosity η^* vs. t_w for 3.5% w/v Laponite suspension.

considerable elasticity in the Laponite suspensions with time.

References

- [1] G. M. Homsy, *Ann. Rev. Fluid Mech.*, **19**, 271-311 (1987).
- [2] S. B. Gorells and G. M. Homsey, *SIAM J. Appl. Math.*, **43**, 79-98 (1983).
- [3] H. J. Pearson, The stability of some variable viscosity flow with application in oil extraction, Cambridge Univ. Report (1977).
- [4] P. G. Saffman and G. Taylor, *Proc. Royal Soc. London Ser. A*, **245**, 312-329 (1958).
- [5] G. Taylor, *Proc. Royal Soc. London A*, **201**, 192-196 (1950).
- [6] B. Gustafsson, R. Teodorescu, A. Vasilev, *Classical and Stochastic Laplacian Growth*, Springer, 2014.
- [7] A. Levermann and I. Procaccia, *Phys. Rev. E*, **69**, 031401 (2004).
- [8] S. Whitaker, *Transport in Porous Media*, **1**, 3-25 (1986).
- [9] N. Maleki-Jirsaraei, A. Lindner, S. Rouhani and D. Bonn, *J. Phys.: Condens. Matter*, **17**, S1219-S1228 (2005).
- [10] M. B. Amar, *Phys. Rev. E*, , R3819-R3822 (1995).

- [11] J. E. Sader, D. Y. C. Chan and B. D. Hughes, *Phys. Rev. E*, **49**, 420-432 (1994).
- [12] H. A. Barnes, J. F. Hutton and K. Walters, *An Introduction to Rheology*, Elsevier, Amsterdam, 1989.
- [13] C. W. Macosko, *Rheology: Principles, Measurements and Applications*, VCH Publishers, New York, 1993.
- [14] P. Moller, A. Fall, V. Chikkadi, D. Derks, and Daniel Bonn, *Phil. Trans. R. Soc. A*, **367**, 5139-5155 (2009).
- [15] J. V. Fontana, S. A. Lira, and J. A. Miranda, *Phys. Rev. E*, **87**, 013016 (2013).
- [16] J. V. Fontana and J. A. Miranda, *Phys. Rev. E*, **88**, 023001 (2013).
- [17] H. van Damme, F. Obrecht, P. Levitz, L. Gatineau and C. Laroche, *Nature* **320**, 731 (1986).
- [18] E. Lemaire, P. Levitz, G. Daccord and H. van Damme, *Phys. Rev. Lett.*, **67**, 2009 (1991).
- [19] F. Pignon, A. Magnin, and J. M. Piau, *J. Rheol.*, **42**, 1349 (1998).

10

Summary and future directions

This chapter describes the main results reported in this thesis and discusses the scope for future research in this field. The main objective of this thesis is to study the colloidal glass transition in aging Laponite suspensions, a model glass former, and connect the observed behaviors with other glass formers. This thesis also describes the flow behavior of aging Laponite suspensions in two contexts - settling of an object through a thixotropic fluid formed by Laponite clay and the formation of fractal patterns in a confined geometry (Hele-Shaw cell) due to instabilities at the interface. The slow dynamics in aging Laponite suspensions is explored mainly by dynamic light scattering (DLS) experiments and supported by ion concentration measurements using an ion meter and rheological measurements using a rheometer. Designs and implementation of falling ball viscometer and Hele-Shaw cell experiments, to study the flow behavior of aging Laponite suspensions, are also discussed in this thesis.

Chapter 1 contains a review of the background information required to understand the experimental observations in this thesis. It describes colloids and colloidal suspensions. It next discusses the main features of the glass transition, with a focus on the

colloidal glass transition. The dynamic slowing down of the relaxation processes in colloidal suspensions and the concomitant increase in viscosity are discussed in detail. This is followed by a discussion of the glass transition of supercooled liquids and other glass formers. This chapter also briefly discusses the main interparticle interactions in colloids. Next, the phase diagram of Laponite suspension is described. Finally, the flow behaviors of colloidal dispersions are discussed.

Chapter 2 discusses the experimental techniques used to performed the experiments in this thesis. This includes the description and measuring protocols used in dynamic light scattering (DLS) measurements, ion concentration measurements, rheology and high speed imaging. Instrumentation involving the design of a falling ball viscometer and Hele-Shaw cell are also described in details.

In chapter 3, we report the dynamic slowing down of relaxation processes of aging Laponite suspensions. Laponite is known as a model glass former. This study relates the relaxation processes in aging Laponite suspensions with the relaxation processes in supercooled liquids. A mapping between waiting time (t_w) for Laponite suspension in the ergodic cage-forming regime with the inverse of temperature ($1/T$) of a supercooled liquid is proposed. In this framework, the comparison between these glass formers reveals the underlying universality of the glass transition processes. Both α and β -relaxations are seen to slow down as the Laponite suspension approaches the glass transition. Coupling between these two relaxation processes is also observed and is related to a similar behavior observed in supercooled liquids. We also relate the observed non-monotonic behavior of the β -relaxation process to the exfoliation of Laponite tactoids. Aging Laponite suspensions are identified as fragile glass formers and the fragility index is also defined for these colloidal glass formers.

Chapter 4 discusses the self-similar nature of relaxation processes for different physicochemical variables *i.e.* Laponite concentration (C_L), salt concentration (C_S) and temperature (T) for spontaneously evolving Laponite suspensions. Comprehensive overlap curves are obtained for both the relaxation timescales and the stretching exponent. This highlights the self-similar nature of the energy landscape dominated

transport of the aging Laponite suspensions. The stretching exponents are seen to decrease linearly with waiting time. The timescale associated with the β -relaxation process is seen to slow down. All these observations and DLVO calculations, together with our sodium ion measurements, indicate the influence of attraction in an overall repulsion dominated environment even for spontaneously evolving Laponite suspensions.

After the glass transition, a glass former achieves a non-equilibrium state and it is not possible to measure its relaxation time as the system does not relax within the observation timescale accessible in the laboratory. Hence, it is customary to study the correlations among different quantities (hypothetical timescales or temperatures) which are associated with the glass transition process and are mostly obtained by extrapolation. The remarkable similarities between the relaxation dynamics of spontaneously evolving Laponite suspensions and molecular glasses makes it possible to explore numerous correlations among different hypothetical timescales associated with the glass transition process of spontaneously evolving Laponite suspensions. Chapter 5 describes the kinetics of the glass transition of fragile soft colloidal suspensions for different physicochemical variables. Fragility parameters D are estimated from the evolutions of the primary relaxation times for different physicochemical variables C_L , C_S and T . It is seen that D is independent of Laponite concentration C_L and salt concentration C_S , but is weakly dependent on temperature T . This also explains the self-similarity of the relaxation process upon change in these variables as seen in chapter 4. Interestingly, the behavior of D corroborates the behavior of fragility in molecular glass formers with respect to equivalent variables. It is seen that a correlation exists between the Vogel time (t_v^∞) and the Kauzmann time (t_k) for all Laponite suspensions with different C_L , C_S and T . This correlation is remarkably similar to an observation reported for fragile molecular glass formers ($D < 10$). A coupling model which was first proposed for molecular glass formers is adapted to account for the t_w -dependence of the stretching exponent and the secondary relaxation time τ_1 , and is used to analyze and explain this correlation.

In the previous chapters, the primary relaxation process was mainly studied. The secondary relaxation process is generally neglected in the study of the vitrification of liquids. However, it is seen that some of the secondary relaxation processes in molecular glass formers have a connection to the glass transition process. The successful application of the coupling model to explain the correlation between t_α^∞ and t_k , discussed in chapter 5, and the coupling between primary and secondary relaxation processes (chapter 3), indicate that the secondary relaxation process might play a crucial role in the relaxation dynamics of spontaneously evolving Laponite suspensions. In chapter 6, the characteristics of the secondary relaxation process of Laponite suspensions are explored by following a conventional route that is often followed for a molecular glass formers. It is seen that the secondary relaxation process of Laponite suspension have many characteristics that are reminiscent of the slow secondary relaxation process of molecular glass formers. For example, the secondary relaxation process of an aging Laponite suspension involves all parts of a Laponite particle. It is also coupled with the primary relaxation process for all the physicochemical variables as the glass transition time t_g is seen to be coupled with the characteristics time t_β^∞ associated with the secondary relaxation process and the width of the primary relaxation process w is correlated to the β -relaxation timescale. Both primary and secondary relaxation times are also shown to be very sensitive to changes in concentration. A correlation between primitive and secondary relaxation processes is also observed. However, this study is done for a spontaneously evolving Laponite suspension where an exfoliation process of Laponite tactoids into smaller entities is present. Additionally, all the correlations are verified from data that are obtained well before the glass transition is achieved as the decay of the autocorrelation function is incomplete for very high waiting times and therefore impossible to analyze. An advanced study is required to be performed in future where the effect of exfoliation could be minimized (possibly by low power ultrasonication of suspension) and for higher waiting times.

In chapters 3-6, the remarkable similarities of the relaxation processes between colloidal glasses of Laponite and fragile supercooled liquids are reported. In future, a

detailed study of the relaxation behavior is needed to be performed for Laponite at very high and low concentrations where they show different phase behaviors. It is worth studying the existence of similar correlations between different dynamical quantities as described in the previous chapters for other concentration regimes. Structural data has to be obtained by X-ray, cryogenic scanning electron microscopy (Cryo-SEM) etc. to improve the understanding and also to determine the presence of any fundamental link between the structure and the dynamics of the different phases of Laponite. Particularly, the structural origin of the fragility in these suspensions needs to be studied. The mapping between the waiting time (t_w) for Laponite suspension with the inverse of temperature ($1/T$) of supercooled liquid has to be verified for other clay dispersions, such as, bentonite, etc.

In chapter 7, the microscopic relaxation processes of aging Laponite suspensions are studied in the presence of probe particles. These probe particles are polystyrene beads with sizes larger than that of the Laponite particles. These particles behave as the less mobile regions in the suspension. Two-step relaxation processes are observed from the intensity autocorrelation function obtained in DLS experiments. The fast relaxation process is identified as due to the diffusion of a Laponite particle inside the cage formed by the neighboring Laponite particles, while the slow relaxation process is interpreted to originate due to relaxation in the presence of the externally added less mobile polystyrene beads. The fragility parameter D is obtained from the evolution of the primary relaxation time for different concentrations and sizes of the polystyrene beads. D is seen to increase with the concentration of polystyrene particles, but decreases as the size of the particles increases. Qualitative agreement in the fragile behavior of the observed relaxation process is demonstrated with simulation results for random pinning in binary mixtures. An advanced study is required to be performed using optical trap to create true quenched defects by pinning different parts of the system in order to make a better comparison with the observations reported for binary mixtures.

The last two experimental chapters report interesting observations regarding the

flow behavior of aging Laponite suspensions. Chapter 8 reports the settling of an object through a thixotropic medium formed by spontaneously evolving Laponite suspensions. Steel balls of different radii are dropped in a long cylindrical tube filled with Laponite suspensions after different waiting times. The motion of each ball is recorded with a high speed video camera. The velocity is seen to increase with the depth of fall for spontaneously evolving Laponite suspensions. This increment is more prominent for larger balls and for lower aging or waiting times of the suspensions. A simple rheological model is constructed based on the concepts of structural kinetics in thixotropic fluids. In contrast to rejuvenated Laponite suspensions, it is seen that the destructuring process is more important than the restructuring process for spontaneously evolving Laponite suspensions over the period of fall. In future, balls with different densities could be dropped in spontaneously evolving Laponite suspensions to understand the structural kinetics under various conditions of structure formation. The analysis should also be performed after considering the possibility of competing restructuring and destructuring phenomena as this may yield better quantitative fits to the experimental data.

Finally, the evolution of fractal patterns when Laponite suspensions of different ages or waiting times are displaced by water (miscible phase) or carbon-tetrachloride (immiscible phase) in a Hele-Shaw cell are reported in Chapter 9. For the miscible phase, a transition from viscous fingering to viscoelastic fracturing is observed with increasing age of the Laponite suspension. However, this transition is absent in the case when the immiscible phase displaces the Laponite suspension. This confirms the role of surface tension in the suppression of viscous fingering. In future, an effort could be made to develop a model to understand these observations quantitatively. It is also important to study if the observed viscoelastic fracturing patterns have any similarities to the patterns formed by natural processes involving various clay/water systems, for example, delta formation by rivers.

This thesis reports a series of experimental studies on colloidal suspensions of

Laponite. The colloidal glass transition and the flow behavior of aging Laponite suspension are highlighted using a wide array of experiments. These studies have shown that Laponite suspensions have the potential to be an excellent model system to study the physics of the glass transition and the flow behavior of aging viscoelastic fluids.